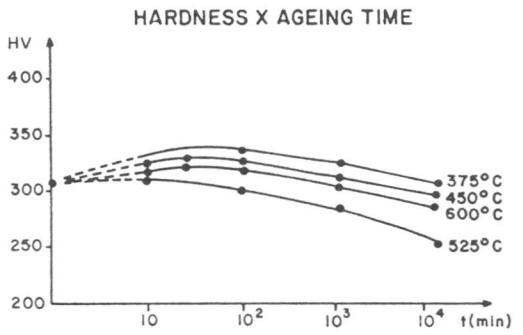

Fig. 6 Ti-7 wt %V

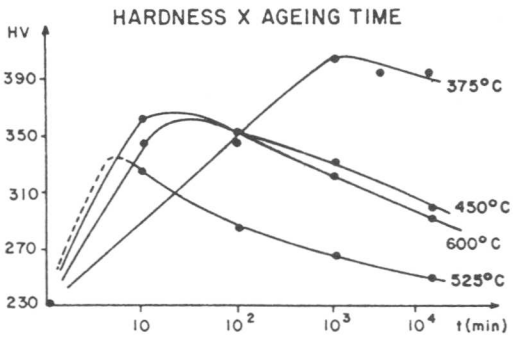

Fig. 7 Ti-12 wt %V

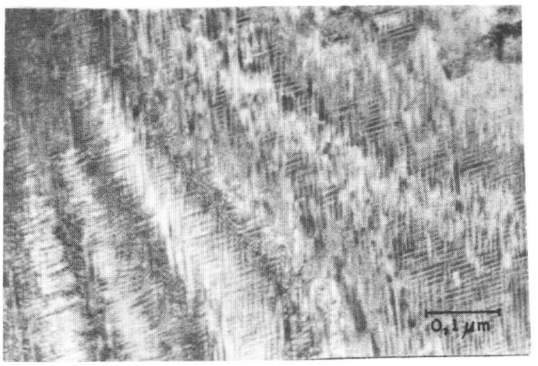

Fig 8. Ti-12 wt %V aged at 375°C, 10^4 min. TEM

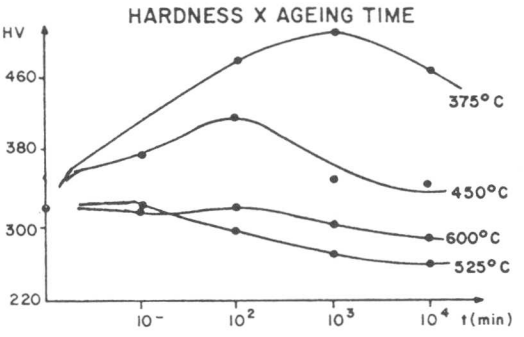

Fig 9. Ti-16 wt %V

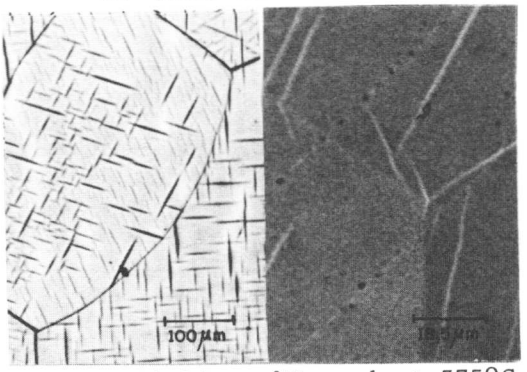

Fig 10. Ti-16 wt %V aged at 375°C 10^4min.

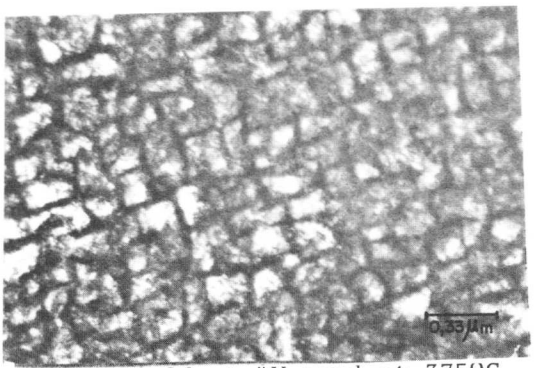

Fig 11 Ti-16 wt %V aged at 375°C 10^4 min. Dark field TEM of ω particles

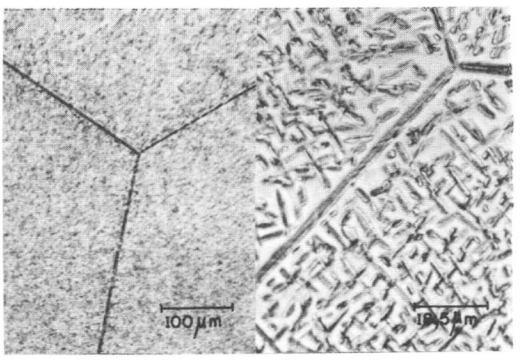

Fig 12. Ti-16 wt %V aged at 600°C, 10^4 min α particles within β grains

Stress and Strain Induced Martensitic Transformations

K. Otsuka* and K. Shimizu*

Abstract

After some discussions on stress-induced vs. strain-induced transformations, some recent developments on the stress-induced transformation in β phase alloys are described. The included topics are successive stress-induced transformations, phase diagrams in temperature-stress coordinates, martensite-to-martensite transformations, the transformation pseudoelasticity and the effect of sense of stress on martensitic transformations.

I. Introduction

The stress-induced martensitic transformation is a current topic among other subjects on martensitic transformations from the following three reasons. Firstly the stress-induced transformation is more easily controlled than the ordinary transformation by cooling, and the associated variables describing a transformation (e.g. CRSS to induce the martensite etc.) is easily obtained when one uses single crystals. Thus, it is more convenient for the study of transformation mechanisms than the latter. Secondly, new phases or new phenomena (e.g. martensite-to-martensite transformations) may appear under stress which are not realized under cooling alone, since stress is a thermodynamic variable independent of temperature. Thirdly interesting mechanical properties are associated with the stress-induced transformation, which have a variety of potential applications, such as the shape memory effect, transformation pseudoelasticity and transformation induced plasticity.

The effect of stress on martensitic transformation has first been explored theoretically by Scheil[1] in early 1930's. A more quantitative theory has been developed by Patel and Cohen[2] to predict the change of transformation temperature as a function of stress, and it has been shown that the transformation temperature increases with uniaxial stress. The same result has been obtained by Burkart and Read[3] by applying the Clausius-Clapeyron equation to shear stress. Until now both theories have been tested successfully by a number of experiments. After 1970 the studies on the stress-induced transformation has become very popular, and the transformation pseudoelasticity has been found and studied in detail in a number of β phase alloys [4, 5]. In the present paper some of the later developments, which have been obtained within a few or several years, will be highlighted.

---

* The Institute of Scientific and Industrial Research, Osaka University, Yamadakami, Suita, Osaka 565, Japan.

II. Stress-induced vs. strain-induced transformations

As described above, an applied uniaxial stress assists the martensitic transformation thermodynamically. This is a stress-induced transformation. In fact, the transformations occurring under stress in β phase alloys above M_s are stress-induced transformations, as evidenced by the conformity to the Clausius-Clapeyron equation and the pseudoelastic behavior at temperatures above A_f. However, it is known in some ferrous alloys under special conditions that a plastic deformation always preceeds the martensitic transformation (e.g. at temperatures above M_s^σ in Fig. 1), and that martensites are often formed at the intersection of two slip bands. This case is controversial as to whether the transformation is stress-induced or strain-induced. In fact, this is a matter of definition to some extent. Some authors[6] call it a strain-induced transformation, simply because the introduction of strains lowers the critical stress to induce martensites from the Clausius-Clapeyron relationship, while others[7] call it a stress-induced transformation because they consider that an applied stress and local stresses around the source of strains add up to the stress required by the Clausius-Clapeyron equation. Based on their nucleation mechanism, Olson and Cohen[8, 9] seem to preserve the term more rigorously such that geometrically favorable nucleation sites are created in the strain-induced transformations. They further claim that the transformation above M_s^σ in Fig. 1 is a strain-induced transformation in their rigorous terminology. However, Tamura and Onodera[10] reported to have obtained experimental results opposing the Olson-Cohen's supposition. Since this is a delicate problem, we will not pursue it any further. See Refs.[9, 10] for further discussion.

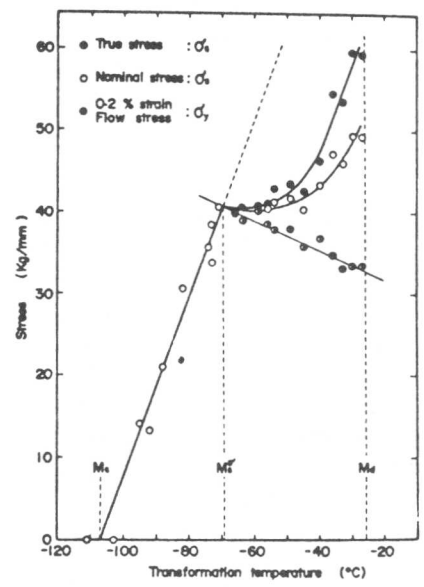

Fig. 1. Stress vs. martensitic transformation temperature in Fe-31.24wt.%Ni-0.21 wt.%C alloy (After Tokizane [35]).

In ferrous alloys such as stainless steels and Fe-Mn-C alloys in proper compositions, the formation of ε martensites and / or a plastic deformation always preceeds the $\gamma \rightarrow \alpha'$ transformation. More complications will arise in these alloys such as the negative temperature dependence of the critical stress to induce the α' martensite and the "window effect"[11]. These will not be discussed in the present paper. Thus, we will solely concern with the stress-induced transformations in the β phase alloys in the next section.

III. Stress-induced transformations and transformation pseudoelasticity.

3.1. Successive stress-induced transformations and phase diagrams.

One of the interesting findings in a recent few years is the successive stress-induced transformations in β phase alloys[12 - 15], as typically shown for a Cu-Al-Ni single crystal in Fig. 2[13]. The reaction occurring on each stage has been determined as indicated by neutron diffraction, x-ray diffraction and two-surface analysis. It has been found [12, 16 - 20] that the structures of the martensites are all long period stacking order structures with the common basal plane as shown in Fig. 2 of Ref.[17].

The unit cells of these martensites have been found to be all monoclinic. The monoclinicity originates partly from the deviation of the stacking positions from the ideal ones and partly from the elastic deformation of martensites under stress. See Ref.[17, 20] to be presented at this symposium for the details of the structure analysis of stress-induced martensites.

By plotting the critical stresses as a

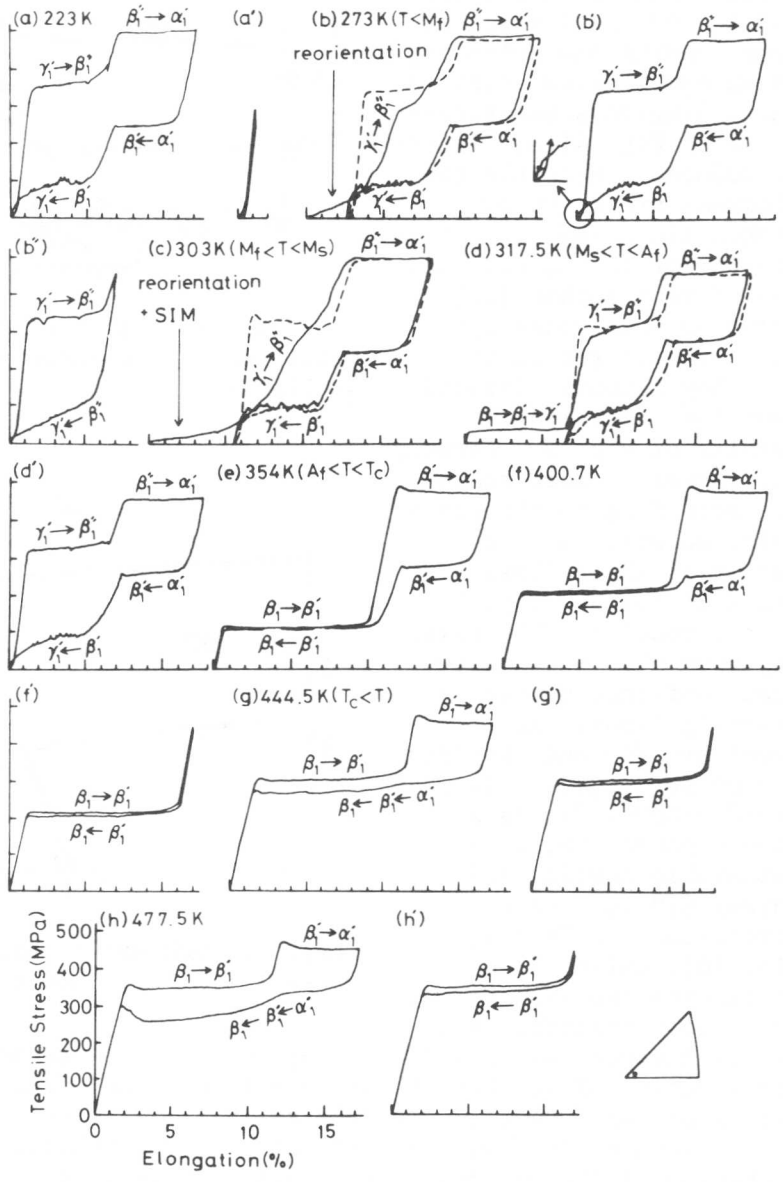

Fig. 2. Stress-strain curves as a function of temperature in a Cu-14.0wt.%Al-4.2wt.%Ni single crystal. Dotted lines in (b), (c) and (d) represent the S-S curves in the second cycle. (a) (b')(b") and (d') are the S-S curves obtained from the stress-induced γ_1' single variant martensite.

function of temperature, we obtain the curves shown in Fig. 3[13]. Since the hysteresis associated with each transformation is very large, the curves are quite complicated. But if one takes a mid-point between the two critical stresses upon loading and unloading as an equilibrium point, a phase diagram schematically shown in Fig. 4[13, 21] may be deduced. Here the two diagrams are drawn by broken lines and full lines. The former is the one which the present authors[12] proposed some years ago, while the latter is the one they recently deduced from the experimental results of Fig. 3. Although the former is more reasonable according to the phase rule, we will use the latter in the following, since it follows experimental results. The following comments, which have been confirmed by further investigations, may be necessary for understanding the phase diagram. In phase field O_1CDO_2, β_1' is a stable phase, while β_1'' a metastable one[13, 21]. Anyway β_1'' is always stress-induced from γ_1' [18, 16], while β_1' is stress-induced from β_1[17, 22]. Both transform into α_1' by further loading[12, 17, 19], but the α_1' transforms back to β_1' irrespective of whether it has been transformed from β_1'' or β_1'[17, 19, 21], indicating that β_1' is stabler than β_1''. The reason why β_1'' is stress-induced from γ_1' in spite of its metastability is that the mechanism of the $\gamma_1' \rightarrow \beta_1''$ transformation is more favorable than that of the $\gamma_1' \rightarrow \beta_1'$ transformation under an uniaxially stressed condition [13]. The β_1' phase in the phase field O_2EFG is also a metastable phase, which appears due to the lack of direct transformation mechanism between β_1 and α_1'[13]. Based on the phase diagram, all the stress-strain curves in Fig. 2 can be consistently explained.

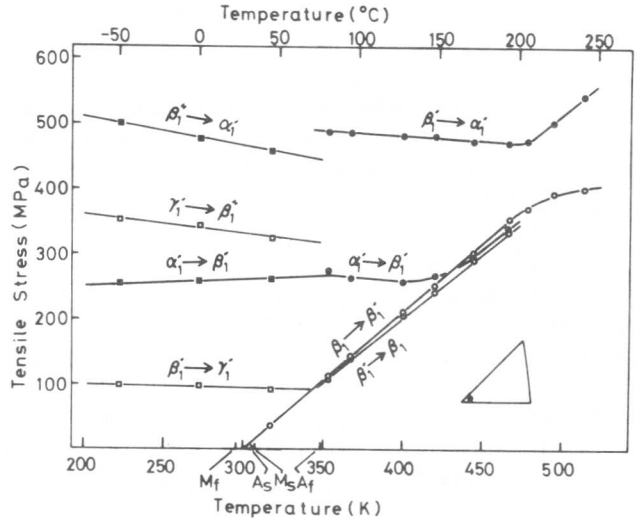

Fig. 3. Critical stress vs. temperature plots for each transformation indicated in Fig. 2.

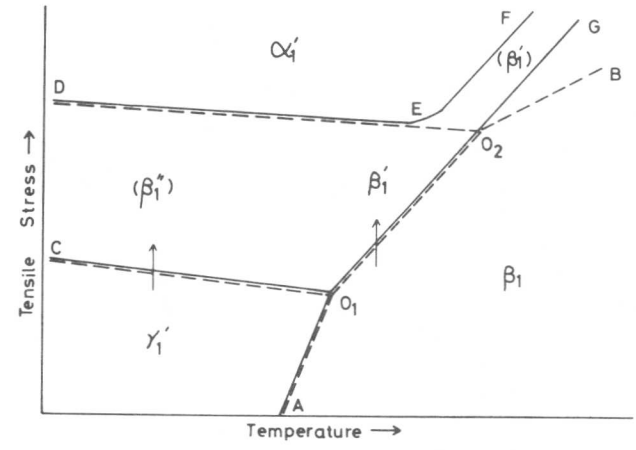

Fig. 4. Schematic phase diagram of a Cu-Al-Ni alloy. See text for details.

We believe Fig. 4 is a prototype of the phase diagram in temper-

ature-stress coordinates in β phase alloys. In fact similar but somewhat different phase diagrams have been proposed in other β phase alloys such as Cu-Zn[14], Cu-Zn-Al[23] and Au-Ag-Cd[15] alloys.

3.2. Characteristics of martensite-to-martensite transformations.

In martensite-to-martensite transformations[24 - 26, 12 - 20] there are some characteristics which are quite distinct from those in usual matrix-to-martensite transformations. Firstly the structural change is very simple, since it is described by a change in stacking sequence alone. Recent studies by neutron diffraction showed that lattice parameters changed linearly even among different martensitic structures[17]. This means that the lattice distorsions are negligible during a transformation under a constant stress. Lattice invariant shears are usually absent except for the $\beta_1'' \rightarrow \gamma_1'$ (or $\beta_1' \rightarrow \gamma_1'$) transformation, since the common basal plane itself is a habit plane[13]. Secondly the number of possible variants in martensite-to-martensite transformations are only two, since the common basal plane is unique and the shear directions are allowed only in the two directions (depending upon tension and compression respectively.). This is quite distinct from the familiar 24 variants in matrix-to-martensite transformations. Because of this, there is a strong orientation dependence on the realization of martensite-to-martensite transformations. That is, martensite-to-martensite transformations or successive stress-induced transformations in Cu-Al-Ni alloys can be realized only in single crystals with such orientations as in the close vicinity of $<001>_{\beta_1}$. This strong orientation dependence has been rationalized[13]. Thirdly the reverse transformations are sometimes not reversible. For example, the transformations on the first stage and the second stage in Fig. 2(b') are irreversible, but the strains completely recover during unloading. The reason for such a recovery will be explained in Section 3.5. The $\gamma_1' \rightleftarrows \beta_1''$ transformation (Fig. 2(b'')) is interesting. It is reversible structure-wise, but the transformation process is not reversible as shown in Fig. 5. The $\gamma_1' \rightarrow \beta_1''$ transformation upon loading proceeds with the habit plane $(001)_{\gamma_1'}$ without introducing any lattice invariant shear, while the $\beta_1'' \rightarrow \gamma_1'$ transformation upon unloading always proceeds by introducing $(\bar{1}01)_{\gamma_1'}$ twins in the γ_1' martensite and the habit plane thus deviates from the $(001)_{\gamma_1'}$. This irreversibility is unique, and the transformation is discussed more in detail in the next section.

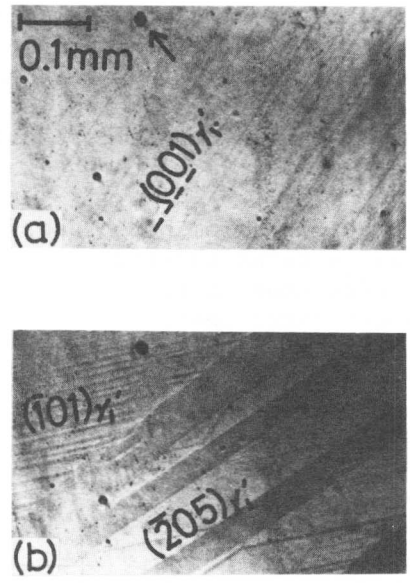

Fig. 5. Optical micrographs indicating the irreversible nature of the transformation process in the $\gamma_1' \rightleftarrows \beta_1''$ transformation in Cu-Al-Ni alloys. (a) the $\gamma_1' \rightarrow \beta_1''$ transformation upon loading, and (b) the $\beta_1'' \rightarrow \gamma_1'$ transformation upon unloading.

3.3. Phenomenological theoretical analysis of the $\beta_1'' \rightarrow \gamma_1'$ transformation.

The $\beta_1'' \rightarrow \gamma_1'$ transformation upon unloading in Cu-Al-Ni alloys is of interest from the following two respects. Firstly it provides a special case in phenomenological theoretical considerations. Secondly it provides a case where the lattice invariant shear is introduced by a source other than the invariant plane condition.

The phenomenological theoretical analysis of this transformation has been carried out based on the W-L-R theory. As seen from Fig. 2 of Ref.[17], the lattice distorsion is described by a shear on $(001)_{\beta_1''}$ plane in $[100]_{\beta_1''}$ direction. The lattice invariant shear is the twinning on $(\bar{1}01)_{\gamma_1'}$ plane in $[101]_{\gamma_1'}$ direction. Since both operations are simple shear, an invariant line, which is the intersection of the $(001)_{\beta_1''}$ plane and $(\bar{1}01)_{\gamma_1'}$ plane, is always present. In other words the solutions of the phenomenological theory are present for any value of the parameter x, a relative twin width, and the invariant plane condition is always satisfied. This is quite distinct from the ordinary case of matrix-to-martensite transformations, where the solutions are present only for a particular value of x. The result of the numerical calculations is shown in Fig. 6. The observed habit planes were found to be pretty close to one of the two solutions for x = 1. The magnitude of the shape strain was found to increase with increasing x. Since the invariant plane condition is satisfied and the shape strain is minimum for x = 0, the introduction of $(\bar{1}01)_{\gamma_1'}$ twins during the transformation cannot be ascribed to the invariant plane condition. We believe this is due to the Le Chatelier principle as follows.

We know from both theory and experiments that the introduction of $(\bar{1}01)_{\gamma_1'}$ twins shorten the specimens in the present experimental conditions. Thus the stress will go up if the $(\bar{1}01)_{\gamma_1'}$ twins are introduced in the γ_1' martensite. Now let us consider the situation where we start unloading from higher stress level in the β_1'' phase. If the $(\bar{1}01)_{\gamma_1'}$ twins are introduced in the $\beta_1'' \rightarrow \gamma_1'$ transformation, the transformation will start from a higher stress level than the case without the twins. This is in accord with the Le Chatelier principle.

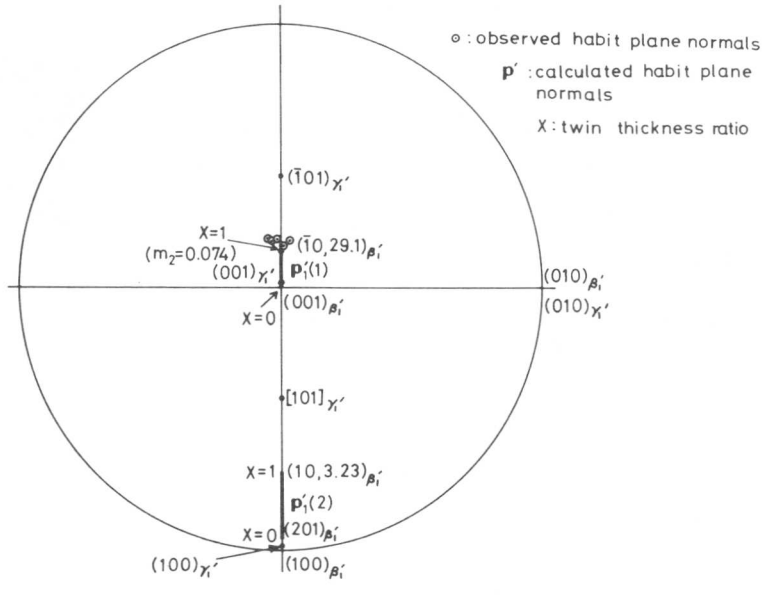

Fig. 6. The results of the phenomenological theoretical calculations for the $\beta_1'' \rightarrow \gamma_1'$ transformation.

By the same argument, the $\gamma_1' \rightarrow \beta_1''$ transformation upon loading will start from a higher stress level if the twins are introduced, but this will violate the Le Chatelier principle. This is the reason why the $(\bar{1}01)_{\gamma_1'}$ twins are not introduced in the $\gamma_1' \rightarrow \beta_1''$ transformation upon loading. Thus, the twinning behavior in the $\gamma_1' \rightleftarrows \beta_1''$ transformation has been rationalized by the Le Chatelier principle.

3.4. Transformation pseudoelasticity.

Various pseudoelastic loops are shown in a series of stress-strain curves in Fig. 2. As described in the figure, all the pseudoelastic behavior is due to the stress-induced martensitic transformations and their reversions. This type of pseudoelasticity has been termed the transformation pseudoelasticity [13]. The driving force for the pseudoelastic behavior is clear from Fig. 4. It is the free energy diffrence of two phases concerned as a function of stress. The recovery of strain during unloading is due to the reversible nature of the transformation of concern, which essentially originates from the ordered structures. In case where the transformation is not reversible as in Fig. 2(b'), a transformation mechanism to account for it will be presented in the next section.

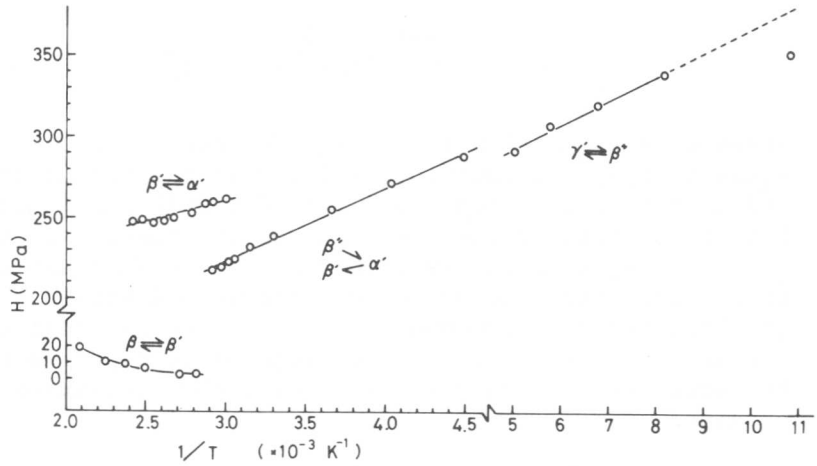

Fig. 7. Temperature dependence of the hysteresis (H vs. 1/T plot) for various transformations in Fig. 2.

The pseudoelastic strains as a function of crystal orientations have been calculated for various transformations using the values of the shape strains calculated from the phenomenological theory. Generally speaking, good agreements have been found between calculated and observed values except for details[5, 13].

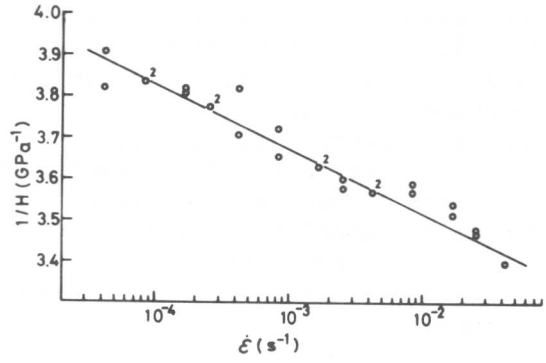

Fig. 8. Strain rate dependence of the hysteresis (1/H vs. $\ell_n \dot{\varepsilon}$ plot) for the $\gamma_1' \rightleftarrows \beta_1''$ transformation in a Cu-14.1wt.%Al-4.2wt.%Ni single crystal.

The effect of temperature and strain rate on the hysteresis of pseudoelastic loops have been measured for various transfor-

mations[13, 27, 28] as typically shown in Figs. 7 and 8[13]. Thus, linear relationships with positive slopes have been found between hysteresis (H) and 1/T, except for the case of the $\beta_1 \rightleftarrows \beta_1'$ transformation. Similarly a linear relationship has been found between strain rate ($\dot{\varepsilon}$) and 1/H. In order to understand these behavior, it is useful to introduce the notion of the effective stress (τ_{eff}) defined as the sum of external stress and chemical stress, which is schematically shown for the $\beta_1 \rightleftarrows \gamma_1'$ transformation in Fig. 9[27]. If the surface dislocation theory, which has originally been developed by Sumino[29] to account for the growth kinetics of the deformation twinning, is applied to the stress-induced transformation, one obtains the following equations[30],

$$U = \alpha A \pi t \left(\frac{Gt}{4\pi(1 - \nu)}\right)^2 \frac{1}{\tau_{eff}} \qquad (3.1.)$$

$$\ell n\, \dot{\varepsilon} = \ell n\, \dot{\varepsilon}_1 - \frac{\alpha^2 A \pi t}{kT} \left(\frac{Gt}{4\pi(1 - \nu)}\right)^2 \frac{1}{\tau_{eff}} \qquad (3.2.)$$

where U is the activation energy for the process, α a constant nearly equal to 5/6, A a function of the critical radius of a step ring (r_c) and a half of the step width (ζ), G a bulk shear modulus, ν the Poisson's ratio, t the magnitude of the Burgers vector of the surface dislocation, $\dot{\varepsilon}_1$ a constant term and k the Boltzman constant. It is easily seen that the above temperature and strain rate dependence of the hysteresis of pseudoelastic loops are rationalized by eq. (3.2.). Furthermore, by measuring the slope of an experimentally obtained hysteresis-strain rate relationship, the activation energy U can be obtained.

The heat of transformation (ΔH) or the entropy of transformation (ΔS) may be obtained from the Clausius-Clapeyron equation by measuring the slopes of σ vs. T curves in Fig. 3, and the result is shown in Table 1[13]. The comparison of these values with those of the corresponding hysteres in Fig. 2 is of quite interest. It is to be noted that in martensite-to-martensite transformations ΔH is very small but the hysteresis is large, while that in the $\beta_1 \rightleftarrows \beta_1'$ transformation ΔH is relatively large but the hysteresis is very small. This result clearly shows that the amout of hysteresis has nothing to do with ΔH, as excepted. Since all the long period stacking order structures have the same internal energy when nearest neighbor interactions alone are taken into account, ΔH is expected to be small in martensite-to-martensite transformations. However, such expectation cannot be held on their hystereses, since the latter represent nucleation barriers in respective transformations.

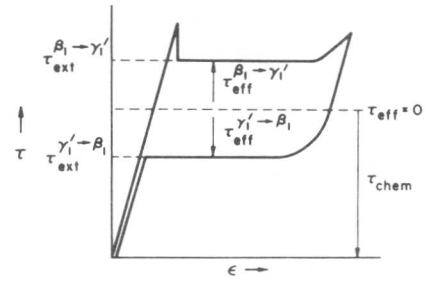

Fig. 9. Definition of an effective stress.

3.5. Mechanism of martensite-to-martensite transformations.

Since the structural changes in martensite-to-martensite transformations

Table 1. The entropy (and enthalpy) of transformation calculated from the Clausius-Clapeyron equation.

Kind of transformation	$\frac{d\sigma}{dT}$ (MPa/K)	ε_o	ΔS (J/mol•K)	ΔH (J/mol)	ΔH (cal/mol)	T (K)
$\gamma_1' \rightleftarrows \beta_1''$	-0.206	0.056	0.086	17.3	4.1	200
$\beta_1' \rightleftarrows \alpha_1'$	-0.139	0.112	0.117	46.7	11.2	400
$\beta_1'' \rightarrow \alpha_1'$, $\beta_1' \leftarrow \alpha_1'$	-0.174	0.145	0.145	36.4	8.7	250
$\beta_1 \rightleftarrows \beta_1'$	2.04	0.085	-1.30	-389	-93.0	300

are so simple, the transformation mechanism in this type of transformations will be of particular interest from theoretical point of view also.

Fig. 10 shows the structural changes when the γ_1' martensite is loaded and unloaded[13]. It is easily seen that these structural changes can be accomplished by the regular slips by partial dislocations with Burgers vectors $b = \pm a/3[100]_{\gamma_1'} = \pm a/3[100]_{\beta_1''}$ etc. as indicated by arrows. Thus, the transformations can be described by successive nucleation of these partial dislocations and their subsequent expansions. We believe from the following evidence that it is not only a formal mechanism but an actual mechanism[13].

Firstly the pseudoelastic behavior is easily explained by contraction or renucleation of these dislocations. Since stacking faults are inevitably associated with the partial dislocations, the cross slip leading to dislocation interactions, which will hinder the strain recovery, will be avoided. The reason why the strain recovers even in irreversible transformations such as the $\beta_1'' \rightarrow \alpha_1'$ transformation upon loading and the $\alpha_1' \rightarrow \beta_1'$ transformation upon unloading (Fig. 3(b')) is easily seen from Fig. 10(b) and (c). That is, the two slips every six layers in (b) is just cancelled by the two slips in opposite direction in (c) as an averaged shear.

Secondly the strain attained on each stage in Fig. 2 has been found to be consistent with that calculated from the above mechanism.

Thirdly the observed habit planes $(001)_{\gamma_1'}$, $(001)_{\beta_1''}$ etc. are consistent with the above

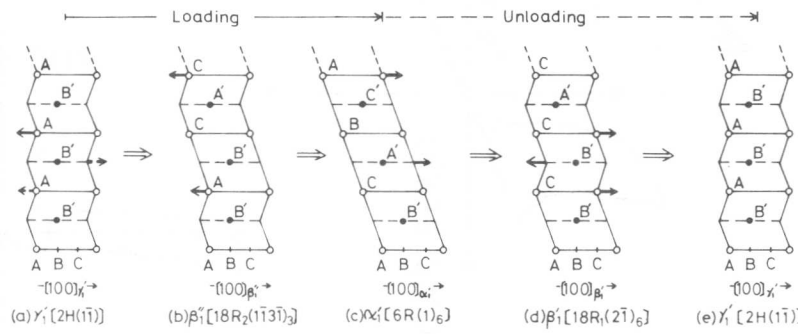

Fig. 10. A mechanism of successive transformations. $\gamma_1' \rightarrow \beta_1'' \rightarrow \alpha_1'$ upon loading and $\alpha_1' \rightarrow \beta_1' \rightarrow \gamma_1'$ upon unloading. Arrows indicate necessary slips to produce the subsequent structure.

mechanism. As noted above, the observed habit plane is different from the basal plane in the $\beta_1'' \rightarrow \gamma_1'$ transformation. This is because the $(\bar{1}01)_{\gamma_1'}$ twins are introduced in this particular transformation.

In the fourth place one may argue the possibility of nucleating partial dislocation loops. The activation energy for such a process can be estimated from eqs. (3.1.) and (3.2.) by inserting the observed value for the slope in eq. (3.2.). The estimated value was roughly 1.1 eV, which was not an unrealistic value for the nucleation of such loops by thermal activation.

3.6. Effect of sense of stress on stress-induced transformations.

In order to see the effect of sense of stress on stress-induced transformations, tension-compression tests have been carried out rather extensively in Cu-Al-Ni alloys. Two typical stress-strain curves are shown in Fig. 11, which have been taken at a temperature above A_f and below M_f respectively. Asymmetric nature is most notable in both of the curves. Previously a stress-strain curve somewhat similar to Fig. 11(a) has been obtained in a Au-Cd alloy by Miura et al.[31] and it has been attributed to different variants of the martensite stress-induced on tension and compression sides. However, it was confirmed in the present study that it was due to the different martensitic transformations on both sides. That is, the $\beta_1 \rightleftarrows \beta_1'$ transformation on tension side and the $\beta_1 \rightleftarrows \gamma_1'$ transformation on compression side. We believe this behavior originates from the non-uniaxiality in compression test.

The asymmetric behavior at temperatures below M_f (B) is due to the difference in deformation modes on tension and compression. It is confirmed that the pseudoelastic behavior on a tension side is due to the $\gamma_1' \rightleftarrows \beta_1''$ transformation, while that the deformation on a compression

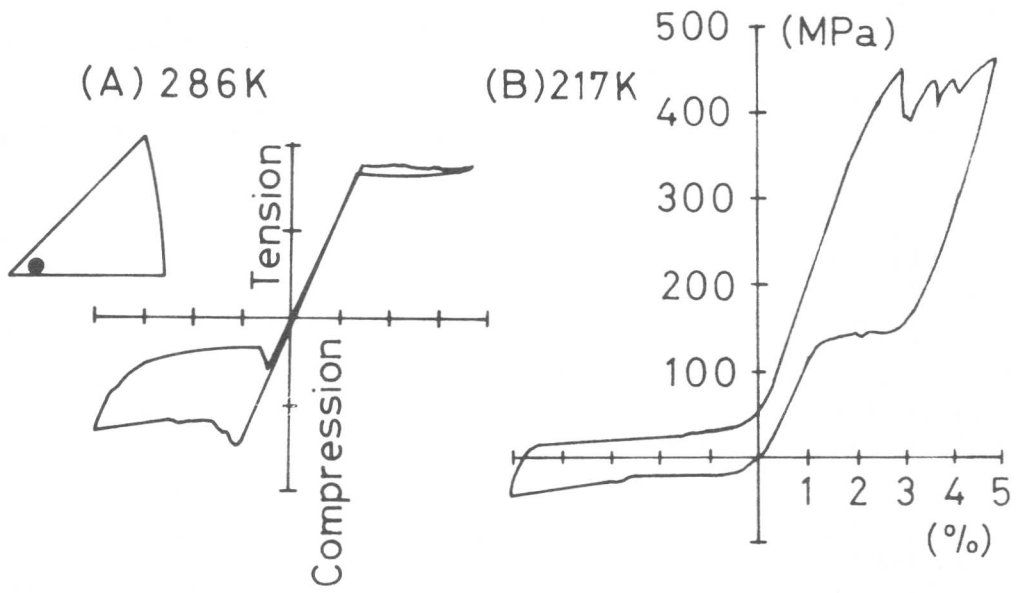

Fig. 11. Typical stress-strain curves in tension-compression tests in a Cu-14.3wt.%Al-4.2wt.%Ni single crystal. M_s = 242K, M_f = 226K, A_s = 250K and A_f = 276K.

side is due to a twinning in the γ_1' martensite. This asymmetry in deformation mode is what is expected from the low symmetry of the martensite. For further details see Ref. [32] to be presented at this conference.

3.7. The shear system which interacts with an applied stress.

It seems established that the Schmid law usually holds in the selection of a variant of the stress-induced martensite[5]. Furthermore it is generally accepted in β phase alloys that the shear system interacting with an applied stress is the shape strain[13, 27, 33]. However, Kato and Mori[34] reported that in stainless steels the interacting shear system was not the shape strain but that the $\{111\}\langle\bar{2}11\rangle_f$ shear originating from the Bogers-Burgers mechanism. This could mean that the interacting shear system in the nucleation stage may be different from the shape strain, as they suggested. Meanwhile it is known in 18-8 stainless steels that the formation of the ε martensite preceeds that of the α' [11]. If that is the case, the formation of the α' phase is not determined solely by the applied stress and the result is not quite reliable. This point is not quite unambiguous.

Acknowledgments

The authors are grateful to Mr. H. Sakamoto and Professor M. Tokonami for useful discussions and collaborations for some of the work included in this paper.

References

[1] E. Scheil: Z. Anorg. Chem., 207(1932)21.
[2] J. R. Patel and M. Cohen: Acta Met., 1 (1953)531.
[3] M. W. Burkart and T. A. Read: Trans. AIME, 197(1953)1516.
[4] L. Delaey, R. V. Krishnan, H. Tas and H. Warlimont: J. Mat. Sci., 9(1974)1521, 1536, 1545.
[5] K. Otsuka and C. M. Wayman: in Reviews on the Deformation Behavior of Materials (P. Feltham, Ed.), Freund Publishing House Ltd., Israel, (1977)vol. II, No.2, p.81.
[6] I. Tamura, T. Maki and H. Hato: Trans. ISIJ, 10(1970)163.
[7] P. C. Maxwell, A. Goldberg and J. C. Shyne: Met. Trans., 5(1974) 1305.
[8] G. B. Olson and M. Cohen: J. Less Common Metals, 28(1972)107.
[9] M. Cohen: Proc. ICOMAT 1977, Kiev, p.69.
[10] I. Tamura and H. Onodera: this conference.
[11] T. Suzuki, H. Kojima, K. Suzuki, T. Hashimoto and M. Ichihara: Acta Met., 25(1977)1151.
[12] K. Otsuka, H. Sakamoto and K. Shimizu: Scripta Met., 10(1976)983.
[13] K. Otsuka, H. Sakamoto and K. Shimizu: Acta Met., in press.
[14] T. A. Schroeder and C. M. Wayman: Acta Met., 26(1978)1745.
[15] S. Miura, M. Ito, F. Hori and N. Nakanishi: Proc. 1st JIM Int. Symp., Suppl. Trans. JIM (1976)p.257.
[16] K. Otsuka, M. Tokonami, K. Shimizu, Y. Iwata and I. Shibuya: Acta Met., in press.
[17] M. Tokonami, K. Otsuka, K. Shimizu, Y. Iwata and I. Shibuya: this conference.

[18] V. V. Martynov and L. G. Khandros: Dokll. Acad. Nauk SSSR, 233 (1977)345.
[19] V. V. Martynov and L. G. Khandros: Dokll. Acak. Nauk SSSR, 237 (1977)1349.
[20] L. G. Khandros and V. V. Martynov: this conference.
[21] K. Shimizu, H. Sakamoto and K. Otsuka: Scripta Met., 12(1978)771.
[22] K. Otsuka, T. Nakamura and K. Shimizu: Trans. JIM, 15(1974)200.
[23] L. Delaey et al.: private communication (1978).
[24] H. Tas, L. Delaey and A. Deruyttere: Scripta Met.,5(1971)1117.
[25] K. Otsuka, H. Sakamoto and K. Shimizu: Shape Memory Effects in Alloys(J. Perkins, Ed.) Plenum Press, (1975), p.327.
[26] C. Rodriguez and L. C. Brown: Met. Trans., 7A(1976)265.
[27] K. Otsuka, C. M. Wayman, K. Nakai, H. Sakamoto and K. Shimizu: Acta Met., 24(1976)207.
[28] J. Van Humbeeck, L. Delaey and A. Deruyttere: Z. Metall., 69 (1978)575.
[29] K. Sumino: Acta Met., 14(1966)1607.
[30] K. Sumino and M. Suezawa: unpublished work (1976). Cited in Ref.[13].
[31] N. Nakanishi, T. Mori, S. Miura, Y. Murakami and S. Kachi: Phil. Mag., 28(1973)227.
[32] H. Sakamoto, M. Tanigawa, K. Otsuka and K. Shimizu: this conference.
[33] T. Saburi, S. Nenno, J. Hasunuma and H. Takii: Proc. 1st JIM Int. Symp. Suppl. Trans. JIM., (1976)p.251.
[34] M. Kato and T. Mori: Proc. 1st JIM Int. Symp. Suppl. Trans. JIM, (1976)p.333.
[35] M. Tokizane: Proc. 1st JIM Int. Symp. Suppl. Trans. JIM., (1976) p.345.

Shape Memory Mechanisms in Alloys

T. Saburi*, S. Nenno* and C. M. Wayman**

Through studies of the shape memory effect in numerous martensitic materials (2H, 3R, 9R and 18R), a generalized explanation of the deformation behavior and subsequent shape recovery process is now possible, even though the martensites are both internally twinned and faulted and possess different crystal structures. In all cases, an initial parent single crystal forms self-accommodating arrangements of martensite variants (plates) characterized by six groups, each consisting of four variants, the average shape strain in each group being essentially zero. For 9R and 18R martensites each variant is a single crystal; the 3R martensite is composed of two orientations, twin-related with respect to a twin plane parallel to the basal (stacking) plane; the 2H martensite features a twin plane inclined to the basal plane.

On stressing below M_f these materials deform by detwinning (2H, 3R only), variant-variant coalescence and twinning processes and further group-to-group coalescence, eventually attaining a single crystal of martensite consisting of that particular variant whose shape strain involves maximum extension in the direction of the applied stress. The deformed martensite persists upon unloading; reverse rearrangements of twins and variants do not occur. The materials regain their initial shape upon heating from A_s to A_f, during which the single crystal of martensite attained by stressing the as-transformed 24-variant configuration transforms back to the original parent phase single crystal in a unique manner. Films demonstrating these mechanisms and the generality of the shape memory effect have been made.

I. Introduction

Although the shape memory effect [1-3] is now a popular phenomenon, the mechanistic understanding of this effect is still incomplete. This is mainly due to insufficient available knowledge on the deformation and recovery processes. In view of this, our recent studies have been focused on detailed observations and crystallographic analysis of the deformation and recovery processes in memory alloys [4-7].

It is generally recognized that the shape memory effect is associated with a thermoelastic martensitic transformation [1]. Another important "selection rule" for memory alloys is that they are ordered [1] (InTl alloys are an exception). Further, the memory martensite structures are of a periodic stacking (3R, 6R, 9R, 18R and 2H)

---

* Osaka University, Osaka, Japan.
** University of Illinois at Urbana-Champaign, Urbana, Illinois 61801

transformed from a B2 or DO_3 ordered parent structure. Also there are many morphological similarities among these memory alloys [5]. Noting these similarities, in this paper we will attempt a generalized explanation of the shape memory mechanisms operative in these martensitic alloys with a periodic stacking structure.

II. Variant Structure in As-formed Martensite

(1) Lattice correspondence

Based on the experimentally observed parent-martensite orientation relationships [8-11], it is now widely believed that in 9R(18R), 2H and 3R(6R) martensites the basal (stacking) plane originates from one of the parent close packed {110} planes. Because of this close relationship between the parent {110} planes and the martensite basal planes, the crystallographic features of the transformations are conveniently described with reference to the parent {110} planes. Figure 1 illustrates the structural changes from a DO_3 ordered parent phase (β_1-A_cB_c) to 6R(α_1'-AB'CA'BC'), 18R(β_1'-AB'CB'CA'CA'BA'BC'BC'AC'AB') and 2H(γ_1'-AB') martensites [12]. Figure 2 is a similar illustration for transformations from a B2 parent (β_1-A_cB_c) to 3R(α_1'-ABC), 9R(β_1'-ABCBCACAB) and 2H(γ_1'-AB) martensites. If we ignore ordering, the 3R and 6R (and also 9R and 18R) are identical in stacking sequence. Therefore, for simplicity we describe only the B2 cases. Three-dimensionally speaking, in any of the cases, 9R, 3R and 2H, one way to describe the structural change on transformation, Fig. 3,* involves i) a homogeneous distortion (expansion along $[011]_{B2}$, contraction along $[100]_{B2}$ and expansion along $[0\bar{1}1]_{B2}$) and ii) a combination of elementary shears in opposite directions, [011] and $[0\bar{1}\bar{1}]$, between two adjacent close-packed planes [12,13]. The homogeneous distortion i) is common for all transformations from B2 to 3R, 9R and 2H, and different combinations of the elementary shears, ii) yield the different martensite structures, 3R, 9R and 2H. The various situations are shown in Fig. 4(a)-(f). Figure 4(a) illustrates the stacking order of the parent $(0\bar{1}1)_{B2}$ plane. The relative displacement between two adjacent planes is $(1/2)(\sqrt{2}a_o)$. If the lattice is sheared on $(0\bar{1}1)_{B2}$ and in the $[0\bar{1}\bar{1}]_{B2}$ direction uniformly** until the relative displacement between two adjacent planes becomes (1/3)a (or (2/3)a)†, a 3R(ABC) structure results (Fig. 4(b)). An equivalent structure is obtained by shearing in the [011] direction, Fig. 4(c), and this is twin-related to that of Fig. 4(b). The actual relative shift taking place between two adjacent planes during transformation is -(1/6)a or (1/6)a (arrows XA_1' and XA_2' in Fig. 3(b)-(c)).†† Since there are six {110} planes,

---

* Although illustrated for the particular case of the $(0\bar{1}1)_{B2}$ plane, equivalent structure changes are similarly possible for the other five $\{110\}_{B2}$ planes.

** As mentioned previously, there is a simultaneous expansion δ_1 along [011] and thus $\sqrt{2}a_o + \delta_1 = a$.

† Strictly, not exactly 1/3.

†† Assuming the shear to occur after the expansion, $(1/3 - 1/2)a = -1/6\ a$ and $(1/2 - 1/3)a = 1/6\ a$.

there are twelve possible combinations of stacking plane and shear direction. These twelve combinations give the possible lattice correspondences in the B2-3R transformation. These are designated as shown in Table I, where the numerals 1-6 specify the parent close-packed planes which generate the martensite basal planes. If the -(1/6)a and (1/6)a shears are combined in a two-to-one sequence, a 9R structure (ABCBCACAB) shown in Fig. 4(d) is obtained. On the other hand, with a one-to-two sequence another 9R stacking (ACBCBABAC) Fig. 4(e) is obtained. This is structurally equivalent and twin-related to that of Fig. 4(d) with respect to their common basal planes. Similar to the 3R case, the twelve correspondences shown in Table I also hold for the B2-9R transformation.

If the -(1/6)a and (1/6)a shears take place in an alternate manner, a 2H structure (AB.. or AC..) shown in Fig. 4(f) results. In this case there is no overall shear since the opposite elementary shears occur alternatively. Therefore, crystallographically there is no difference between two correspondences with and without a prime symbol (for example, 1 and 1′). Thus there are only six lattice correspondences (1-6) for the B2-2H transformation.

(2) Inhomogeneous transformation shear and structure of a martensite plate

In general a homogeneous lattice distortion alone does not satisfy the crystallographic requirement for an invariant (unrotated and undistorted) habit plane and a specific inhomogeneous shear is needed besides the homogeneous lattice distortion. For a 3R martensite plate this shear is provided by a combination of the two opposite shears in Fig. 4(b) and (c). The two structures obtained (with correspondences 1 and 1′) are in a twin relation with respect to the basal plane and thus the variant is composed of thin twin crystals [14,15]. This variant is designated as 11′ ("matrix" regions of correspondence 1 and "twin" regions of correspondence 1′).* Another combination 1′1 ("matrix" regions of correspondence 1′ and "twin" regions of correspondence 1) also provides the required shear but this is in the opposite direction to that of 11′. In this manner, 12 combinations of twin-related correspondences are possible, and for each of these there are two different but crystallographically equivalent invariant habit planes. We differentiate between these two situations by using plus and minus signs. Thus there are 24 martensite variants, 11′(+), 11′(-), 1′1(+), ... which can occur.

For a 9R martensite plate the inhomogeneous shear provides the structure itself (ABCBCACAB), with the exact invariant plane condition being adjusted by occasional "random" stacking faults [13]. Thus each variant plate is a single crystal, apart from the stacking faults. Each of the 12 correspondences in Table I yields two variants, each of which has a crystallographically equivalent but different habit plane. Thus, like the 3R case, 24 variants also occur in the 9R structure and these are designated 1(+), 1(-), 1′(+), ... 6′(-).

---

*e.g., the matrix-twin ratio is about 2:1 in Ni-Al martensite [15].

For a 2H martensite plate the inhomogeneous shear is provided by twinning on $\{111\}_{2H(B2)}$ [10] ($\{121\}_{2H(DO_3)}$ [9]).* This twin plane is not the martensite basal plane, although it is also derived from one of the $\{110\}_{B2}$ planes. Thus a variant plate of 2H martensite is composed of twin lamellae but the twin structure is different from that of a 3R martensite plate. The twin structure in a 2H plate is also conveniently described using the 6 correspondences in Table I. For example, correspondences 5 and 1 are twin-related with respect to $(101)_{B2}$ and combination of these two yields variant 5-1 ("matrix" regions of correspondence 5 and "twin" regions of correspondence 1). On the other hand, variant 1-5 is composed of "matrix" regions 1 and "twin" regions of 5. Since variants 5-1 and 1-5 differ in the twin-ratio, their habit planes are different (although crystallographically equivalent). Since 24 crystallographically equivalent combinations of correspondence are possible, 24 variants appear also in 2H martensite.

Thus, in any of the cases, 3R, 9R and 2H, all the single crystalline subunits which compose the bulk martensite have a one-to-one correspondence with the parent crystal. For 9R, each of the variant plates is a single crystal and is related uniquely to the parent crystal by one of the 12 correspondences. For 3R and 2H, each of the twin-related regions in a variant plate is a single crystal and has its own unique correspondence with the parent: one of the twelve in Table I for 3R and one of the six without a prime symbol for 2H.

(3) Self-accommodation

Although the 3R, 9R(18R) and 2H martensites are different (both in crystal structure and mode of inhomogeneous shear), a common feature is found in their variant grouping during transformation. That is, in all cases self-accommodation is achieved by forming variant groups (I-VI), each of which consists of four variants with habit plane normals clustered about one of the six {110} poles of the parent phase [4,5,15-17].** An example for all 24 variants is shown in Fig. 5 for a Cu-Zn-Ga alloy [6]. Further, in all cases four variants in a group always appear in a so-called "diamond" type morphology [4,5]. Therefore, the self-accommodating structures are visualized for convenience by referring to the parent close-packed planes. Fig. 6(a), (b) and (c) illustrate the self-accommodating diamond-like plate group configuration in Group IV for each of the 9R, 3R and 2H structures. The Group IV variants of 9R, Fig. 6(a), are 5′(-), 3(+), 4′(-) and 6(+) and there are specific relations among these. Referring to Fig. 6(d) which shows the crystallographic disposition of the parent close-packed plane poles, it is easily seen that variants 5′(-) and 3(+) (and 4′(-) and 6(+)) which form a "spear" pair are in twin relation with respect to the $(01\bar{1})_{B2}$ plane. Variants 5′(-) and 6(+) (and 3(+) and 4′(-)), which show a "fork" morphology, are in another

---

* 2H(B2): 2H transformed from B2, 2H(DO_3): 2H transformed from DO_3.

** The {011} "grouping" planes are not to be confused with the {011} planes which generate the stacking sequences or transformation twins.

twin relation with respect to $(100)_{B2}$. Further, variants 5'(-) and 4'(-) (and 3(+) and 6(+)) are twin-related with respect to $(011)_{B2}$. However, it is to be noted that the interface between 5'(-) and 4'(-) is not a twin plane (about 90° away from (011)) but is an "impingement" plane.

A Group IV diamond of 3R martensite is composed of 5'5(-), 33'(+), 66'(+) and 4'4(-), Fig. 6(b). Although each variant is composed of twins, the "matrix" regions have the lattice correspondences 5', 3, 6 and 4' with the parent and their relative arrangement is identical to that of the 9R martensite.

A Group IV diamond of 2H martensite is composed of 5-1, 3-1, 6-1 and 4-1, Fig. 6(c). Variants 5-1 and 3-1 (and 6-1 and 4-1) form a spear and variants 5-1 and 6-1 (and 3-1 and 4-1) show a fork morphology. The "matrix" regions of the four variants have the correspondences 5, 3, 6, and 4 with the parent and their relative arrangement is identical to those of 9R and 3R martensites (note that correspondences with and without prime symbols are identical in 2H). Similar to the 9R and 3R cases, "matrix" regions 5 and 3 (and 6 and 4) are twin-related with respect to $(01\bar{1})_{B2}$ and "matrix" regions 5 and 6 (and 3 and 4) are twin-related with respect to $(100)_{B2}$. Although "twin" regions of all the four variants have the same correspondence, 1, with the parent, their actual lattice orientations are slightly different from each other due to the rigid body rotation of the transformation [18].

For the other five groups, similar variant arrangements are found, as shown in Fig. 7. An important point about this diamond-like configuration is that the shape strains of the four variants in a particular group essentially cancel each other and thus the net shape change on transformation becomes nearly zero for the group [5,17,19]. This zero macroscopic shape change is important in the shape memory effect in that it enables the shape memory materials to deform under low stresses (substantially lower than that to move ordinary slip dislocations) by variant coalescence.

III. Deformation

Shape memory materials change their shapes on stressing by means of detwinning within each variant (internally twinned martensites), variant-to-variant coalescence in a group and further group-to-group coalescence [4,6,7,20-23]. Through these processes the materials attain a new variant arrangement where variants are most favorably disposed with respect to the applied stress. Typically under a tensile stress the final product is a single crystal of martensite of the particular variant which gives the largest extension in the direction of the applied stress. Examples are shown in Figs. 8(a),(b) and 9(a),(b) for 18R and 2H martensites, respectively [6,7]. The deformation processes to attain the single crystal state of martensite are different for each structure, and further, are different for each variant group, depending also on the relative arrangement of the groups involved.

(1) 9R(18R)

When a tensile stress is applied in a particular direction within the standard stereographic triangle (001-011-$\bar{1}$11), variant coalescence takes place as follows [6].

a) Groups I and II

1′, 2, 5, 6′ → 1′

In Groups I and II, both of which contain the 1′ variant,* the four variants coalesce to the 1′ variant (differentiation between 1′(+) and 1′(-) becomes meaningless after stress-induced variant coalescence).

b) Groups III and IV

3, 4′, 5′, 6 → 4′ → 1′

In Groups III and IV, the four variants coalesce first to variant 4′ which gives the largest extension in the group, and then 4′ changes to variant 1′ which gives the largest extension of all. The latter process, 4′ → 1′, is characterized by nucleation and growth of 1′ variant plates in the 4′ region and the surface traces of the plates are parallel to the (110) trace of the original parent. Since correspondences 4′ and 1′ are in twin relation with respect to the parent (110) plane, the process 4′ → 1′ is very likely to be twinning.

c) Groups V and VI

1, 2′, 3′, 4 → 1 → 1′

In Groups V and VI, the four variants coalesce first to variant 1, and then 1 changes to variant 1′ by twinning.

d) Groups I and III

3, 4′, 5′, 6 → 1′

The processes b) and c) above involve an intermediate stage where the most favorable variant in the group (4 and 1) initially dominates, and then yields the variant 1′. However, direct coalescence from Group III to the variant 1′ has also been observed. This happens when small regions of Group I are scattered within a large region of Group III; the variant 1′ in the Group I regions consumes the other three variants in the group and it also grows directly into the Group III region.

---

* The variant which gives the largest extension along the stress direction.

(2) 2H

For 2H martensites, the coalescence processes are somewhat different from the 9R(18R) case and more complex since each variant plate is composed of extremely thin twin-related crystals. Though some details of the coalescence processes for 2H are yet to be resolved, it has clearly been shown that detwinning in a variant plate and also variant-to-variant coalescence can occur easily under an applied stress [7]. The 2H-type behavior is expected to apply to TiNi alloys.

(3) 3R

Judging from the structural similarities to 9R(18R) and 2H martensites, it is expected that reorientation among 12 correspondences takes place easily.

The most important point concerning these deformation processes is that deformation is achieved by twinning and variant coalescence* rather than ordinary slip mechanisms. This enables the deformed materials to recover their original shape on heating.

IV. Shape Recovery

When the applied stress is released below the A_s temperature, the produced shape change remains since reverse rearrangement of twins and variants does not occur. However, upon heating through the A_s and A_f temperatures the materials regain their original shape by a reverse transformation from martensite to parent. A single crystal of martensite attained by tensile stressing the self-accommodating variants transforms back to the original single crystal state of the parent, Fig. 8(c)(d) and Fig. 9(c)(d). In 18R(9R) martensites, the reverse transformation takes place by nucleation and growth of thin plates of the parent, Fig. 8(d), and the habit plane is close to $(515)_{DO3}$ or $(\bar{5}15)_{DO3}$. As mentioned before, two habit planes are equivalently possible for each parent-martensite correspondence. When the variant 1′ transforms back to the parent, the two habit planes, $(515)_{DO3}$ and $(\bar{5}15)_{DO3}$ can occur. The obtained shape strains in the direction of the original applied stress (contraction) are identical for these two cases [6]. On the other hand, reverse transformation from a 2H martensite single crystal to the parent single crystal proceeds by the propagation of complex self-accommodating boundary regions as seen in Fig. 9(c). It is not crystallographically possible for a single crystal of a 2H martensite plate to have an unrotated and undistorted interface with respect to its parent, unlike the situation for 9R and 18R martensites. This explains the complex reverse transformation in interface regions in 2H.

---

* In essence, interchange from one correspondence to another.

Although no observation has yet been made for the 3R case, similar complex interfaces are also expected to form in this case for the same reason as for the 2H case. Although the reverse transformation processes are different for each structure, the end product is invariably the original parent single crystal in all cases. Thus the materials regain their original shape.

V. General Discussion

Although details are different for each shape memory material, the basic mechanisms and essential processes involved are common for all the materials. The four stages which involve the effect are schematically illustrated in Fig. 10.

On cooling, the parent single crystal transforms into many martensite variants in a self-accommodating manner. In all cases, six groups of four variants form from the parent, and the average shape strain (macroscopic net shape change) in each group becomes nearly zero as a result of the mutual cancellation of individual shape strains. Thus, the initial length L of the material does not change.

On stressing (tensile) below M_f, deformation (elongation) occurs by detwinning within a variant plate (2H and 3R only), variant-to-variant coalescence and then group-to-group coalescence. The end result is a single crystal of martensite with the particular correspondence whose shape strain involves the maximum extension in the direction of the applied stress. By this process the specimen is elongated from L to $L + \varepsilon$. The elongation ε depends on the structure and intrinsic shape strain of the martensite and also on the orientation of the parent lattice with respect to the applied stress.

On releasing the applied stress, the elongation (ε) remains since the reverse rearrangement of twins and variants does not occur.

On heating the single crystal of martensite, the reverse transformation to the parent phase takes place. Since the martensite single crystal has a unique lattice correspondence with the parent lattice, the retransformed parent is in exactly the same state as initially, and the original length L is again assumed. The importance of an ordered structure for a one-way reverse transformation has been discussed in references [1] and [24]. Although the processes metnioned here were deduced for a tensile stress essentially the same deformation processes by variant coalescence are expected for compression and bending.

As a necessary condition for the shape memory effect, it is often stated that the transformation must be reversible, where, typically speaking, the reverse transformation occurs by the shrinkage of plates which have nucleated and grown during the forward transformation. Although reversibility does apply, the operative processes in the memory effect are not reversible in that the forward and reverse paths are different. For example, the numerous variants of 9R martensite produced thermoelastically on cooling coalesce to a single

variant of 1′ under a tensile stress (forward path), which on heating transforms directly to the parent phase (reverse path). Color films demonstrating the various phenomena involved in the shape memory effect in 18R and 2H martensites have been produced.

Acknowledgements

This work was supported by the Division of Materials Research, National Science Foundation (USA), Grant DMR-77-00363, and the Ministry of Education of Japan.

REFERENCES

[1] C. M. Wayman and K. Shimizu, Metal Sci. J., 6(1972), 175.
[2] L. Delaey, R. V. Krishnan, H. Tas and H. Warlimont, J. Mat. Sci., 9(1974), 1521, 1536, 1545.
[3] J. Perkins (Editor), *Shape Memory Effects in Alloys*, Plenum Press, New York (1975).
[4] T. A. Schroeder and C. M. Wayman, Acta Met., 25(1977) 1375.
[5] T. Saburi and C. M. Wayman, submitted to Acta Met.
[6] T. Saburi, C. M. Wayman, K. Takata and S. Nenno, submitted to Acta Met.
[7] T. Saburi and C. M. Wayman, submitted to Acta Met.
[8] S. Sato and K. Takezawa, Trans. Japan Inst. Met., 9(1968), 925.
[9] K. Otsuka and K. Shimizu, Japan J. Appl. Phys., 8(1969), 1196.
[10] T. Tadaki, S. Hamada and K. Shimizu, Trans. Japan Inst. Metals, 18(1977), 135.
[11] S. Chakravorty and C. M. Wayman, Met. Trans., 7A(1976), 555.
[12] Z. Nishiyama and S. Kajiwara, Japan J. Appl. Phys., 2(1963), 478.
[13] T. Saburi and S. Nenno, Scripta Met., 9(1975), 887.
[14] K. Enami, S. Nenno and K. Shimizu, Trans. Japan Inst. Metals, 14(1973), 161.
[15] S. Chakravorty and C. M. Wayman, Met. Trans., 7A(1976), 569.
[16] H. Tas, L. Delaey and A. Deruyttere, Met. Trans., 4(1973), 2833.
[17] T. Saburi, S. Nenno, S. Kato and K. Takata, J. Less Common Metals, 50(1976), 223.
[18] K. Otsuka and K. Shimizu, Trans. Japan Inst. Metals, 15(1974), 103.
[19] J. De Vos, L. Delaey and E. Aernoudt, Z. Metall., 69(1978), 511.
[20] K. Otsuka, Japan J. Appl. Phys., 10(1071), 571.
[21] H. Tas, L. Delaey and A. Deruyttere, J. Less Common Metals, 28(1972), 141.
[22] H. Tas, L. Delaey and A. Deruyttere, Z. Metall., 64(1973), 862.
[23] L. Delaey and J. Thienel, p. 341, reference [3].
[24] K. Otsuka and K. Shimizu, Scripta Met., 11(1977), 757.

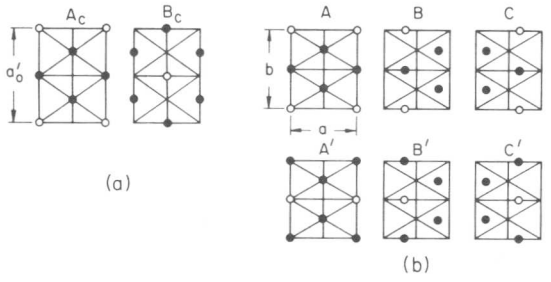

Fig. 1 Structural changes from DO_3 to 18R, 6R and 2H. (a) DO_3 $(0\bar{1}1)$: A_cB_c (b) martensite (001) 18R:AB'CB'CA'CA'BA'BC'BC'AC'AB', 6R:AB'CA'BC', 2H:AB'.

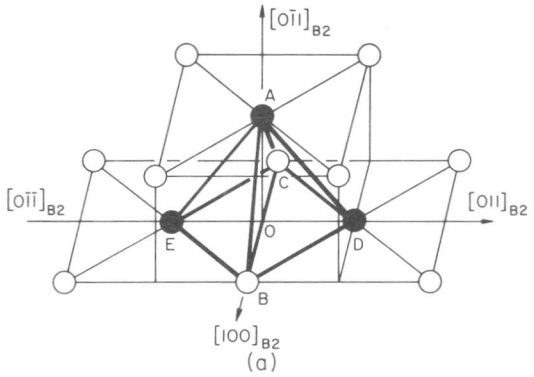

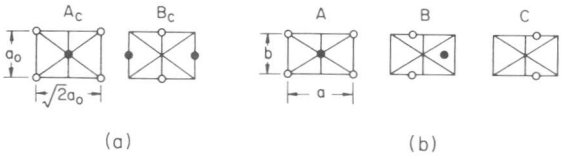

Fig. 2 Structural changes from B2 to 9R, 3R and 2H. (a) B2 $(0\bar{1}1)$: A_cB_c (b) martensite (001) 9R:ABCBCACAB, 3R:ABC, 2H:AB.

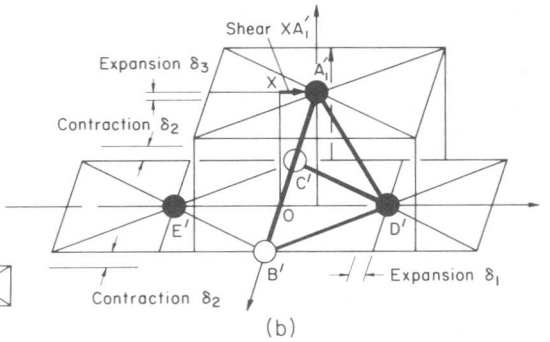

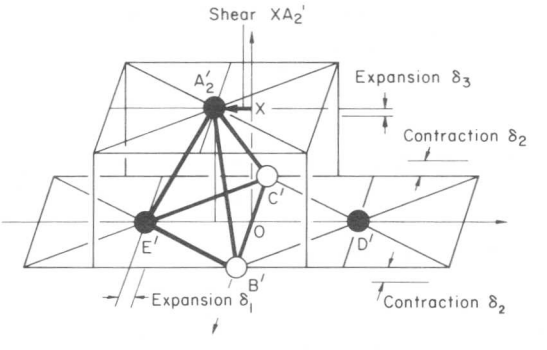

Fig. 3 Change in interatomic relations on transformation. (a) B2 (b) martensite, homogeneous distortion and shear XA_1' (c) martensite, homogeneous distortion and shear XA_2'

Table I Parent-Martensite Lattice Correspondences
P: Parent (B2, DO_3)
M: Martensite (3R, 9R, 18R, 2H)

	$[100]_M$	$[010]_M$	$(001)_M$
1	$[011]_P$	$[\bar{1}00]_P$	$(0\bar{1}1)_P$
1′	$[0\bar{1}\bar{1}]_P$	$[\bar{1}00]_P$	$(0\bar{1}1)_P$
2	$[0\bar{1}1]_P$	$[\bar{1}00]_P$	$(0\bar{1}\bar{1})_P$
2′	$[0\bar{1}1]_P$	$[\bar{1}00]_P$	$(011)_P$
3	$[101]_P$	$[0\bar{1}0]_P$	$(10\bar{1})_P$
3′	$[\bar{1}0\bar{1}]_P$	$[0\bar{1}0]_P$	$(10\bar{1})_P$
4	$[10\bar{1}]_P$	$[0\bar{1}0]_P$	$(\bar{1}0\bar{1})_P$
4′	$[10\bar{1}]_P$	$[0\bar{1}0]_P$	$(101)_P$
5	$[110]_P$	$[00\bar{1}]_P$	$(\bar{1}10)_P$
5′	$[\bar{1}\bar{1}0]_P$	$[00\bar{1}]_P$	$(\bar{1}10)_P$
6	$[\bar{1}10]_P$	$[00\bar{1}]_P$	$(\bar{1}\bar{1}0)_P$
6′	$[\bar{1}10]_P$	$[00\bar{1}]_P$	$(110)_P$

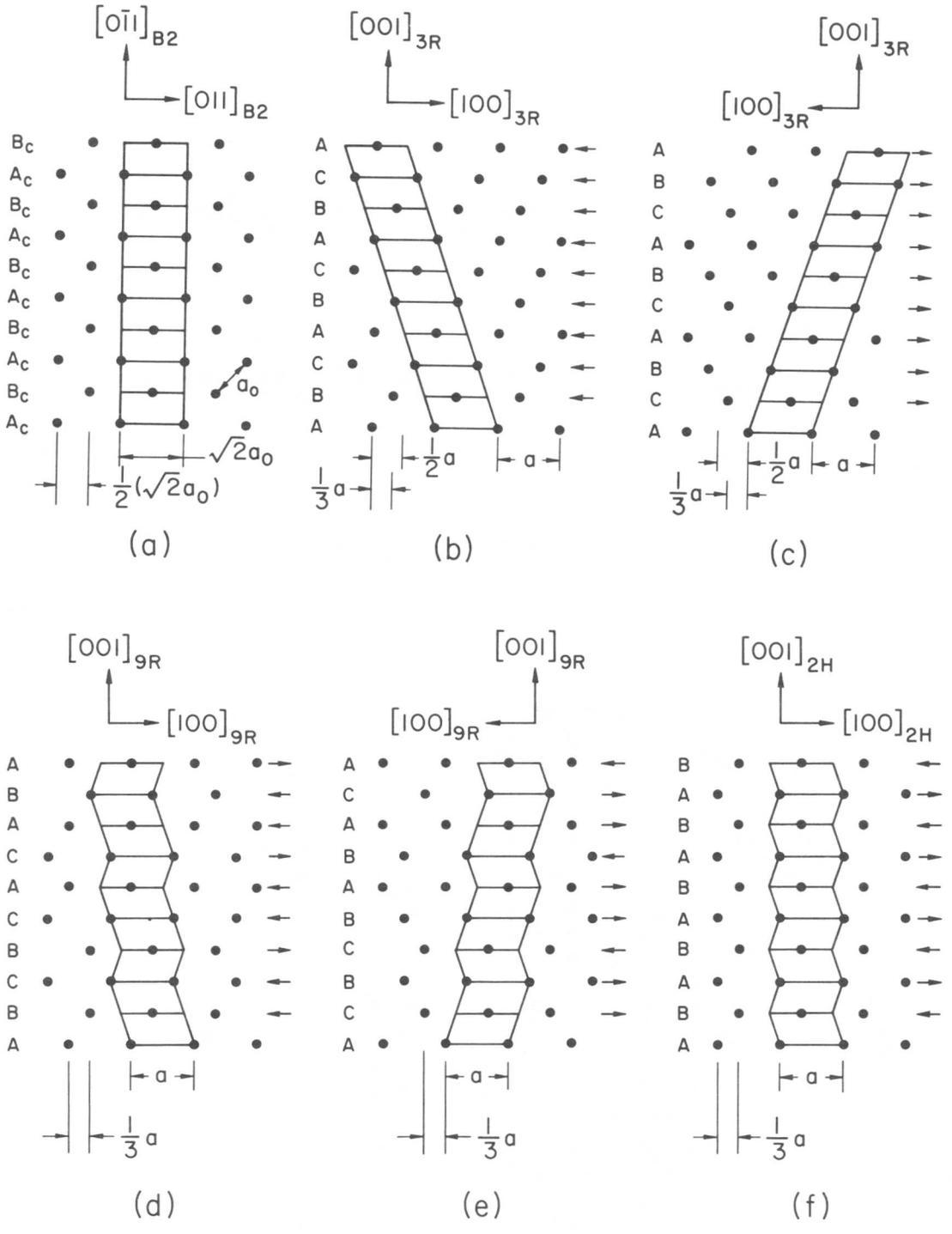

Fig. 4 Stacking order of parent (0$\bar{1}$1)and martensite (001) planes. (a) B2 (b) 3R(ABC) (c) 3R(ACB) (d) 9R(ABCBCACAB) (e) 9R(ACBCBABAC) (d) 2H(AB).

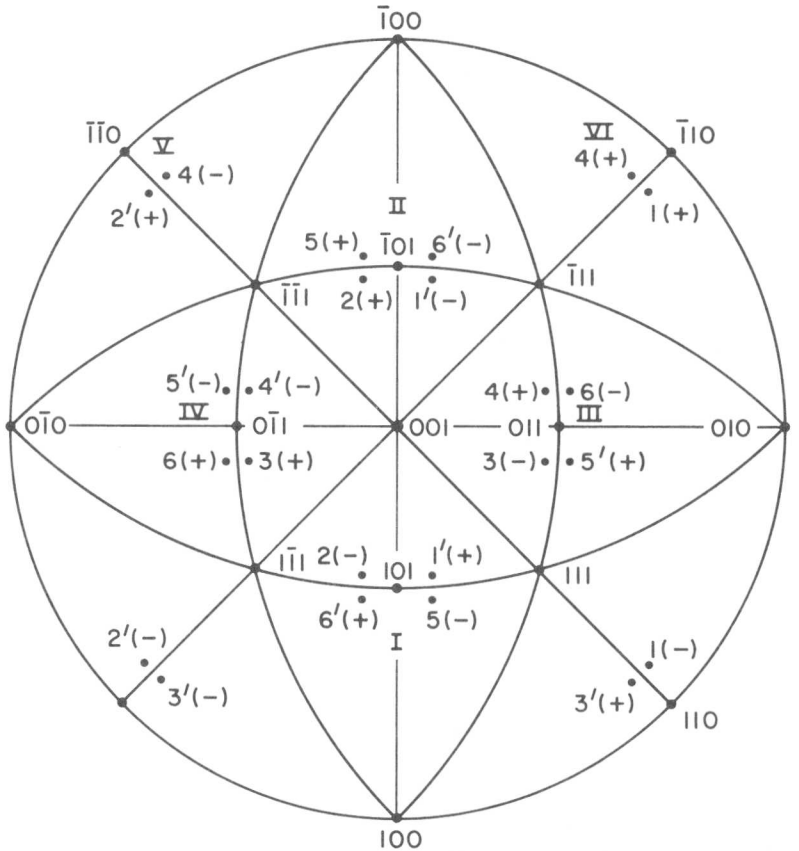

Fig. 5 Calculated habit plane poles for 24 martensite variants for a CuZnCa alloy. Six {110} plate groups are designated as I-VI.

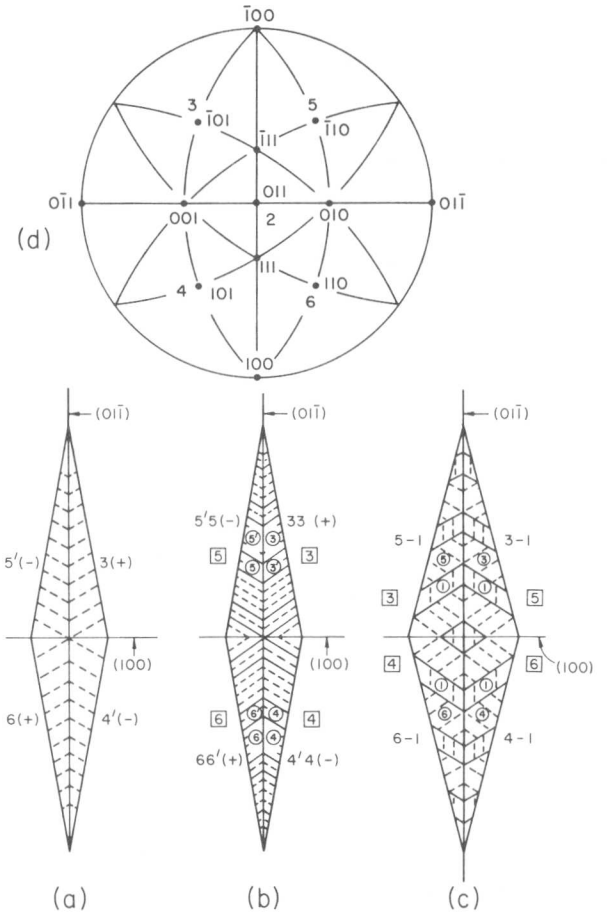

Fig. 6 Self-accommodating diamond-like plate group (Group IV). (a) 9R (b) 3R (c) 2H (d) crystallographic disposition of the parent close-packed planes, {110}, (011) projection. Solid line: variant and twin boundaries. Dashed line: basal planes. ⑤, ③, etc.: correspondence. [5], [3], etc.: twinning plane.

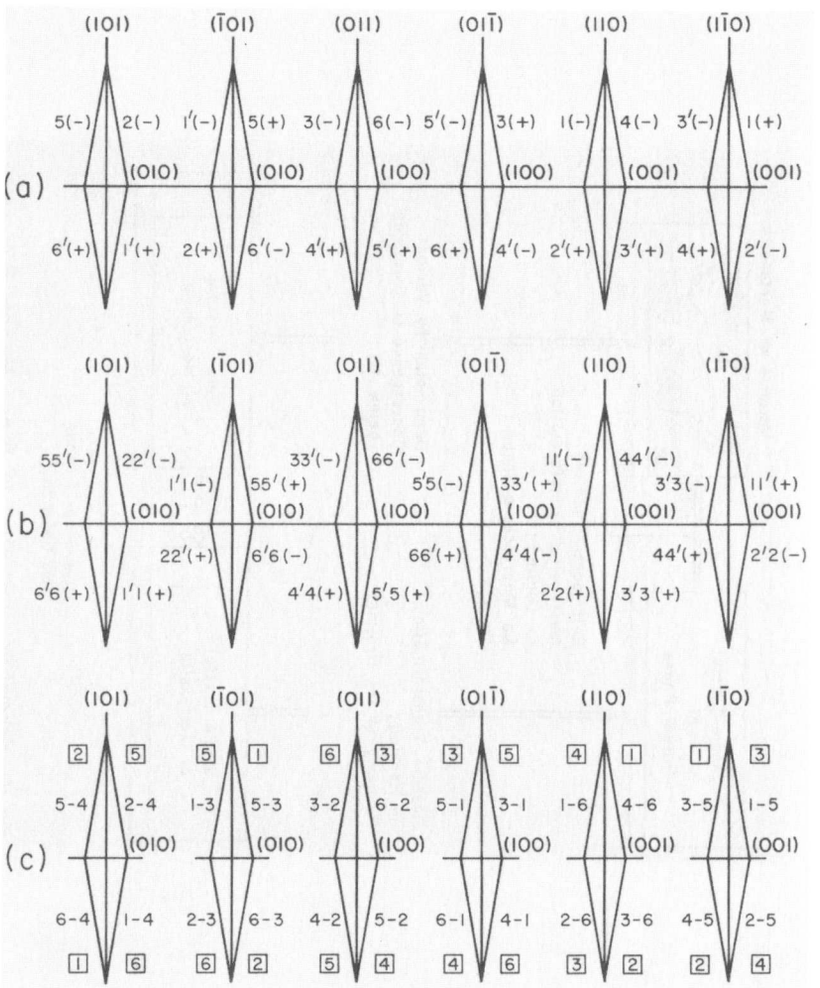

Fig. 7 Variant arrangement in six {110} plate groups. (a) 9R(18R) (b) 3R(6R) (c) 2H.

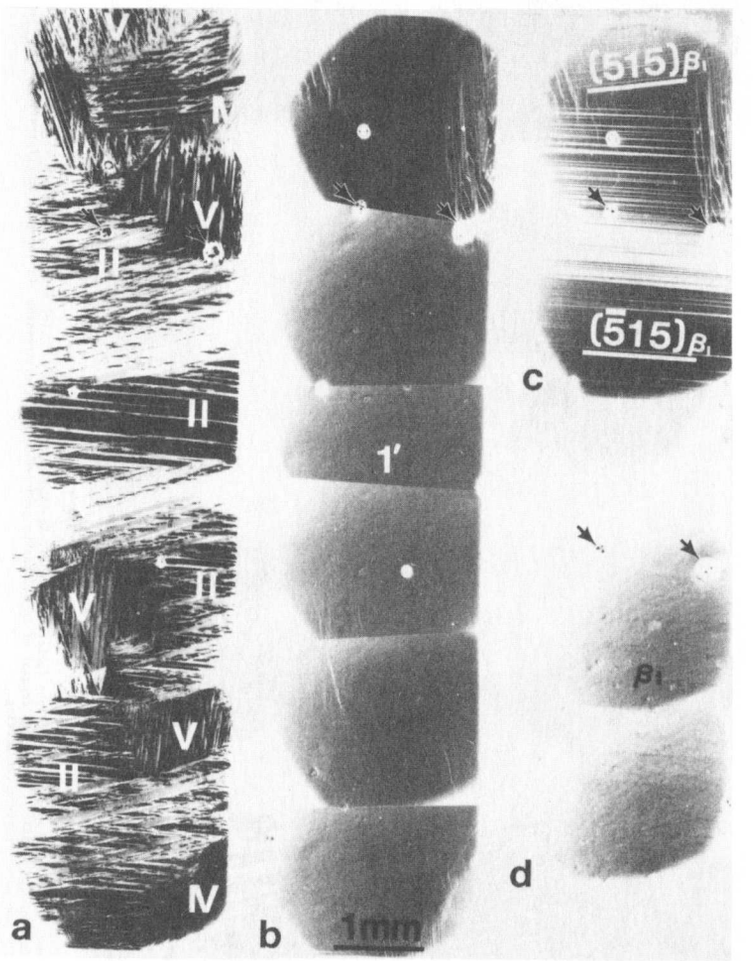

Fig. 8 Shape memory processes, optical micrographs (polarized light), Cu-20.4Zn-12.5Ga (at.%) (M_s:35°C). (a) as cooled self-accommodating structure below M_f(25°C) (b) single crystal of 18R martensite produced by tensile stressing (c) reverse transformation on heating (d) single crystal of the parent phase, after heating.

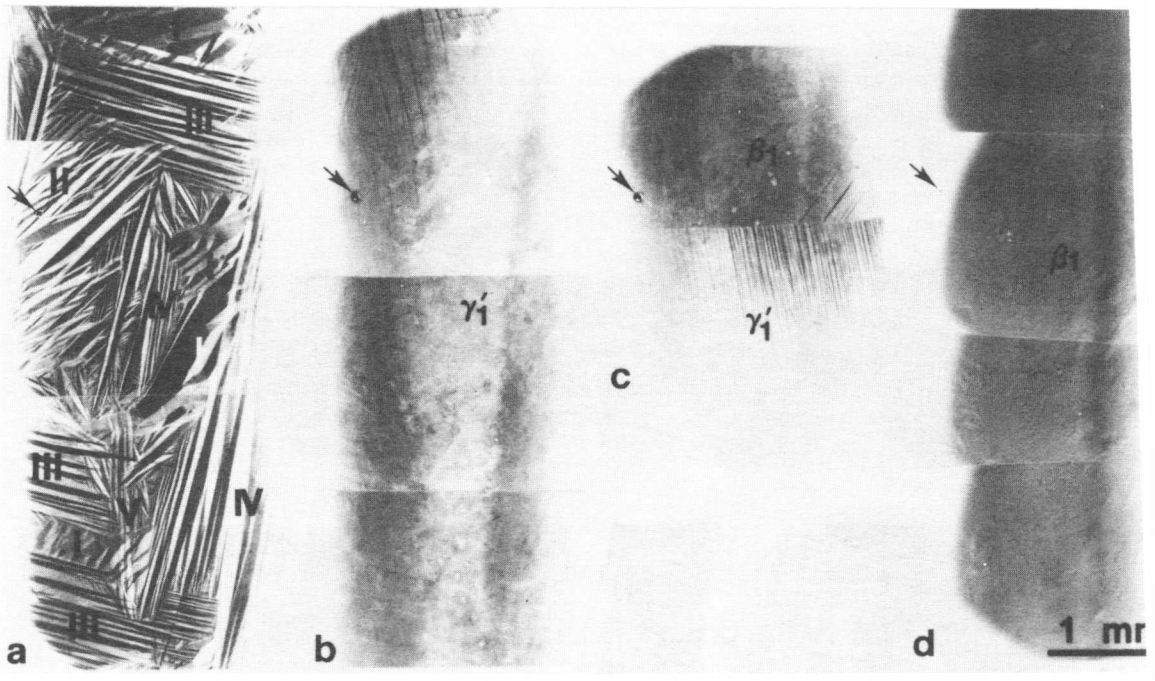

Fig. 9 Shape memory processes, optical micrographs (polarized light), Ag-45Cd(at.%) (M_s:-60°C). (a) Self-accommodating variants of 2H martensite pro on cooling below M_f (-85°C) (b) single crystal of 2H martensite produced by tensile stressing (c) reverse transformation on heating (d) sin crystal of the parent phase after heating.

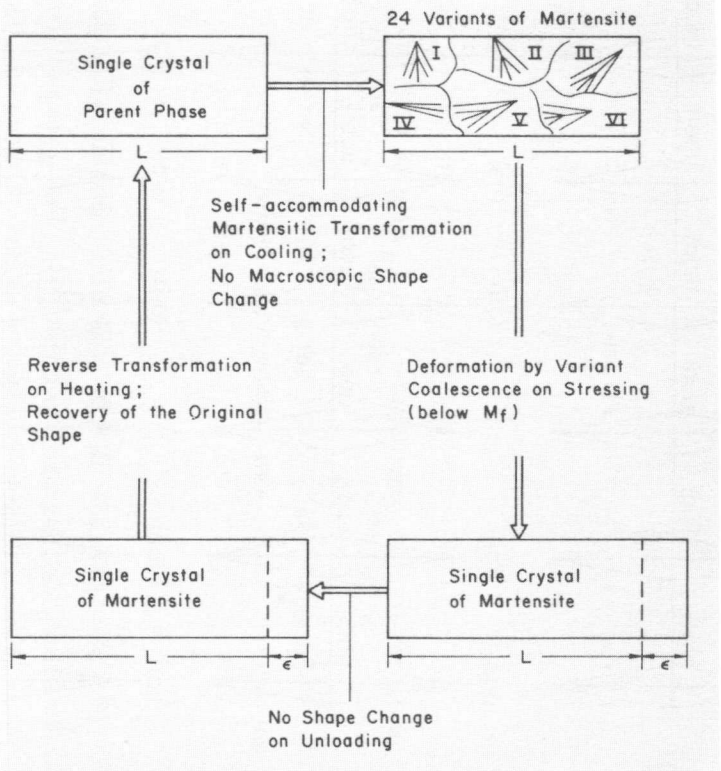

Fig. 10 Schematic Illustration of Shape Memory Processes

Effect of Tensile and Compressive Stress on Martensitic Transformations and Deformation Behavior of Cu-Al-Ni Alloys

H. Sakamoto*, M. Tanigawa+, K. Otsuka* and K. Shimizu*

Abstract

Tension-compression tests, in combination with optical microscopy, have been carried out for Cu-Al-Ni single crystals in a wide temperature range covering both above and below the M_S point, in order to see the effect of sense of external stress on martensitic transformations and associated pseudoelasticity.

The pseudoelastic stress-strain curves obtained are remarkably unsymmetric on tension and compression sides. In a temperature range above M_S, a small hysteresis loop characteristic of the $\beta_1 \rightleftarrows \beta_1'$ transformation is seen on a tension side, while a large one characteristic of the $\beta_1 \rightleftarrows \gamma_1'$ transformation on a compression side. In compression tests, the $\beta_1 \rightarrow \gamma_1'$ transformation occurs from the beginning at temperatures a little above M_S, but it is preceded by the $\beta_1 \rightarrow \beta_1'$ transformation at the very beginning at temperatures above Af. The critical temperature, which is determined by extrapolation of the Clausius-Clapeyron relationship to zero stress, has been found to be different in tensile and compressive stress. In a temperature range below A_S, the pseudoelastic loop in a tension side is due to the $\gamma_1' \rightleftarrows \beta_1''$ transformation, while the deformation mode on a compression side due to twinning in the γ_1' martensite, reflecting the anisotropy of the martensite. A phase diagram in tensile-compressive stress and temperature coordinate has been deduced from the stress-strain curves. A possible origin for the above effect of sense of stress on martensitic transformations is discussed.

Introduction

Stress-induced martensitic transformations and associated pseudoelasticity in Cu-Al-Ni alloys under tensile stress have been extensively investigated previously [1, 2, 3]. A few works have been done on the stress-induced transformations under a compressive stress [4]. There are some pioneering works on mechanical properties of Au-Cd and Au-Cu-Zn alloys under tensile-compressive stress [5, 6, 7]. However, the temperature dependence of deformation behavior and the microstructural change associated with the stress-induced transformations were not investigated in detail. Further, a single crystal martensite is expected to show a remarkably unsymmetric behavior in a tension-compression test due to the anisotropy (lower symmetry) of martensite crystal. Thus, stress-induced martensitic transformations and associated pseudoelasticity under tensile-compressive stress have been initiated in the present study using Cu-Al-Ni single crystals.

---

* The Institute of Scientifica and Industrial Research, Osaka University, Yamadakami, Suita, Osaka 565, Japan.
+ Graduate School, Osaka University.

Experimental Procedure

Three single crystals with the orientations shown in Fig. 1 have been used. The compositions and characteristic temperatures of the crystals are shown in Table 1. The specimens were subjected to the final heat treatment of 1273 K x 7200 s → W. Q. Then they were spark cut into the shape suitable for tension-compression tests. The tension-compression tests were carried out using Instron Machine of TT-CM-L type equipped with a temperature control chamber. The dimension of specimens was about 5 x 5 x 16 (mm) in its parallel guage length portion. In order to observe microscopical change under stress, a small tension-compression apparatus has been used. The details of specimen preparation and single crystal fabrication are described in Ref.[8].

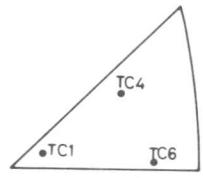

Fig. 1. Orientations of the specimens used.

Table 1.

	Compositions (wt.%)	M_s (K)	M_f	A_s	A_f
TC1	Cu-14.3Al-4.2Ni	242	226	250	276
TC4	Cu-14.0Al-4.0Ni	267	242	273	299
TC6	Cu-13.7Al-4.0Ni	303	292	322	337

Results and Discussion

(1) Stress-strain curves as a function of temperature

The results of tension-compression tests are typically shown in a series of stress-strain (S-S) curves as a function of temperature in Fig. 2. The curves are remarkably unsymmetric on tension and compression sides throughout the tested temperature range. The unsymmetric nature is explained in more detail in the followings by dividing the temperatures into two regimes.

(I) $M_s < T$: (A1) to (A7) show the S-S curves obtained at tmperatures above M_s. In a temperature region above A_f, pseudoelastic loops are obtained as shown in (A1) to (A4). Big differences are notable in the hysteris curves on tension and compression sides. The small hysteresis loop on a tension side is characteristic of the $\beta_1 \rightleftarrows \beta_1'$ transformation, while the large one on a compression side the $\beta_1 \rightleftarrows \gamma_1'$ transformation, as previously verified [8]. However, the transformation on a compression side is preceded by the $\beta_1 \rightarrow \beta_1'$ one at the very beginning. The initial plateau of the curves on a compression side corresponds to the occurence of the $\beta_1 \rightarrow \beta_1'$ transformation, and a large load drop after the plateau region corresponds to the beginning of the $\beta_1 \rightarrow \gamma_1'$ transformation. If stress is released before the load drop, only a small hysteresis loop characteristic of the $\beta_1 \rightleftarrows \beta_1'$ transformation is obtained on a compression side, (B). The load drop in (A1) occurs after 2.1% strain, while no load drop is seen even after 4.4% strain in another specimen (TC6), as seen in (C). Such a difference in the range of plateau regions is due to a test temperature relative to M_s and to a specimen orientation. Although a little difference exists from specimen to specimen, one important characterisitic of the sense of stress in this temperature region is that the $\beta_1 \rightarrow \gamma_1'$ transformation occurs more easily

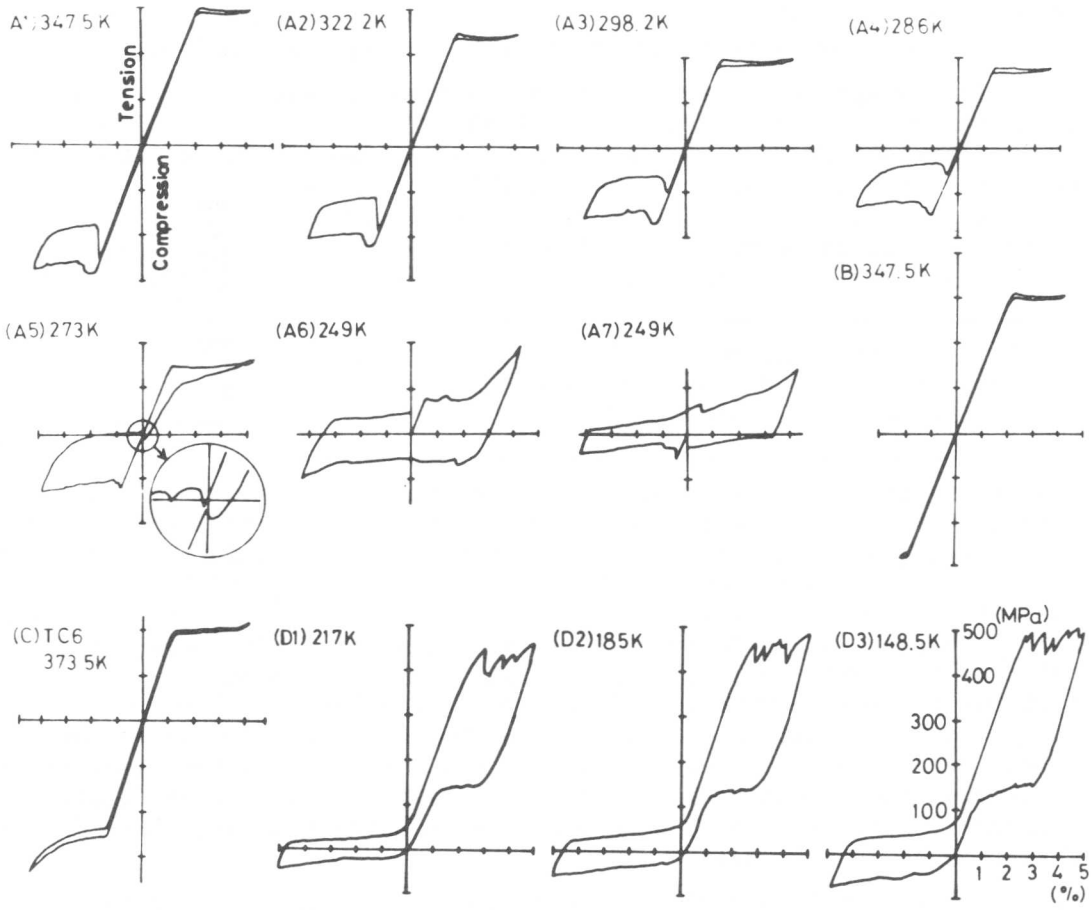

Fig. 2. Tension-compression stress-strain curves obtained from Specimen TC1 except for (C). Strain rate was 3×10^{-4}/sec.

on compression side even if the $\beta_1 \rightarrow \beta_1'$ transformation always occurs in tension side.

In a temperature region between A_f and M_s, different shapes of S-S curves are obtained as shown in (A5) to (A7). In (A5), which was taken at a temperature a little below A_f, the $\beta_1' \rightarrow \gamma_1'$ transformation is initiated at the end of the plateau region on a tension side (as evidenced by stress increases [1]), and because of this the hysteresis becomes so large near the origin. On the contrary, the $\beta_1 \rightarrow \gamma_1'$ transformation occurs from the beginning on a compression side, exhibiting a characteristic large hysteresis. The γ_1' martensite thus produced retains after the release of stress, and the retained one transforms to the β_1 matrix when stress is applied subsequently in the opposite direction, as seen from the enlarged portion in (A5). (A6) and (A7) were obtained at a temperature a little above M_s. The two curves correspond to the cases where the tests have been initiated from a tension side and a compression side respectively. At this temperature, the γ_1' martensite is stress-induced on both tension and compression sides, and it retains after the removal of stress. The retained γ_1' martensite does not transform to the β_1 matrix even if stress is applied subsequently in the opposite direction, being different from the case of (A5). Therefore, the deformation

mode after the initial $\beta_1 \rightarrow \gamma_1'$ transformation on another side of stress may be twinning or detwinning in the retained γ_1' martensite.

(II) $T < A_s$: A single variant γ_1' martensite with $(101)_{\gamma_1'}$ twins has been prepared by the procedure described before [9, 10], and the S-S curves obtained from the γ_1' martenstie are shown in (D1) to (D3), which are remarkably unsymmetric. They exhibit a pseudo-elastic loop on a tension side due to the $\gamma_1' \rightleftarrows \beta_1''$ transformation and a yield on a low stress level due to twinning on a compression side. The reason

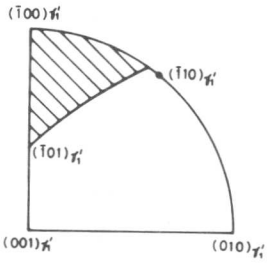

Fig. 3. Stereographic projection of the possible orientations of single variant γ_1' martensite stress-induced form the β_1 matrix.

why the $\gamma_1' \rightleftarrows \beta_1''$ transformation occurs only on a tension side and twinning occurs on a compression side can be explained as follows; The orientation of the single variant γ_1' martensite stress-induced from the β_1 matrix situates in the hatched area in Fig. 3. The Schmid factors for six twin systems, i. e. four $\{121\}_{\gamma_1'}$ twins and two $\{101\}_{\gamma_1'}$ twins of the γ_1' martensite have been found to be all negative. This means that no twinning is operative on a tension side. This is the reason why the martensite-to-martensite transformation is realized on a tension side. On the contrary there are many twinning modes, which operate on low stress levels on a compression side. Thus, the martensite-to-martensite transformation is not realized on a compression test. In one test, a compressive stress as high as 600 MPa was applied but the $\gamma_1' \rightleftarrows \beta_1''$ transformation was not induced.

(2) Optical microscopy of transformation and deformation behavior

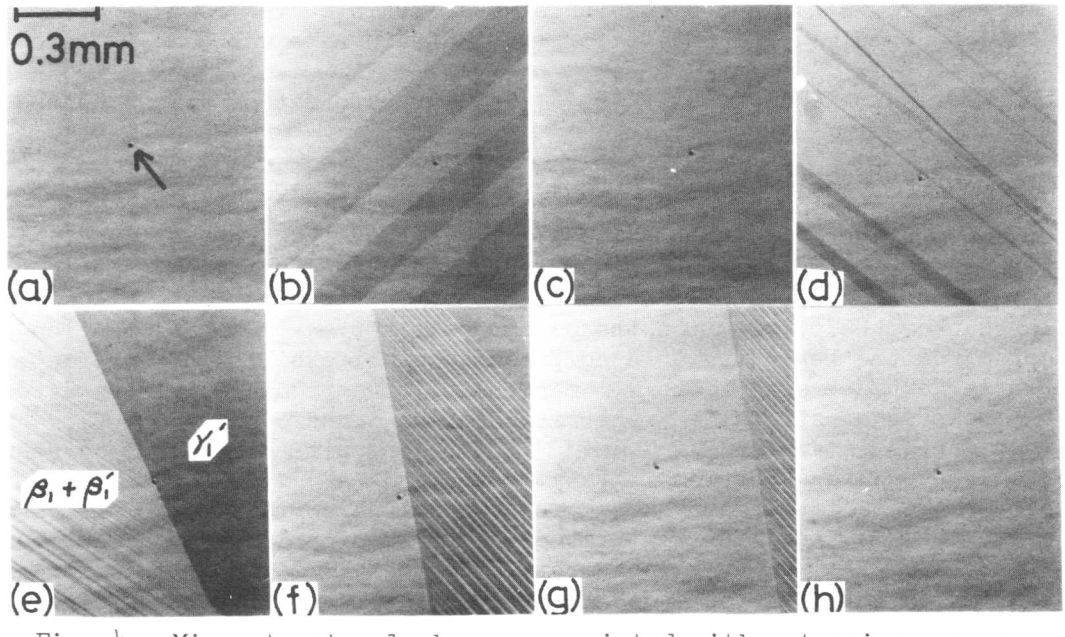

Fig. 4. Microstructural change associated with a tension-compression test, which was taken from Specimen TC4 at room temperature ($T > A_f$). Arrow (↑) in (a) represents a fiducial marker.

Fig. 4 is a series of optical micrographs of transformation and deformation behavior occurring in a tension-compression test at a temperature above A_f. (a) shows an initial single crystal state of the β_1 matrix, and (b) the β_1' martensites stress-induced on a tension side. The β_1' martensites transform back to the β_1 matrix upon releasing stress, (c). Applying a compressive stress, two variants of β_1' martensites are first stress-induced with different habit planes from that in (b), as seen in (d), and then a large plate of γ_1' martensite is stress-induced, (e). The γ_1' martensite plate grows at the expense of the β_1 matrix and the β_1' martensites already stress-induced. With decreasing compressive stress, the γ_1' martensite reverts to the β_1 matrix, and transformation twins are introduced inside the γ_1' martensite to satisfy the invariant plane strain condition of the $\gamma_1' \rightarrow \beta_1$ transformation, (f), and the transformation proceeds by the movement of the interface, (g), finally reverting to the β_1 matrix, (h). These microscopical changes are consistent with the S-S curves shown in Fig. 1 (A1) to (A4).

(3) Critical stresses as a function of temperature for various transformations and deformation

Fig. 5(A) and (B) show two schematic S-S curves in two temperature regions of $A_f < T$ and $M_s < T < A_f$, respectively. Critical stresses to induce a transformation and twinning are defined in the figure. These critical stresses have been plotted as a function of temperature in Fig. 6. Those for the $\beta_1 \rightleftarrows \beta_1'$ and $\gamma_1' \rightleftarrows \beta_1''$ transformations on the tension side are linear with respect to temperature, which are consistent with those previously obtained for tensile tests [3, 8]. On the compression side, however, the $\gamma_1' \rightleftarrows \beta_1''$ transformation does not occur, and not only the β_1' but also the γ_1' martensites are stress-induced from the β_1 matrix. In this way, transformation behavior is remarkably different on the

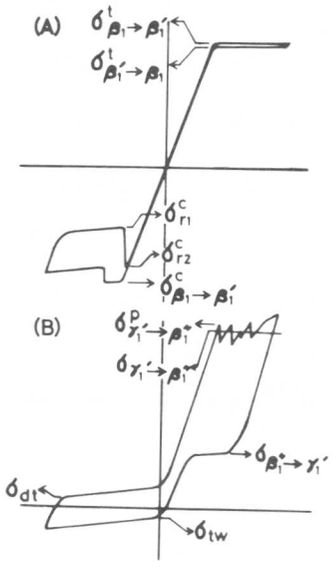

Fig. 5. Definition of critical stresses for transformation and twinning.

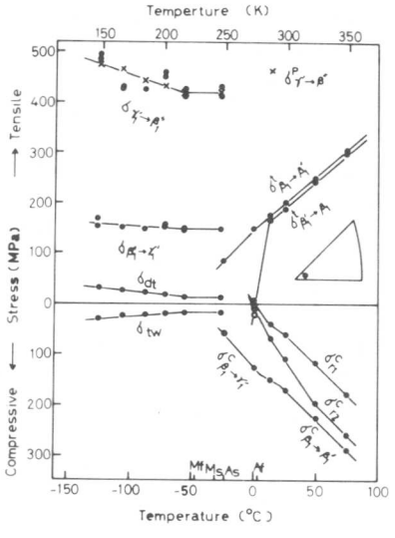

Fig. 6. Critical stresses as a function of temperature. The specimen (TC1) orientation is indicated in the inserted stereographic triangle.

tension and compression sides. The formation of γ_1' martensite on compression side may be explained by a non-uniform stress distribution due to an inferior uniaxiality in compression tests. That is, the γ_1' martensite can easily accomodate the non-uniform stress since many twinning modes are available. Hysteresis of the critical stresses for twinning and detwinning on the compression and tension sides, respectively, increases with decreasing temperature. This is probably due to the increase in frictional resistance of twin boundary movements with decreasing temperature.

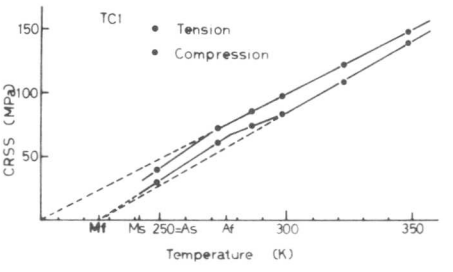

Fig. 7. Temperature dependence of the critical resolved shear stress for the $\beta_1 \rightarrow \beta_1'$ and $\beta_1 \rightarrow \gamma_1'$ transformations in tension-compression tests.

Fig. 7 shows a temperature dependence of the critical resolved shear stress (CRSS) for the $\beta_1 \rightarrow \beta_1'$ and $\beta_1 \rightarrow \gamma_1'$ transformations in tension-compression tests when we assumed that a variant of the β_1' or γ_1' martensite was formed with the maximum Schmid factor. It is immediately noticed that the CRSS is always lower and the critical temperature extrapolated to zero stress is higher on the compression side than on the tension side. This may be again explained by the non-uniaxiality in compression tests, that is, the CRSS is lowered by buckling due to non-uniaxiality on a compression side.

References

[1] K.Otsuka, H.Sakamoto and K.Shimizu; Scripta Met., 10 (1976), 983.
[2] K.Shimizu, H.Sakamoto and K.Otsuka; Scripta Met., 12 (1978), 771.
[3] K.Otsuka, H.Sakamoto and K.Shimizu: Acta Met., in press.
[4] L.A.Shepard; Shape Memory Effects in Alloys, ed. by J.Perkins, Plenum Publ., New York, (1975), 419.
[5] N.Nakanishi. Y.Murakami, S.Kachi, T.Mori and S.Miura; Phys. Lett., 37A (1971), 61.
[6] D.S.Lieberman, M.Schmerling and R.W.Karz; Shape Memory Effects in Alloys, ed. by J.Perkins, Plenum Publ., New York, (1975), 203.
[7] N.Nakanishi, T.Mori, S.Miura, Y.Murakami and S.Kachi; Phil. Mag., 28 (1973), 277.
[8] K.Otsuka, C.M.Wayman, K.Nakai, H.Sakamoto and K.Shimizu; Acta Met., 24 (1976), 207.
[9] K.Otsuka, H.Sakamoto and K.Shimizu; Scripta Met., 9 (1975), 491.
[10] K.Otsuka, H.Sakamoto and K.Shimizu; Shape Memory Effects in Alloys, ed. by J.Perkins, Plenum Publ., New York, (1975), 327.

Neutron Diffraction Studies of Crystal Structures of Stress-induced Martensites in a Cu-Al-Ni Alloy

M. Tokonami*, K. Otsuka*, K. Shimizu*, Y. Iwata** and I. Shibuya**

Abstract

The structure analysis of pseudoelastic martensites in a Cu-Al-Ni alloy has been carried out by neutron diffraction under tension. The crystallographic data such as the space groups, stacking sequence and lattice parameters of these martensites have been determined. It has been found that the structures except for that of the γ_1' martensite are all monoclinic, reflecting the deviations of stacking positions from the ideal ones. The effect of stress on the lattice parameters of these martensites are also discussed.

I. Introduction

The multistage pseudoelasticity recently found in Cu-Al-Ni, Cu-Zn, Au-Ag-Cd and Cu-Zn-Al alloys is of keen interest to many workers[1]. This effect is caused by successive stress-induced martensitic transformations and their reversions[2, 3]. It is vitally important to know the crystal structures of martensites stress-induced on various stages in order to understand the transformation mechanisms and pseudoelastic behavior. Since the pseudoelastic martensites are present only under stress, and the required stress level are very high (300 - 500 MPa), the structure determination must be carried out under stress in bulk specimens. This is a special aspect of the present structure analysis which is distinct from the ordinary one. In order to overcome this difficulty, we employed the neutron diffraction technique using a single crystal diffractometer. The purpose of the present paper is to report the results of the structure analysis of various stress-induced martensites appearing in a Cu-Al-Ni alloy by utilizing the above technique.

Martynov and Khandros[4, 5] have done a similar work by applying the X-ray oscillation photograph method to thinner wire specimens. However, their specimens are possibly too thick to obtain quantitative data by X-ray diffraction, and too thin to produce homogeneous transformations throughout specimens. The advantage of the present technique is to enable to obtain quantitative data from a large area of the reciprocal space, from which lattice parameters and atomic parameters can be determined.

Four martensitic phases γ_1', β_1', β_1'' and α_1' appear in the present alloy, and a phase diagram relating these phases in temperature and stress coordinates have been reported elsewhere[1, 3, 6].

---

* Institute of Scientific and Industrial Research, Osaka University, Yamadakami, Suita, Osaka 565, Japan

** Research Reactor Institute, Kyoto University, Kumatori, Sen'nan, Osaka 590-04, Japan

Table 1. Compositions and characteristic temperatures of used specimen

Specimen No.	Composition (at.%)	M_S(K)	M_f	A_S	A_f
T 27	Cu-27.6Al-3.6Ni	300	293	300	330
D 4	Cu-27.6Al-3.8Ni	312	296	305	338

II. Experimental Procedure

The single crystals were prepared by the modified Bridgman technique as described previously[3]. Two specimens were used, and their compositions and characteristic temperatures are shown in Table 1. The orientations of the specimens are shown in Fig. 1, along with those of the crystal axes of the stress-induced γ_1' martensite, which have been determined by the back reflections Laue method. The orientations of crystal axes of other stress-induced martensites did not change appreciably from these orientations.

The neutron diffraction experiment has been carried out by utilizing the 4 circle neutron diffractometer at KUR (Research Reactor Institute of Kyoto University). Incident neutron beam is monochromated by Cu(220) plane and has wave length of 0.1007 nm. A special tensile device has been made, which fits to the 4 circle goniometer[7]. The specimen size in the gauge length portion was 3.25 x 1.23 x 200 (mm) for Specimen D4, and was 2.75 x 1.68 x 600 (mm) for Specimen T27.

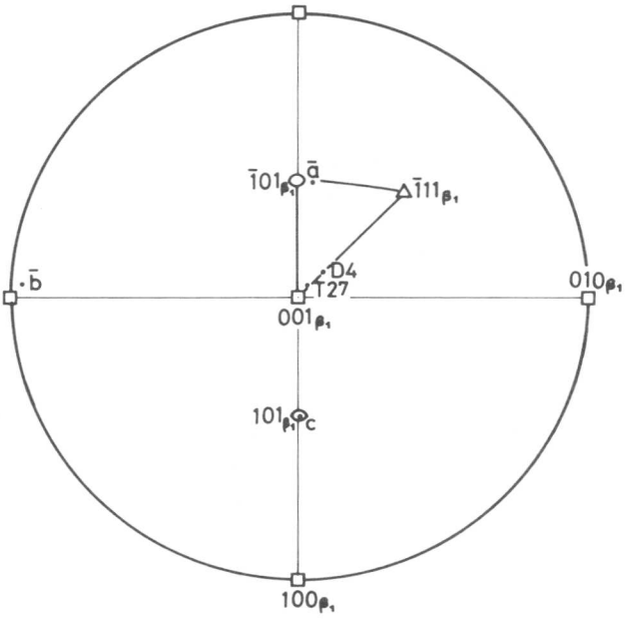

Fig. 1. Orientations of specimens and those of stress-induced martensites.

III. Results and Discussion

Before presenting experimental details, the essence of the crystal structures of the four martensites is given in Fig. 2. The experimental evidence of each structure except for that of well-established γ_1', is given below.

3.1. The structure of the β_1'' martensite

A detailed structure analysis has been carried out for this phase, and the result is published elsewhere[7].

3.2. The structure of the β_1' martensite

This structure has been studied previously by electron diffraction [8]. The present study confirmed the previous result concerning the stacking sequence. However, it further revealed that the x-coordinates of the stacking positions were deviated from the ideal ones such as 0,

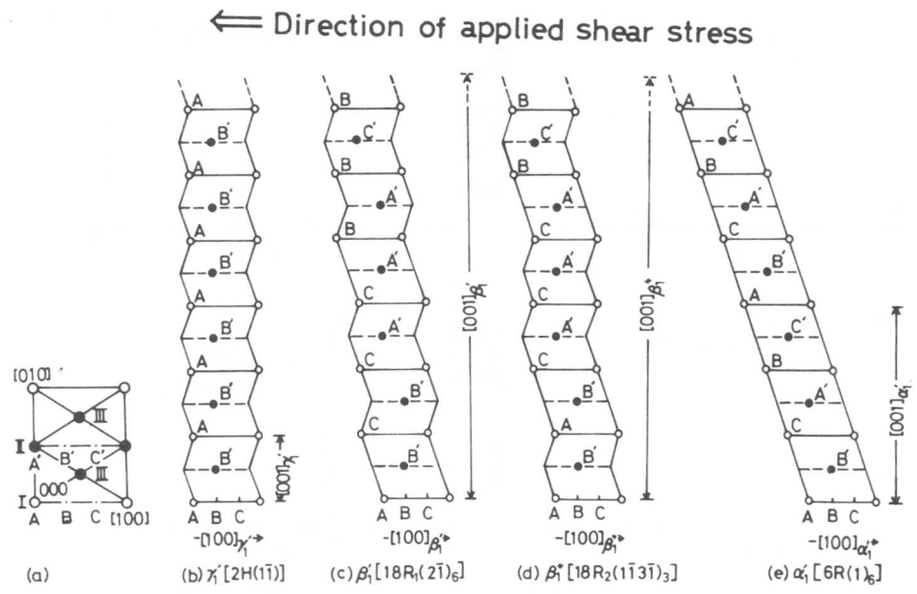

Fig. 2. Crystal structures of various stress-induced martensites. (a) Atomic arrangement and possible stacking sites in the common basal plane. Stoichiometric Al atoms occupy site I, extra Al atoms site II, Ni atoms site III, Cu atoms in balance sites II and III. (b) - (e) represent stacking sequence of each structure, viewed from $[010]_{\gamma_1'}$ = $[010]_{\beta_1''}$ etc.

1/3 and 2/3 and that the unit cell was monoclinic rather than orthorhombic because of this.

3.3 The structure of the α_1' martensite

The α_1' martensite is stress-induced either from β_1' or β_1'' [1, 3 6]. The intensity distribution along c* axis was found to be slightly different in the two cases. Thus typical intensity distributions are shown separately in Figs. 3 and 4. In these figures the indices for $\underline{\ell}$ are given for the perfect 6R structure. Thus, if the structure is of perfect 6R, strong peaks should appear at the indexed positions. However, the presence of subsidiary maxima and the displacement of main peaks are observed when $\underline{h}$ is not a multiple of 3, while neither the splitting nor the displacement of peaks are observed when $\underline{h}$ is a multiple of 3. This is a clear evidence that the spitting and displacement are due to the presence of stacking faults on the basal plane. In the following the two cases are discussed separately.

First we discuss the case of the α_1' martensite stress-induced from β_1''. The intensity distribution with subsidiary maxima as shown in Fig. 3(a) and (b) can be explained by introducing stacking faults rather regularly[10]. Since the α_1' martensite has been stress-induced from β_1'' with the stacking sequence $(1\bar{1}3\bar{1})_3$, the stacking sequence of the α_1' martensite with regular faults may be represented by a formula $(6\underline{n}-1, \bar{1})$ in Zhdanov symbol, where $\underline{n}$ is an integer. If a fault is introduced every $6\underline{n}$ layers, then the separation between a main peak and a subsidiary maxima becomes $1/6\underline{n}$ of the reciprocal lattice unit corresponding to an interplanar spacing of the basal plane. The averaged value of the

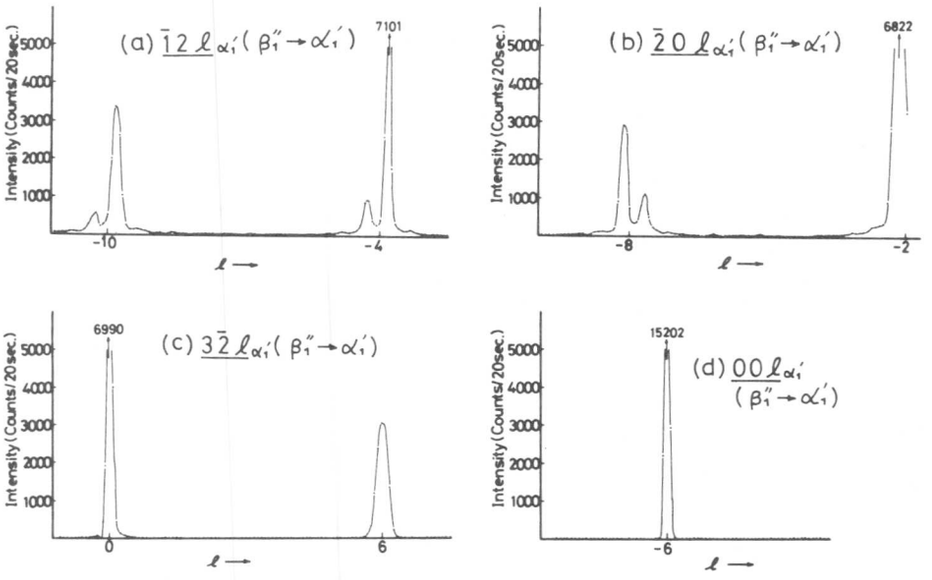

Fig. 3. Typical uncorrected intensity distribution along the c* axis of α_1' martensite stress-induced from β_1''.

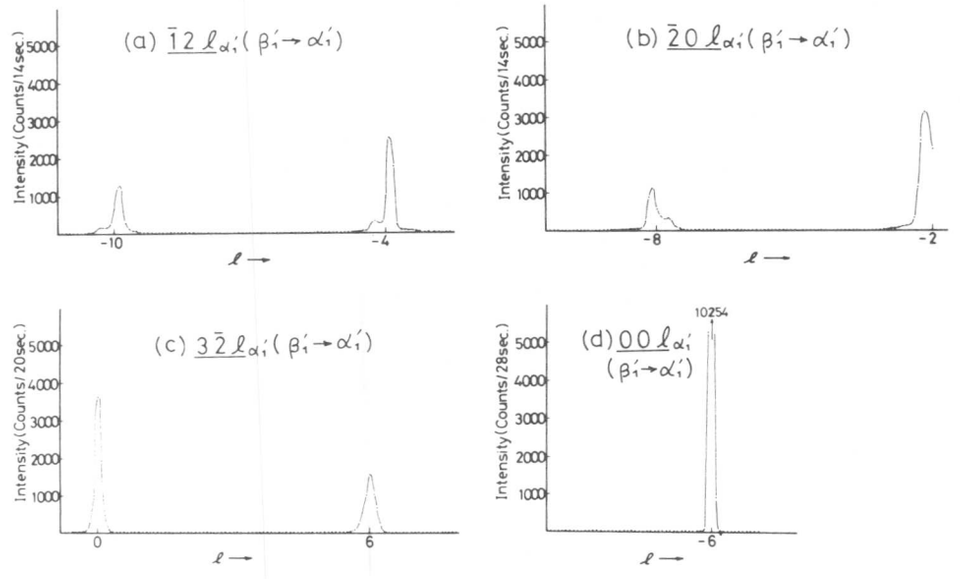

Fig. 4 Typical uncorrected intensity distribution along the c* axis of α_1' martensite stress-induced from β_1'.

separation was found to be about 1/13, which is very close to 1/12 [n=2]. Thus, the sequence may be represented as $(11, \bar{1})_3$. The intensity ratio of a main peak and a subsidiary maximum in this case is calculated to be about 1/4, assuming no deviation of stacking positions. However, the intensity ratio in Fig. 3(a) and (b) are different from this value. This discrepancy has been rationalized by taking into account the deviation of stacking positions from the ideal ones. The deviation of the separation from the ideal value of 1/12 may be interpreted as due to the mixing of the stacking sequence of $(11, \bar{1})_3$ and $(17, \bar{1})_3$[n=3]. Martynov and Khandros[5] reported that the stacking sequence was represented as $(14, \bar{1})_6$. This assignment of the stacking sequence may not be appropriate, since the stacking sequence do not conform to the above stacking sequence formula.

The case of the α_1' martensite stress-induced from β_1' is rationalized similarly. In this case (Fig. 4), the subsidiary maxima are more diffuse than the previous case and they are not well separated from the main peaks. Again this may be interpreted as due to the mixing of regular faults with different periods. Since the sequence formula is represented by $(3\underline{n}-1, \bar{1})$, in which the density of subsidiary maxima upon changing $\underline{n}$ is higher, it is easy to understand why the subsidiary maxima are more diffuse than the previous case. The average separation between subsidiary maxima and main peaks was found to be about 1/18. Thus the average stacking sequence may be represented as $(17, \bar{1})_3[\underline{n}=6]$.

Although the above diffraction patterns were deviated from that of the ideal 6R structure, they were consistently explained by introducing stacking faults rather regularly. These faults are possibly the ones left over during the transformation from β_1'' to α_1' or from β_1' to α_1' under the present experimental condition*. We believe that the specimen will have the ideal 6R structure if the stress is increased high enough. This point will be experimentally examined in the near future.

3.4. Lattice parameters of various martensites as a function of stress.

The crystallographic data including space group and the lattice parameters etc. are summarized in Table 2. Since all the data except for that of β_1'' were taken from the same specimen, the lattice parameters are directly comparable. By plotting the lattice parameters as a function of stress, linear relationships have been obtained with positive slope for the $\underset{\sim}{a}$ and $\underset{\sim}{c}$ axes and a negative one for the $\underset{\sim}{b}$ axis. This tendency is the one what is expected from the orientations of the stress-induced martensites shown in Fig. 1.

The behavior of the β angle as a function of stress is also interesting. The value of the β angle is determined by two factors. One is the elastic deformation of a stress-induced martensite, and the other is the deviation of stacking positions from ideal ones[7, 9]. The former tends to make the β angle larger as seen from Fig. 2, while the latter tends to make it smaller as verified in the previous work[7]. Thus the

---

* In order to avoid the fracture of the specimen, the transformed region was restricted to a certain region of the specimen, which is subject to neutron scattering.

Table 2. Crystal structures of various stress-induced martensites in Cu-14.0Al-4.2Ni (wt.%) alloy

Phase	γ_1'	β_1' ($\beta_1 \rightarrow \beta_1'$)	β_1'' ($\gamma_1' \rightarrow \beta_1'$)	α_1' ($\beta_1'' \rightarrow \alpha_1'$)	α_1' ($\beta_1' \rightarrow \alpha_1'$)
Space group	Pnmm	A2/m	$P2_1/m$	A2/m	
Stress (MPa)	100	150	400	500	500
Lattice parameters					
a (nm)	0.4418	0.4430	0.4437	0.4503	0.4500
b	0.5344	0.5330	0.5301	0.5239	0.5235
c	0.4242	3.819 (0.4243x9)	3.814 (0.4238x9)	1.277 (0.4257x3)	1.276 (0.4253x3)
β	90.2°	89.0°	89.2°	89.3°	89.2°
Ramsdel notation	2H	$18R_1$	$18R_2$	6R	
Zhdanov symbol	$1\bar{1}$	$(2\bar{1})_6$	$(1\bar{1}3\bar{1})_3$	$(1)_6$	
Stacking sequence	AB'	AB'CB'CA' CA'BA'BC' BC'AC'AB'	AB'AB'CA' CA'CA'BC' BC'BC'AB'	AB'CA'BC'	
Specimen No	T27	T27	D4	T27	

two effects are opposite in sense. Since the β angle of the γ_1' martensite is determined by the elastic effect alone, the elastic effect for each stress-induced martensite is calculated from this value, assuming that the shear modulus is the same for all martensites. The other effect is easily obtained by subtracting the elastic effect from the observed β angle of the β_1' martensite. Since both effects are known, it is possible to estimate the β angle of the α_1' martensite under a stress of 500 MPa. The calculated value was 89.1°, consistent with the observed value. Thus, the behavior of the β angle as a function of stress has been well rationalized.

References

[1] K. Otsuka and K. Shimizu: this conference.
[2] K. Otsuka, H. Sakamoto and K. Shimizu: Scripta Met., 10(1976)983.
[3] K. Otsuka, H. Sakamoto and K. Shimizu: Acta Met., in press.
[4] V. V. Martynov and L. G. Khandros: Dokll. Akad. Nauk SSSR, 233 (1977)345.
[5] V. V. Martynov and L. G. Khandros: Dokll. Akad. Nauk SSSR, 237 (1977)1349.
[6] K. Shimizu, H. Sakamoto and K. Otsuka: Scripta Met., 12(1978)771.
[7] K. Otsuka, M. Tokonami, K. Shimizu, Y. Iwata and I. Shibuya: Acta Met., in press.
[8] K. Otsuka, T. Nakamura and K. Shimizu: Trans. JIM., 15(1974)200.
[9] T. Tadaki, M. Tokoro and K. Shimizu: Trans. JIM., 16(1975)285.
[10] S. Kajiwara: J. Phys. Soc. Japan, 27(1969)712.

Pseudoelastic Transformation and Reorientation in β_1-Cu-Zn-Al Alloys

L. Delaey, J. Janssen, J. Van Humbeeck, J. Luyten and A. Deruyttere

Abstract

The pseudoelastic transformation, the reorientation and the martensite-to-martensite stress induced transformation have been studied in β- and martensitic Cu-Zn-Al alloys. The present paper only summarizes the main topics and results which are to be presented in the oral communication.

The pseudoelastic behaviour of Cu-Zn-Al β-phase alloys was studied on single, bi- and polycrystals [1]. For one single crystal it was shown that the (σ^{P-M} - T)-curve existed of two straight lines with different slopes. It was suggested that this may be due to a stress-induced martensite-martensite transformation. This aspect of the pseudoelastic transformation is now analysed in more detail. A single crystal was tested at various temperatures above the A_s-temperature, the results are summarized in figure 1. The two types of stress-strain curves, which are observed in two different temperature ranges, are schematically represented on the same figure. The most important points of deflection in those stress-strain curves are marked by different numbers. Fig. 1 shows clearly the difference in stress-strain behaviour in the two temperature ranges $T \leqslant TO_2$ and $T \geqslant TO_2$. The ($\sigma^{P \rightarrow M}$ - T)-curve consists of two straight lines with different slopes. Curve 1 is valid for the $\beta_1 \rightarrow \beta_1'$ (18R-type) stress-induced transformation and curve 2' is valid for $\beta_1 \rightarrow \alpha_1'$ (6R). Curve 1' is the stress needed to nucleate the α_1'-martensite. Curve 3 is the stress needed for inducing the α_1'-martensite from β_1'.

The hysteresis for $\beta_1 \rightleftarrows \beta_1'$ (curve 1 and 6) is independent on temperature whereas the hysteresis for $\beta_1 \rightleftarrows \alpha_1'$ (curves 2' and 6') is dependent on temperature. The difference between the nucleation stress (curve 1') and the equilibrium stress (curve 2') also increases with increasing temperature.

Until now it is believed that the stress-induced martensite (β_1') has the same crystal structure and internal plate morphology (stacking faults and lamellae) as the thermally induced martensite. Electron microscopy of deformed β_1 shows that the retained martensite plates have not the same internal structure. Figure 2 shows an electron diffraction pattern (2a) and a micrograph (2b) of a deformed β_1-phase. It clearly shows that the martensite is internally twinned, the twinning occurs along the 18R-basal plane. The thus obtained 18R-orientation does not coincide with one of the 24 possible thermally induced 18R-variants. Plastic deformation occurs in the β_1-phase (fig. 2b).

Department of Metallurgy, Katholieke Universiteit Leuven, de Croylaan 2, B-3030 Heverlee-Leuven (Belgium).

It is generally accepted that deformation of martensite below M_f occurs primarily by reorientation, all the 24 variants reoriented finally to the same single variant.

Electron microscopy however shows that during the deformation of martensitic polycrystals a 18R-twinned microstructure forms (fig. 3).

The internal microstructure of the stress-induced as well as that of the deformed thermally induced martensite thus clearly differs from the microstructure of the undeformed thermally induced martensite.

This result indicates that in the β_1'-phase region on figure 1 an extra curve should be drawn delignating the twinned from the untwinned 18R-structure. The fact that shape memory occurs in the deformed and reoriented martensite, the exact mechanism for the reverse transformation and for the shape memory will be revised.

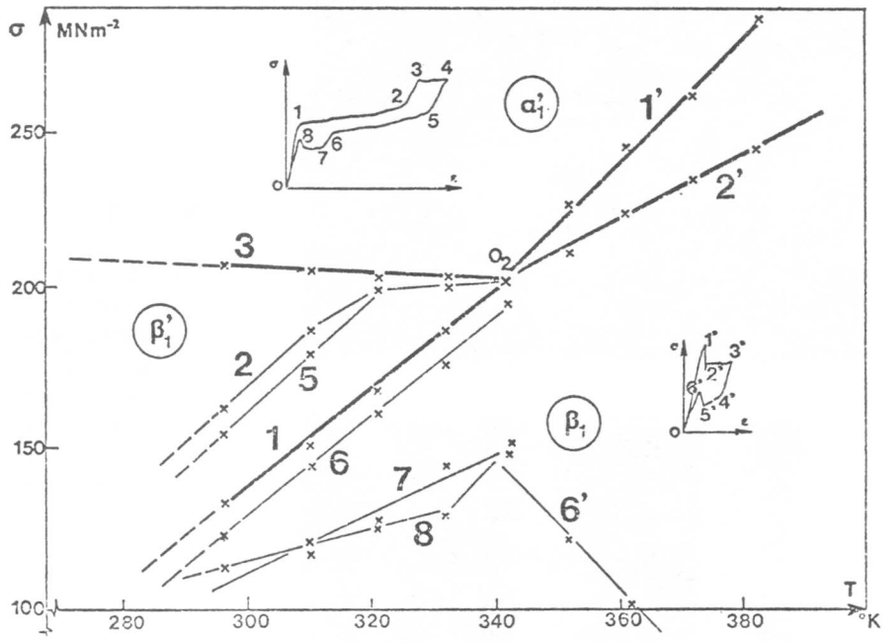

Fig. 1 : Temperature dependence of critical stresses with temperature.
Curve 1 : stress needed to induce β_1' from β_1
2 : stress at the end of the $\beta \rightarrow \beta_1'$ transformation
3 : stress needed to induce α_1' from β_1'
5 : stress corresponding with the start of the $\beta_1' \rightarrow \beta_1$ transformation
6 : stress corresponding with the end of the $\beta_1' \rightarrow \beta_1$ transformation
7 : stress corresponding with the start of the $\alpha_1' \rightarrow \beta_1$ transformation
8 : stress corresponding with the end of the $\alpha_1' \rightarrow \beta_1$ transformation
1': nucleation stress for the α_1' martensite from the β_1-matrix
2': equilibrium stress to proceed the $\beta_1 \rightarrow \alpha_1'$ transformation of the nucleation step (curve 1')
6': stress associated with the end of the $\alpha_1' \rightarrow \beta_1$ transformation

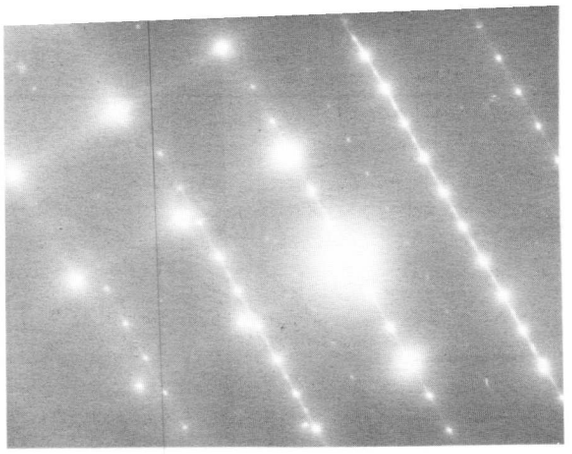

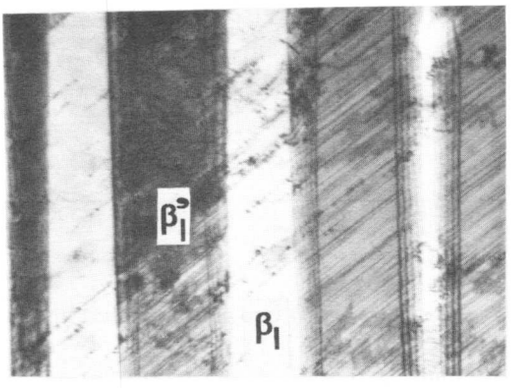

Fig. 2 :

a. 18R with bcc diffraction pattern which shows the twinnings in the martensite.
b. plastic deformation in the β_1-parent phase.

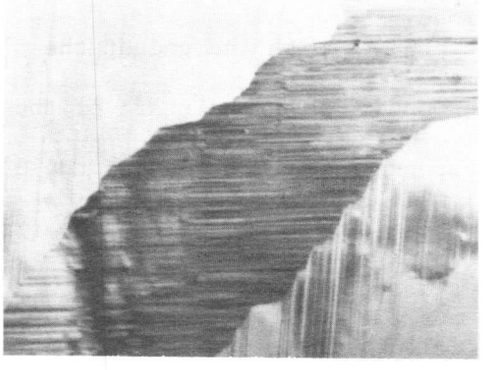

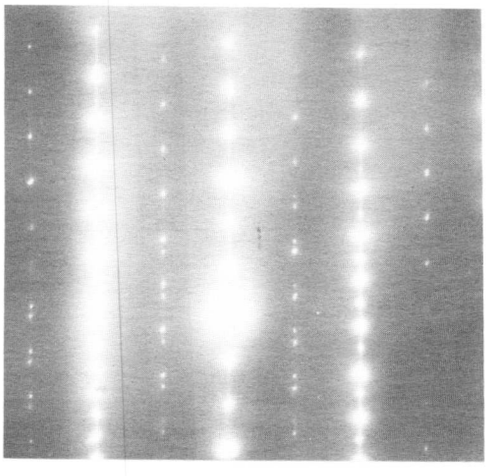

Fig. 3 :

a. internal twins in the martensite (18R).
b. diffraction pattern showing the twins in the martensite.

The Influence of Cycling on the Rubberlike Behavior in CuZnAl Martensite

M.Ahlers* and G.Barceló*

Abstract: The rubberlike behavior has been studied in martensitic single crystals of CuZnAl alloys with M_S=50°C. The behavior is due to the stress induced formation of a new martensite variant which disappears on unloading and restores the original shape after the deformation cycle. The maximum revertible strain decreases with the number of cycles. Reasons for this behavior are analysed. It is shown that twinning occurs in the martensite during the cycling which do not disappear on unloading and inhibit the stress induced formation of the martensite variant, that leads to the rubber like behavior.

I. Introduction

A martensitic single crystal is obtained by straining a β' phase single crystal above its M_S temperature in tension and then cooling it below M_S under constant stress. If this martensitic crystal is compressed it deforms plastically. However, on releasing the stress the induced deformation disappears again and the original shape of the martensite is restored. This rubber effect which occurs in the martensite is to be distinguished from the pseudoelasticity which is caused by stress inducing martensite in the β' phase. The rubber effect has been frequently observed for martensites with a hexagonal structure, but recently has also been found in CuZnAl alloys with the orthorhombic 3R structure [1]. After the initial report [1], more detailed studies were made [2], which were mainly concerned with the crystallography of the transformation. An attempt had been made to explain the rubber like behavior [3] on the basis of this crystallographic study. Another aspect that is of interest and may be important for possible technological applications is the change in the rubber like behavior with repeated stress cycling. In this paper some experimental results on the cycling behavior are reported and discussed.

II. Experimental procedure and results

β' single crystals of nominally 70 at% Cu-12 at% Zn and 18 at% Al were prepared in the usual way by the Bridgman method in sealed vycor tubes from master alloys which had been obtained by melting together the pure metals, also in quartz. The single crystals had an M_S=50°C. In

*Centro Atómico Bariloche, Comisión Nacional de Energía Atómica (8400) S.C. de Bariloche - Argentina

order to produce the martensitic single crystals, the β' phase samples were deformed in tension above the A_f temperature. The formation of the martensite bands in the β' phase was visible optically and the strain at which all material had transformed to martensite could easily be recognized. The crystals were then cooled to room temperature, and subsequently the stress was released leaving a martensitic single crystal for further studies. From the single crystals of ≈3mm diameter, compression samples of 10mm length were cut by spark machining. A sample was deformed at room temperature in compression, and then unloaded after a certain stress was reached. This loading-unloading cycle was repeated many times. In figure 1 are shown the engineering stress (σ) versus engineering strain (ε) curves for the various cycles. When the crystal was loaded for the first time, deformation started at a critical stress and proceeded with little hardening to $\varepsilon \approx 10\%$, whereafter the

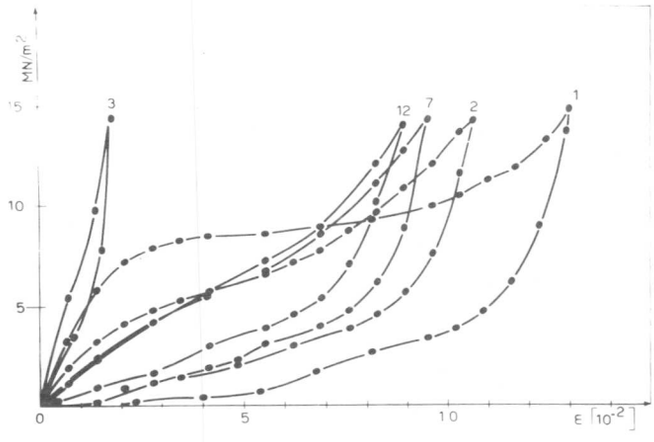

Fig.1:Stress σ versus strain ε for various deformation cycles, denoted by the number of the cycles.

hardening increased. The sample was then unloaded, and as seen in fig.1 the sample expanded until at zero stress it had recovered nearly its original length. The residual strain was partially due to deformation at the sample ends, and also due to some deformation remaining in the center. All subsequent cycles have been plotted starting at a zero strain. The second cycle differed from the first one in several aspects: The deformation started at a lower stress, the hardening rate was higher and the upper stress was reached at lower strains, probably due to the deformation retained after the first cycle. The retransformation curve was nearly the same as that of the first cycle, implying that the hysteresis stress had become smaller. During the following 25 cycles the hysteresis curves changed relatively little, the hardening increased slowly and the maximum stress, which was the same in all cycles, was reached at steadily decreasing strains. After 25 cycles the hardening started to increase rapidly, the revertible strain becoming small.

These results have been supplemented by optical microscopy studies. A sample was deformed repeatedly while under observation. The deformation during the first cycle started with the formation of bands

which extended across the whole cross section of the sample. The bands had plane interfaces with the original martensite. Generally the deformation proceeded by the broadening of the bands and by the appearance of new ones, until the entire central part of the sample had transformed. Though no surface traces were visible any more in the center, traces remained however at the sample ends. On unloading retransformation occured by the formation and growth of bands of the original martensite. When the stress was completely released traces remained at the sample ends, and a few bands were visible in the center part. The remnant deformation found in the stress strain curve probably is due to this effect. During the next 25 cycles the behavior did not change much. The bands appeared and disappeared in the same way as during the first cycle. The number of bands that remained after the unloading, did not increase noticeably, except at the sample ends. After 25 cycles changes were observable, more bands remained after unloading and between the bands new traces had appeared whose number increased rapidly on further cycling. Some traces crossed into the bands, whereas others were confined to the region between the bands. In figure 2 is shown an area

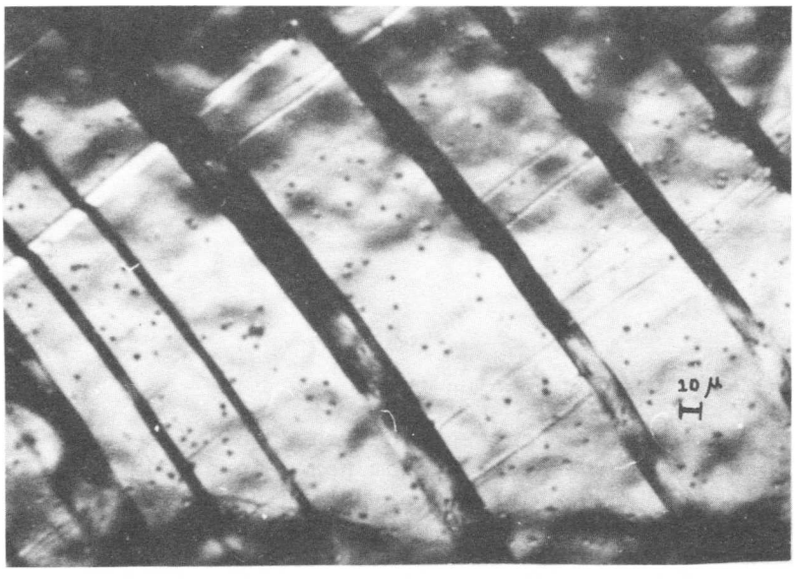

Fig.2:Sample surface with retained bands of the compression induced martensite and with the thin twins nearly normal to them.

after unloading which contains the bands and some of the new traces nearly perpendicular to the bands. The disappearance of the rubber effect apparently was related to the formation of the additional markings, as no bands appeared during the compression in the region where they were present. The orientation of the new plates was determined by multisurface analysis. In figure 3 the orientation of the sample axis (T), the plane normal of the bands (P)and of the new traces (P_{II}) are shown plotted in a stereographic projection. The shear direction d of the bands could be measured within $\pm$ 5°, whereas the shear direction for the other markings could not be determined with sufficient precision, and therefore only the theoretical d_{II}(to be discussed below) is shown in the projection. The orientation of the martensite

had been determined by x-rays before the cycling was started. In figure 3 are shown the axes of the orthorhombic martensite, $[100]_o$ $[010]_o$ and $[001]_o$ of the original martensite variant. Finally, from the known orientation relationship between martensite and the high temperature β' phase, the cubic axes of the β' have also plotted as filled squares.

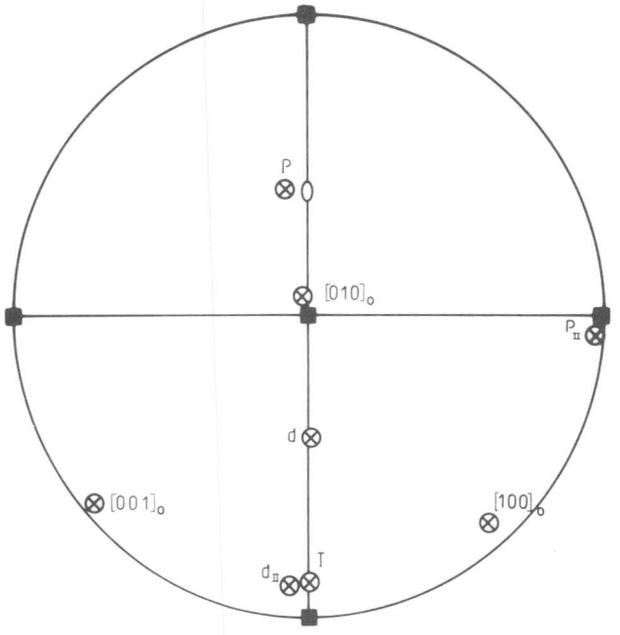

Fig.3:Stereographic projection of measured band interface normal (P), the corresponding shear (d), the twin interface normal (P_{II}) and the calculated twin shear direction(d_{II}) with respect to the sample axis (T), the orthorhombic axis system of the original martensite and the β' phase axes, denoted by filled squares.

III. Discussion

The rubber-like behavior has been explained in detail elsewhere by the existence of short range disordered atom pairs in a long range ordered martensite [3]. The bands which appear during compression are a new variant of the same structure as the original martensite [2].The disordered pairs which are present in thermal equilibrium when the original martensite is left for sufficient time at or above room temperature transform to another configuration which is no longer in thermal equilibrium and has a higher energy, thus providing the driving force for the retransformation when the stress is released [3].

After the cycling, in addition to the bands of the new martensite variant secondary traces appear. The pole P_{II} of these traces lies away from $[001]_o$ and close to $[100]_{\beta'}$ direction. The traces cannot therefore be due to shears on the $(001)_o$ compact plane of the orthorhombic lattice, or due to a third martensite variant with an interface close to $(110)_{\beta'}$. It is however likely that the traces are due to twins within the martensite. Twins in the martensite have indeed been observed by Speidel and Warlimont [4] in orthorhombic and hexagonal martensite in the Cu-Al system after plastic deformation. The twins in

the hexagonal martensite, were analysed and it was concluded from TEM diffraction patterns that the twins in the orthorhombic martensite are similar. However due to the severe deformation no quantitative evaluation was possible. Tas, Delaey and Deruyttere [5] analysed the interfaces that can exist between different martensite variants which belong to the same self accomodating group of martensite plates, and which have their habit planes close to one $(110)_{\beta'}$ pole of the β' phase. They found three types of interfaces for the orthorhombic martensite in Cu-Al alloys two of these have their interfaces close to a $(110)_{\beta'}$ pole and the third one has an interface close to $(100)_{\beta'}$, which they called twins of the second kind. In addition to growing alongside other existing variants under stress, the twins were also found inside a variant, as thin straight markings similar to those observed in our samples. The orientation of the twin interface agrees closely with our observed P_{II}, and the twinning direction is parallel to d_{II}, shown in figure 3. Since shears in directions other than d_{II} on the observed plane P_{II} would lead to structural changes, it is concluded that the markings which form during cycling are identical to the twins of the second kind discussed by Tas et al [5], and also to those seen by Speidel and Warlimont [4] during plastic deformation. For better visualisation the atom positions normal to the twin plane are shown in figure 4 for the 3R structure

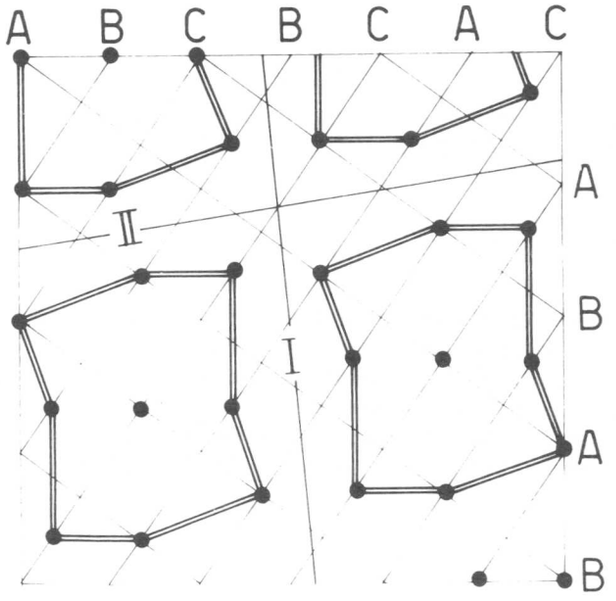

Fig.4:Projection of a $[010]_o$ plane in the 3R martensite. Atom rows in $[100]_o$ and $[001]_o$ normal to them. Two possible twin shear planes contain lines I and II, and $[010]_o$ normal to the projected plane.

with ABCBCACAB stacking, containing the $[001]_o$ and $[100]_o$ directions. Groups of atoms are joined by lines to show better the symmetry. The groups lie parallel to the lines denoted by I and II. Twinning occurs now by a displacement of the groups as a whole and an additional shuffle to restore the correct positions of the atoms within the group.

The twinning can occur on a plane containing line I or II in a direction parallel to them. The observed twinning plane with pole P_{II} is that which contains line II. The predicted angle between this twin plane normal and $[00\bar{1}]_o$ is 43.3°, in good agreement with the observed angle of 45° between $[00\bar{1}]_o$ and P_{II}. The calculated amount of twin shear of 0.105 is small, and therefore the orientation for which the markings disappear (and thus the shear direction) can be determined only with a large error margin.

Finally it is necessary to consider why the twins do not disappear on unloading, whereas the bands do. This behavior can easily be understood in terms of the model for the rubberlike behavior [3], since every atom pair is transformed into the same configuration during twinning; thus the total energy of the disordered pairs does not change, and consequently no additional driving force is created during twinning which would restore the original martensite variant.

In conclusion, therefore, it has been shown in this paper that rubber-like behavior in CuZnAl martensite depends strongly on the number of deformation cycles. This is due to the competitive formation of deformation twins that do not disappear with the stress and which prevent the martensite variant, responsable for the rubber-like behavior to be stress induced.

The presentation of this paper was made possible by
a grant from the Organization of American States
(Multinational Program for Physics).

References

[1] R.Rapacioli,M.Chandrasekaran,M.Ahlers and L.Delaey, in "Shape Memory Effects in Alloys", ed.J.Perkins,Plenum Press 1975
[2] G.Barcelo,R.Rapacioli and M.Ahlers, Scripta Met 12 (1978) 1069.
[3] M.Ahlers,G.Barcelo and R.Rapacioli, Scripta Met 12 (1978) 1075.
[4] M.O.Speidel and H.Warlimont, Z.Metallkde 59 (1968) 841
[5] H.Tas, L.Delaey and A.Deruyttere, Met.Trans 4 (1973) 2833

On the Mechanism of Reversible Shape Memory Effect in Cu-Zn-Al Alloys

Kazuyoshi Takezawa and Shin'ichi Sato

In the previous studies on the reversible shape memory effect in Cu-Zn-Al alloys, it has been verified that a planar structure consisting of α_1' and β_1' martensites is constructed after heating the specimen under constraint or by deforming it severely. The composite structure is expected to produce a special stress field by which the original β_1' martensite is induced on subsequent cooling.

In the present paper, the above mechanism is crystallographically examined by the phenomenological theory. The shape deformations due to the two-step transformation, $\beta_1 \rightarrow \beta_1' \rightarrow \alpha_1'$, and the reverse transformation, $\alpha_1' \rightarrow \beta_1'$, are formulated assuming a shear deformation on the close-packed planes in the second transformation, $\beta_1' \rightarrow \alpha_1'$. The numerical calculations using these formulae with the measured lattice parameters indicate that a β_1' martensite having different orientation (variant 2) from the original β_1' (variant 1) can be formed under the influence of the $\beta_1' \rightarrow \beta_1$ reverse transformation of the original one. It is also theoretically confirmed that around the retained α_1', with which the β_1' (variant 2) construct the composite structure, the stress field in a sense to produce the original β_1' martensite is reasonably formed.

I. Introduction

The reversible or two way shape memory effect(RSM) is closely related to the thermoelastic nature of martensitic transformation. The phenomenon has so far been found in Ni-Ti, Cu-Zn-Al-Ti, Cu-Zn-Ga, Ni-Al, Cu-Zn, Cu-Al-Zn and Cu-Zn-Al alloys. In most of the studies on these alloys the RSM were produced by the severe deformation. The present authors, on the other hand, have found that the RSM can also be generated by heating deformed β_1 specimens of Cu-Zn-Al alloy under constraint [1]. They have made a series of investigations on the RSM and have concluded that the following evidences are closely connected with the RSM[2, 3].

(i) The stress-induced transformation occurs in two steps, i.e., $\beta(B2) \rightarrow \beta_1'(9R) \rightarrow \alpha_1'(3R)$

(ii) The α_1' martensite, produced either by severe deformation or by heating under constraint, often retains in the matrix crystal upon unloading.

(iii) The retained α_1' martensite forms a composite structure with the β_1' martensite which has a different orientation (variant 2) from the original one (variant 1).

Department of Applied Physics, Faculty of Engineering, Hokkaido University, Sapporo, Japan

Because of the displacive nature of martensitic transformation, the shape deformation can be evaluated by the phenomenological theory assuming that the change in crystal strucutre directly reflects the macroscopic shape change during the transformation. Several workers[4-7] have already tried to make the phenomenological consideration on the β_1(B2 or DO_3)$\rightarrow\beta_1'$(9R or 18R) transformation. In the present study, following and extending one of the calculations by Saburi and Nenno[8], an attempt was made to calculate the shape changes due to the multi-step transformation, $\beta\rightarrow\beta_1'\rightarrow\alpha_1'\rightarrow\beta_1'$, and to understand how the composite structure is constructed and why the RSM appears.

II. Formulation and Calculation of Shape Change

The structural change and lattice correspondence in the $\beta_1\rightarrow\beta_1'\rightarrow\alpha_1'$ two-step transformation are represented in Fig. 1. The $\beta_1\rightarrow\beta_1'$ lattice distortion matrix $\mathbb{F}$ can be expressed by a product of the shear $\mathbb{S}(\beta_1\rightarrow\beta_1')$ on $(110)_{\beta_1}$ plane in $[\bar{1}10]_{\beta_1}$ direction and the lattice expansion or contraction $\mathbb{B}(\lambda_i,\ i=1\sim3)$. The shear $\mathbb{S}$ is expressed by the following equation

$$\mathbb{S}(\beta_1 \rightarrow \beta_1') = \mathbb{I} + (1 - 2x)g\mathbb{d}_g\mathbb{p}_g' \quad , \tag{1}$$

where x is the existing rate of AC stacking in β_1' structure in Fig. 1, $\mathbb{d}_g$ and $\mathbb{p}_g$ are the unit vectors in $[\bar{1}10]_{\beta_1}$ direction and in the direction normal to $(110)_{\beta_1}$, respectively, and g is the magnitude of shear.
So that,

$$\mathbb{F} = \mathbb{B}\mathbb{S} = \mathbb{B} + (1 - 2x)\lambda_1 g\mathbb{d}_g\mathbb{p}_g' \quad , \tag{2}$$

where λ_1 is the ratio of the lengths $[100]_{\beta_1'}$ and $[\bar{1}10]_{\beta_1}$. The magnitude of x will be determined by the condition that the hanit plane contains no distortion, i.e., $\det(\mathbb{F}'\mathbb{F} - \mathbb{I})=0$. Moreover, the continuity of material across the habit plane requires that the rigid body rotation $\mathbb{R}$, opposite to the rotation included in $\mathbb{F}$, is neccessary. Therefore, the net deformation in the $\beta_1\rightarrow\beta_1'$ transformation can be written as an invariant plane strain(IPS) as follows:

$$\mathbb{P}(\beta \rightarrow \beta_1') = \mathbb{R}\mathbb{F} = \mathbb{I} + m\mathbb{d}\mathbb{p}' \quad , \tag{3}$$

where $\mathbb{d}$ and $\mathbb{p}$ are the unit vectors in the direction of distortion and the normal to the plane of IPS, respectively, and m is the magnitude of shear. Using the relation $\mathbb{P}'\mathbb{P}=\mathbb{F}'\mathbb{F}$. one knows

$$\mathbb{p} = \frac{1}{\sqrt{2(\lambda_1^2\lambda_3^2-\lambda_2^2)}}\begin{bmatrix}\lambda_1\sqrt{\lambda_3^2-1}+\sqrt{\lambda_1-1}\\ \lambda_1\sqrt{\lambda_3^2-1}-\sqrt{\lambda_1^2-1}\\ \sqrt{2(1-\lambda_2^2)}\end{bmatrix}, \quad \mathbb{d} = \frac{1}{\sqrt{2(\lambda_1^2\lambda_3^2-\lambda_2^2)}}\begin{bmatrix}\lambda_2(\lambda_1\sqrt{\lambda_3^2-1}+\sqrt{\lambda_1^2-1})\\ \lambda_2(\lambda_1\sqrt{\lambda_3^2-1}-\sqrt{\lambda_1^2-1})\\ -\lambda_1\lambda_3\sqrt{2(1-\lambda_2^2)}\end{bmatrix},$$

$$\text{and} \quad m = \lambda_1\lambda_3-\lambda_2 \quad , \tag{4}$$

Under the assumption that the $\beta_1'\rightarrow\alpha_1'$ transformation proceeds as a simple shear on $(001)_{\beta_1'}$ plane in $[\bar{1}00]$ direction in Fig. 1, the lattice distortion can be expressed as

$$\mathbb{S}(\beta_1' \rightarrow \alpha_1') = \mathbb{I} + n\mathbb{d}_s\mathbb{p}_s' \quad , \tag{5}$$

where $\mathbb{d}_S$, $\mathbb{p}_S$, and n are similarly defined as before. Therefore, after the two-step transformation the net deformation will be expressed as follows

$$\mathbb{P}(\beta_1 \rightarrow \beta_1' \rightarrow \alpha_1') = \mathbb{S}(\beta_1' \rightarrow \alpha_1')\, \mathbb{P}(\beta_1 \rightarrow \beta_1') \quad . \tag{6}$$

The shear deformation due to the reverse transformation, $\alpha_1' \rightarrow \beta_1'$, will be described as the reciprocal of Equation (5). In this case the α_1' will be reverted to the previous β_1'. However, since the α_1' has fct structure, four variants of β_1' can possibly be produced during the reverse transformation. The deformation is written as

$$\mathbb{S}(\alpha_1' \rightarrow \beta_1') = \mathbb{I} + n\mathbb{d}_r\mathbb{p}_r' \tag{7}$$

where $\mathbb{d}_r$, $\mathbb{p}_r$ and n are similarly defined as before. Finally, the total shape deformation of multi-step transformation can be obtained by

$$\mathbb{P}(\beta_1 \rightarrow \beta_1' \rightarrow \alpha_1' \rightarrow \beta_1') = \mathbb{S}(\alpha_1' \rightarrow \beta_1')\, \mathbb{P}(\beta_1 \rightarrow \beta_1' \rightarrow \alpha_1') \quad . \tag{8}$$

Utilizing the measured values of lattice constant, i.e., a_o=2.9405Å for matrix crystal, A=4.462Å, B=2.658Å, C=19.23Å for β_1' martensite, and a_f=3.757A and C_f=3.884Å for fct α_1' martensite, the shape deformations for various transformation modes are calculated by the above equations. Table I shows the obtained values of $\mathbb{P}$ which correspond to the changes shown in Fig. 1. The possible shape changes caused by the $\beta_1 \rightarrow \beta_1'(i)$ transformations with i=1~8 which can be induced by elongation are shown in Table II. The total deformations due to the multi-step transformation $\beta_1 \rightarrow \beta_1'(1) \rightarrow \alpha_1'(1) \rightarrow \beta_1'(1,j)$ for j=a~d are calculated as in Table III.

III. Mechanism of the RSM

The experimental results so far obtained are summarized in Fig. 2. The RSM is always predominant where a composite structure is retained in the matrix crystal. We now discuss how this particular structure is produced as an origin of the RSM. Suppose that the $\beta_1'(1)$ is initially produced in β_1 and that the phase boundary AB moves to CD in Fig. 3 by the reverse transformation due to the various treatments in Fig. 2. The region ABCD should be deformed as follows:

$$\mathbb{P}\{\beta_1'(1) \rightarrow \beta_1\} = \mathbb{P}^{-1}\{\beta_1 \rightarrow \beta_1'(1)\} = \mathbb{I} - \frac{m}{1 - m\mathbb{p}'(1)\mathbb{d}(1)}\mathbb{d}(1)\mathbb{p}'(1). \tag{9}$$

So that, the retained $\alpha_1'(1)$ in $\beta_1'(1)$ such as A'B'C'D' in Fig. 3 is subjected to the effect of shape change in surroundings.

It is now worth noting that one obtains $\mathbb{p}_r(1,b) \simeq \mathbb{p}(1)$ and $-\mathbb{d}_r(1,b) \approx \mathbb{d}(1)$ as shown by * and ** in Table II and III, respectively. Moreover, the amount of shear in Equation(9) is close to and a little smaller than that for $\mathbb{S}\{\alpha_1'(1) \rightarrow \beta_1'(1,b)\}$. Accordingly, it is expected that a part of the region A'B'C'D' is reverted to $\beta_1'(1,b)$ and a composite structure is formed. Since it is also calculated that the crystal axes of $\beta_1'(1,b)$ coincide with those of $\beta_1'(2)$ within 2°, one may use $\beta_1'(2)$ instead of $\beta_1'(1,b)$.

In order to interprete the special stress field around the composite structure arrows indicating directions of shape deformation with respect to the original shape are written in Fig. 3. Although the horizontal arrows run through the composite structure, the vertical ones retain in $\alpha_1'(1)$. So taht, the stress field having a sense that it would produce the deformation $\mathbb{P}\{\beta_1 \rightarrow \beta_1'(1)\}$ in the matrix crystal near $\alpha_1'(1)$ will appear as shown by the dotted arrows. The stress field will produce $\beta_1'(1)$ on subsequent cooling and the RSM works as shown in Photo. 1(a) and (b).

The authors acknowledge partial support of this work by the Grant-in-aid for Co-operative Research by the Ministry of Education in Japan (Sōgō: 1977).

References

[1] K. Takezawa and S. Sato: Proc. 1st. JIM Intern. Sympo. "New Aspects of Martensitic Transformation", Kobe, (1976) 233
[2] K. Takezawa, K. Adachi and S. Sato: J. Japan Inst. Met., 43, (1979) No. 3, 229
[3] K. Takezawa, H. Sato, Y. Abe and S. Sato: J. Japan Inst. Met., 43, (1979), No. 3, 235
[4] I. Cornelis and C.M. Wayman: Acta Met., 22, (1974) 291, 301
[5] S. Kajiwara: Trans. Japan Inst. Met., 17, (1976) 435
[6] T. Saburi, S. Nenno, S. Kato and K. Takata: Less. Common. Met., 50, (1976) 223
[7] J. De Dos, E. Aernoudt and L. Delaey: Z. f. Metallk., 69, (1978) 438
[8] T. Saburi, S. Nenno: Scripta Met., 9, (1975) 887

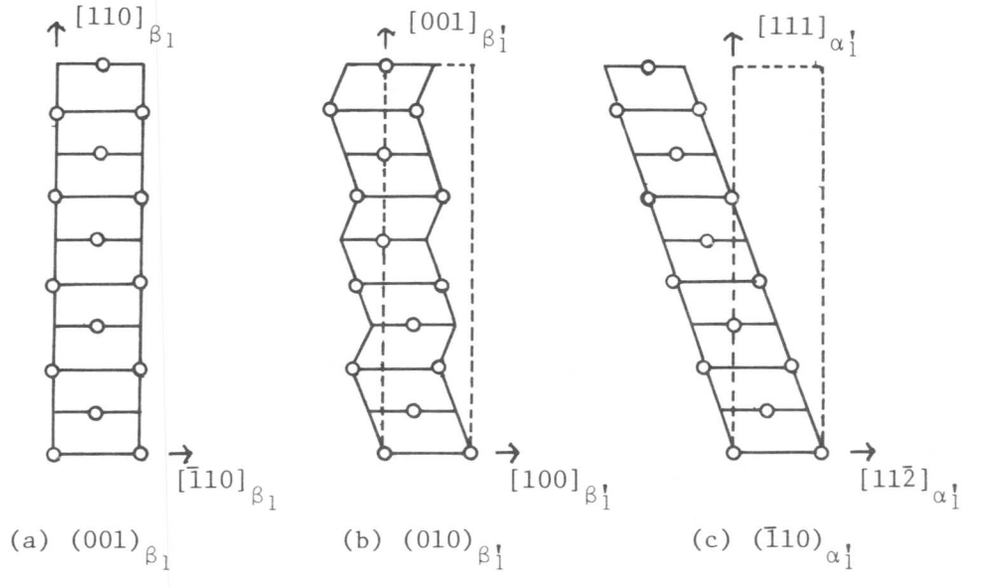

Fig. 1 Lattice correspondence between β_1 matrix(B2), β_1'(9R) and α_1'(fct or 3R) martensites.

Table I Calculated shape changes due to the $\beta_1 \rightarrow \beta_1' \rightarrow \alpha_1'$ transformation in Cu-Zn-Al alloy

	$\mathbb{P}(\beta_1 \rightarrow \beta_1')$			$\mathbb{p}$	$\mathbb{d}$	m
$\beta_1 \rightarrow \beta_1'$	1.0920	-0.0200	0.0871	0.7174	0.6485	
	-0.0200	1.0044	-0.0189	-0.1560	-0.1410	0.1978
	-0.1062	0.0231	0.8995	0.6790	-0.7481	
	$\mathbb{S}(\beta_1' \rightarrow \alpha_1')$			$\mathbb{p}_s$	$\mathbb{d}_s$	n
$\beta_1' \rightarrow \alpha_1'$	1.1062	0.1162	-0.0078	0.6736	0.7328	
	-0.0978	0.8929	0.0072	0.7375	-0.6751	0.2151
	-0.0123	-0.0135	1.0009	-0.0497	-0.0852	
	$\mathbb{P}(\beta_1 \rightarrow \beta_1' \rightarrow \alpha_1')$					
$\beta_1 \rightarrow \beta_1' \rightarrow \alpha_1'$	1.2065	0.0944	0.0871			
	-0.1254	0.8989	-0.0189			
	-0.1195	0.0098	0.8995			

Table II Values of $\mathbb{p}(i)$ and $\mathbb{d}(i)$ of possible stress-induced $\beta_1(i)$ variants produced by elongation. Eight variants show that the strain $\varepsilon = |\mathbb{P}\{\beta_1 \rightarrow \beta_1'(i)\} \cdot \mathbb{u}| - 1 > 0$ where the tensile direction $\mathbb{u}(u_1, u_2, u_3)$ satisfies the conditions $u_1 > |u_2| > |u_3|$, $u_2 < 0$ and $u_3 < 0$.

Variant i	$\mathbb{p}(i)$	$\mathbb{d}(i)$	Variant i	$\mathbb{p}(i)$	$\mathbb{d}(i)$	Variant i	$\mathbb{p}(i)$	$\mathbb{d}(i)$
1	*0.7174	* 0.6485	4	0.7174	0.6485	7	0.7174	0.6485
	-0.1560	-0.1410		0.1560	0.1410		-0.6790	0.7481
	0.6790	-0.7481		0.6790	-0.7481		0.1560	0.1410
2	0.7174	0.6485	5	0.7174	0.6485	8	0.7174	0.6485
	0.6790	-0.7481		-0.1560	-0.1410		0.1560	0.1410
	-0.1560	-0.1410		-0.6790	0.7481		-0.6790	0.7481
3	0.7174	0.6485	6	0.7174	0.6485			
	0.6790	-0.7481		-0.6790	0.7481			
	0.1560	0.1410		-0.1560	-0.1410			

Table III Possible four variants in the reverse transformation $\alpha_1'(1) \rightarrow \beta_1'(1, j)$. Total shape deformations due to the multi-step transformations, $\beta_1 \rightarrow \beta_1'(1) \rightarrow \alpha_1'(1) \rightarrow \beta_1'(1,j)$, are also tabulated.

Variant j	Shear in $\alpha_1'(1)$	$\mathbb{P}_r(1,j)$	$\mathbb{d}_r(1,j)$	$\mathbb{S}\{\alpha_1'(1) \rightarrow \beta_1'(1,j)\}$			$\mathbb{P}\{\beta_1 \rightarrow \beta_1'(1) \rightarrow \alpha_1'(1) \rightarrow \beta_1'(1,j)\}$		
a	(111) $[11\bar{2}]$	0.674	-0.733	0.894	-0.116	0.008	1.092	-0.020	0.087
		0.737	0.675	0.098	1.107	-0.007	-0.020	1.004	-0.019
		-0.050	0.085	0.012	0.014	0.999	-0.106	0.023	0.900
b	$(\bar{1}11)$ $[\bar{1}1\bar{2}]$	**0.667	*-0.738	0.894	0.012	-0.118	1.091	0.094	-0.028
		-0.078	0.070	0.010	0.999	0.012	-0.114	0.899	-0.008
		0.741	0.672	0.096	-0.011	1.107	-0.015	0.010	1.004
c	$(1\bar{1}1)$ $[1\bar{1}\bar{2}]$	0.512	-0.852	0.906	0.008	0.157	1.073	0.094	0.220
		-0.044	0.095	0.105	0.999	-0.018	-0.111	0.899	-0.034
		-0.858	-0.514	-0.056	0.005	1.095	-0.200	0.010	0.980
d	$(11\bar{1})$ $[112]$	-0.506	0.857	0.907	0.159	0.012	1.073	0.228	0.087
		0.860	0.510	-0.055	1.094	0.007	-0.205	0.979	-0.019
		0.067	-0.072	0.008	-0.013	0.999	-0.108	-0.002	0.900

(A) Heating under constraint (H.C.)

(a) Large-grained(bamboo) specimen

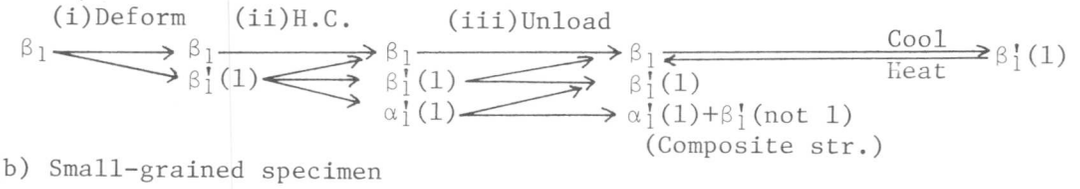

(b) Small-grained specimen

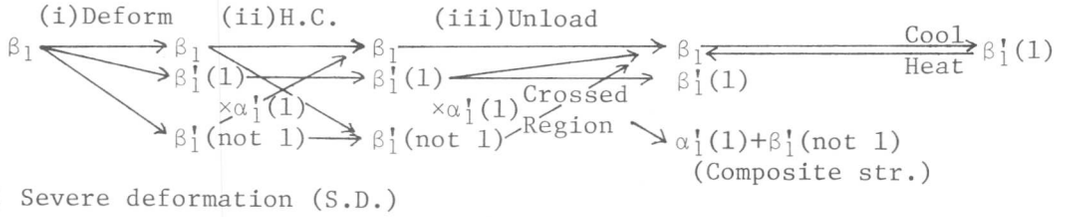

(B) Severe deformation (S.D.)

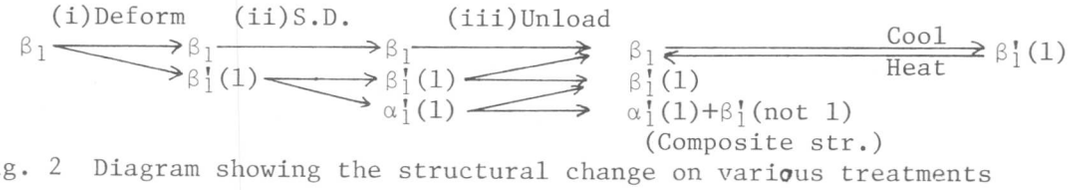

Fig. 2 Diagram showing the structural change on various treatments

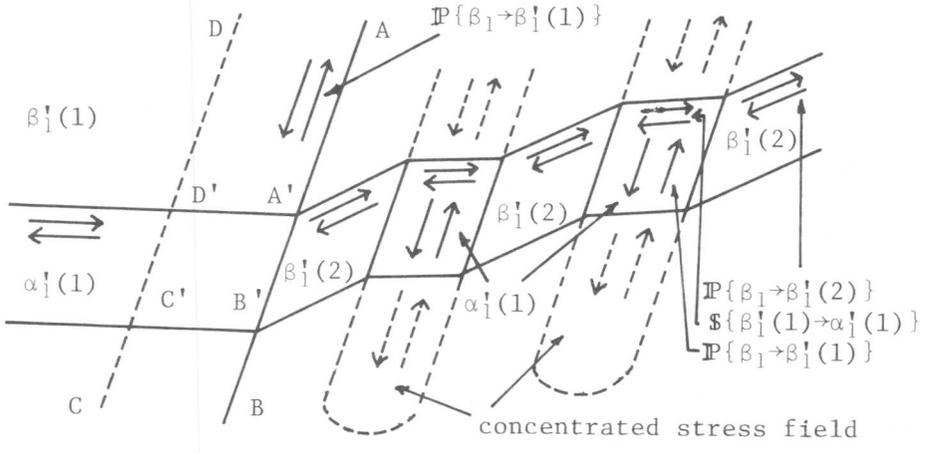

Fig. 3 Schematic representation of the reverse transformation $\alpha_1'(1) \rightarrow \beta_1'(2)$ induced by $\beta_1'(1) \rightarrow \beta_1$. The shape deformations and stress fields are also shown.

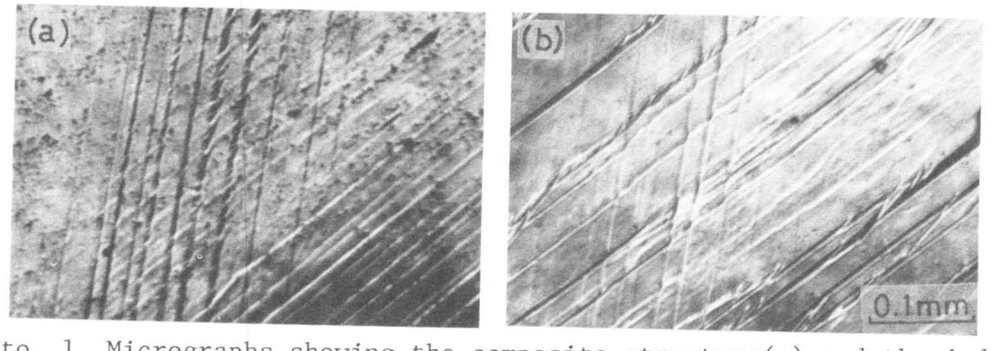

Photo. 1 Micrographs showing the composite structure(a) and the induced $\beta_1'(1)$ on subsequent cooling(b).

Effect of Applied Stress on the Character of Reversible Shape Memory in Cu-Zn-Al Alloy

Kazuyoshi Takezawa, Shoichi Edo and Shin'ichi Sato

As a basic investigation for industrial use of the reversible shape memory effect (RSM), the effect of applied stress on the shape change in Cu-Zn-Al alloy is studied. Polycrystalline ribbon specimens are heat-treated under constraint to produce the RSM. The shape changes on cooling and heating are then measured under bending load in opposite sense to the shape recovery. It is observed that the amount of shape recovery on cooling rapidly decreases as increasing applied stress. This can be interpreted by the formation of martensites which disturb the behavior of active martensites associated with the shape recovery. Upon heating, the decrease in shape recovery is not so remarkable as on cooling, because the martensites at low temperature are reverted to the original matrix crystal. As heating and cooling are repeated, the specimens are gradually yielded by applied stress to the shapes between which the RSM works. The origin of the gradual yielding is discussed in detail.

I. Introduction

The reversible shape change due to the appearance and disappearance of the stress-induced martensite (SIM) with temperature has been called the reversible shape memory effect (RSM). The phenomenon can be utilized as a conversion technique of low-grade thermal energy to mechanical or other usefull forms. The RSM alloy used as the energy conversion element will be obliged in thermal cycles under stress. The present work is undertaken for studying the behavior of SIM under the applied stress which disturbs the progress of transformation.

The RSM is known to be generated by the severe deformation or by a heat-treatment under constraint. The latter method [1] has an advantage that the amount of shape change can be controlled easier than the former. In this study the RSM was generated by the latter method in Cu-Zn-Al alloys.

II. Experimental Procedure

Ingots of Cu-39.0at%Zn-4.6at%Al alloy were prepared from 99.9%Cu, 99.9%Zn and 99.99%Al by melting at 1150°C in argon atmosphere. The ingots were hot-forged to 3~4 mm in thickness and then two kinds of specimens with different thickness, 0.3~0.5 mm and about 2 mm, were prepared for different modes of deformation used. These specimens were heat-treated for 5 min. at 870°C and quenched into water at room temperature. The M_s temperature was set to be at room temperature.

Department of Applied Physics, Faculty of Engineering, Hokkaido University, Sapporo, Japan.

Two modes of deformation, bending and tensile deformation, were used in the present work. The bending was performed by winding straight ribbon specimens with dimensions of about 100×20×0.3~0.5 mm on the side surface of a steel cylinder and binding it by a steel belt. The amount of deformation, called the initial strain ε_i, is defined by the strain on the surface of specimen calculated from the radius of the cylinder. The specimen wound on the cylinder was heated for 5 min. at 100°C and then the constraint was removed at room temperature. By this procedure, the RSM character was allowed to the specimen. The radius of curvature of specimen was measured at temperatures between which the RSM worked. The surface strains obtained from the measured radii at the high and low temperatures are designated by ε_P and ε_M, respectively. The difference between ε_P and ε_M, which is a measure of the amount of RSM, will be called the RSM strain, hereafter.

The specimens about 30×2×2 mm in dimension were extended by an Instron-type tensile testing machine. To produce the RSM, the specimen was first extended up to a fixed strain, called the initial strain, ε_i', then heated for 5 min. at 100°C without changing elongation. On the specimen which gained the RSM nature during the above treatment the gauge length was measured at the two temperatures by using an instrument for measuring small displacement with a differencial transformer. The RSM strain was obtained from the difference between measured ε_P' and ε_M', similarly as in the bending case.

A pulley and weight system was specially designed and constructed to measure the amount of RSM under the applied stress. A weight was set through a pulley at one end of the circularly bent RSM specimen, the other end being pinned. The displacement of the weight was measured at the two temperatures as before. Since the amount of the shape change obtained from these displacements is different from the RSM strain defined above, we call this amount the RSM value. Fig. 1 illustrates the experimental procedure used in the measurement of shape change under bending load during the thermal cycles between two temperatures. First, starting from the measurement of length $L_h(0)$ at the high temparature, which is taken as the standard length, the measurements of length $L_{h,\ell}(0,-W)$ were successively made in the order, a→b→c→d as indicated by arrows in Fig. 1. After a series of measurements, one can calculate the RSM value, ε_h, by using Equation(1)*. The other series of measurements in the order a→b'→c'→d'→a in Fig. 1 will give the other RSM value ε_c by Equation(2).

$$\varepsilon_h = \{L_h(-W) - L_\ell(-W)\}/\, L_h(0) \qquad (1)$$

$$\varepsilon_c = \{L_\ell(W) - L_h(W)\}/\, L_h(0) \qquad (2)$$

---

* $\varepsilon_h^*=\{L_h(-W)-L_\ell(0)\}/L_h(0)$ and $\varepsilon_c^*=\{L_\ell(W)-L_h(0)\}/L_h(0)$ were used as the RSM values instead of (1) and (2), respectively, when $L_\ell(-W)$ were difficult to measure. The sign of W is defined as shown in Fig. 1 for convenience.

III. Results and Discussion

(1) The RSM without applied stress

Photo. 1 shows examples indicating the character of the RSM with no load in the Cu-Zn-Al alloy. The specimens with 0.45 mm in thickness were heat-treated under the bending forces so as to give the initial strains ε_i=0.6, 0.9 and 1.8%. The shape changes between 95°C and -20°C are shown in the photograph with the obtained values of ε_P and ε_M. A large number of measurements as in Photo. 1 drew a conclusion that ε_P and ε_M linearly increase as ε_i. One more important character of the RSM recognized in the bending experiment is that the shape changes are homogeneous on the whole surface of specimen.

The RSM strain was examined for specimens with different thickness and no remarkable change in the RSM strain was obtained in the bending case. Since the β_1 grain size of the alloy is usually as large as the thickness of the specimen, it is to be said that the RSM strain produced by bending is less dependent on the grain size. However, it was observed, on the other hand, that the RSM strain produced by the tensile deformation was strongly sensitive to the crosssectional area of the specimen.

Detectable RSM tensile strains were usually observed for specimens having more than several β_1 grains in the crosssectional area but not observed for specimens having a few β_1 grains. Moreover, the scattering in data on the RSM strain was observed for large-grained specimens. There was a tendency that the smaller the grain size was, the smaller value of ε'_i the RSM started from. These phenomena will be understood that the only particular grains were selectively and favourably deformed for the RSM in the case of tensile deformation.

(2) The RSM with applied stress

Fig. 2 shows an example of the results obtained from the measurements for a Cu-Zn-Al polycrystalline ribbon with a dimension of 100×20×0.5 mm. The high and low temperatures were set to 60°C and -10°C, respectively. The RSM value ε^*_h on heating with W=0 was about 0.43 which decreased gradually with increasing the load and reached to 0 at about 350gr. The RSM value ε^*_c on cooling, on the other hand, rapidly decreased from 0.4 to 0 as one sees on the right hand side in Fig. 2. The load at which the RSM was suppressed was only about 60gr. So that, it is unfortunately doublfull to expect enough powers of conversion upon cooling when the alloy is used as the energy conversion element.

It has been observed that the amount of RSM without load decreases during early 20~30 thermal cycles and reaches to a constant value after 50~100 cycles [2]. A similar experiment was performed under load in the present work. The cycle of a→b→c→d→a was repeated more than 50 times with a weight of 200gr. The obtained yielding behaviors in $L_h(0)$ and $L_h(-W)$ are represented in Fig. 3. At the low temperature the weight of 200gr was enough to deform the specimen severely to $L_e(-W)=0$ and since the severe deformation was thought to be the origin of the yielding phenomenon in Fig. 3, the following test with a stopper for preventing the severe deformation at the low temperature was undertaken. A result is shown in Fig. 4 which indicates a less decrease in $L_h(0)$ and $L_h(-W)$ on the thermal cycles. The result that the heatings at 100°C after 20 thermal cycles recovered the original form was also observed as shown by

the arrows in Fig. 4.

(3) Metallography

It is not difficult to understand that the rapid decrease in ε_C^* by the load will be due to the formation of martensites which disturb the behavior of the active martensite associated with the RSM. This point was metallographically verified as shown in Photo. 2.

As far as the yielding phenomenon in Fig. 3 is concerned, it was supposed that the β_1' martensite having the same orientation as that associated with the RSM retained after increasing the thermal cycles. To check if this supposition is true, a metallographic examination was made as follows: A specimen, having the bending RSM character, was first electropolished at 60°C to remove the surface relieves due to the retained martensite (Photo. 3(a)). The polished specimen was then treated by the thermal cycles of 40 times. After this treatment a large number of relieves were observed as in Photo. 3(b). The structure in this photograph is similar to the composite structure which produces the RSM so far observed in our laboratory [3~5]. The reason why the structure increases in number after increasing cycles will be that the specimen was subjected to the severe deformation at the low temperature and also that the deformation at the high temperature gave a similar effect as the heat-treatment under constraint [1,3~5]

The authors acknowledge partial support of this work by the Grant-in-aid for Co-operative Research by the Ministry of Education in Japan (Sōgō: 1978).

References

[1] K. Takezawa and S. Sato: Proc. 1st. Intern. Sympo. "New Aspects of Martensitic Transformation", Kobe, (1976) 233
[2] T. Saburi and S. Nenno: Scripta Met., 8, (1974) 1363
[3] K. Takezawa, K. Adachi and S. Sato: J. Japan Inst. Met., 43, (1979) 229
[4] K. Takezawa, H. Sato, Y. Abe and S. Sato: J. Japan Inst. Met., 43, (1979) 235
[5] K. Takezawa and S. Sato: Proc. ICOMAT-79, Boston, (1979)

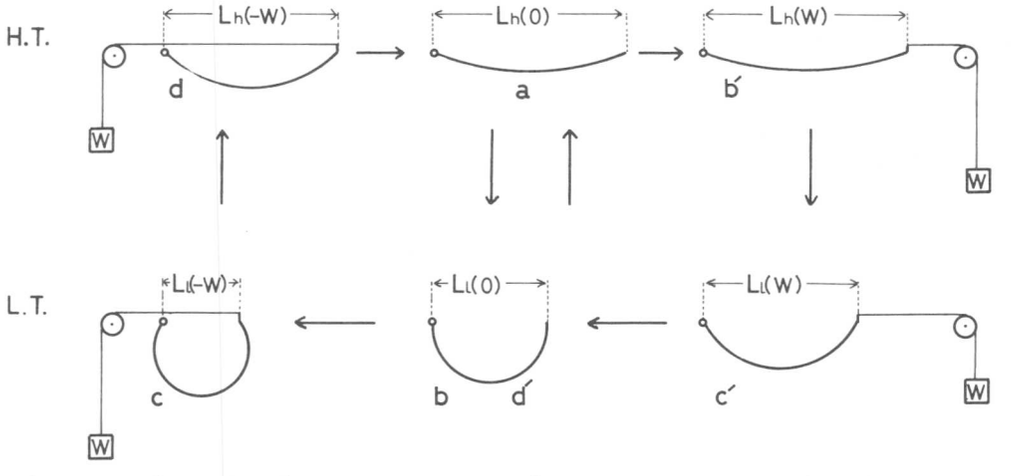

Fig. 1 Procedure in the measurement of RSM character under load

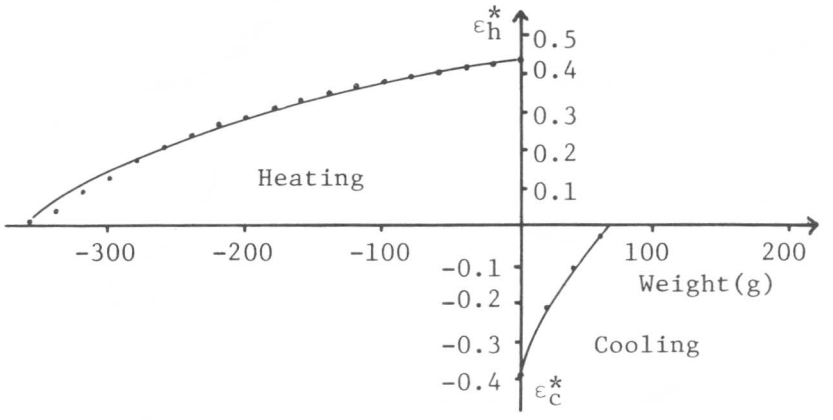

Fig. 2 Variations of ε_h^* and ε_c^* with W. Temperatures: 60°C, -10°C

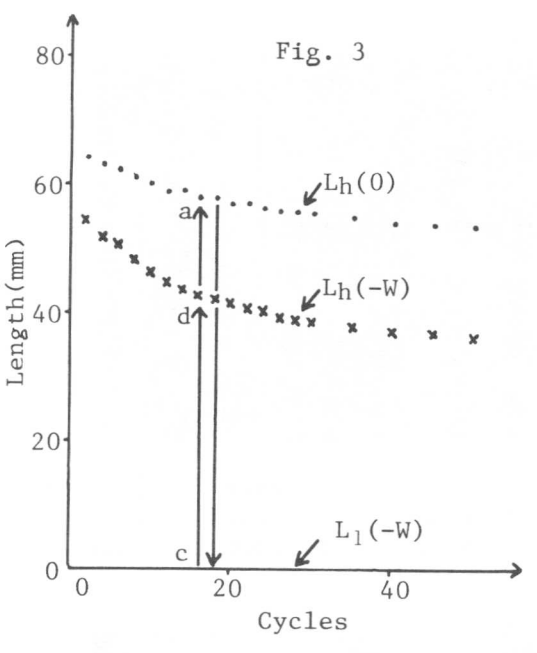

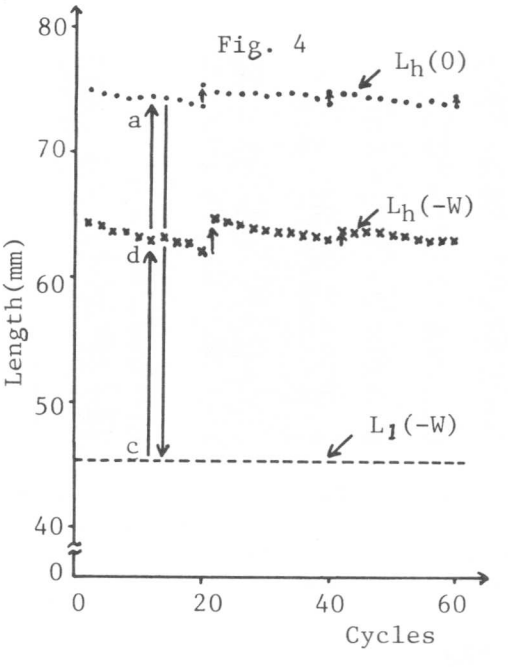

Fig. 3 Effect of the thermal cycles on the RSM character.
Temperatures: 60°C, -10°C Weight: 200gr

Fig. 4 Effect of the thermal cycles on the RSM character. The severe deformation was prevented by fixing $L_\ell(-W)$=45mm.
Temperatures: 60°C, -10°C Weight: 200gr

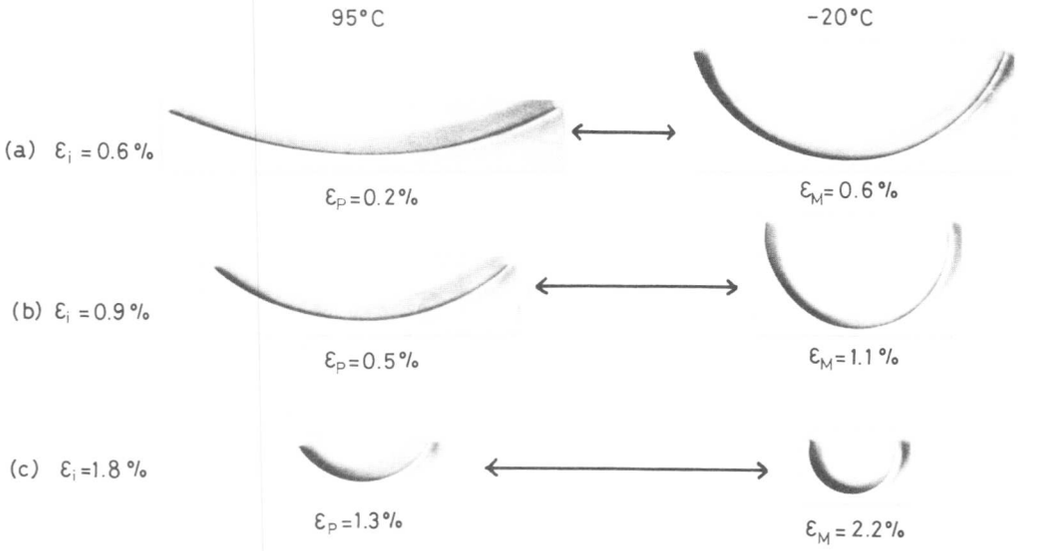

Photo. 1 Macroscopic shape changes of the Cu-Zn-Al RSM alloys.
ε_i: Initial strains ε_p: Surface strains at 95°C
ε_M: Surface strains at -20°C

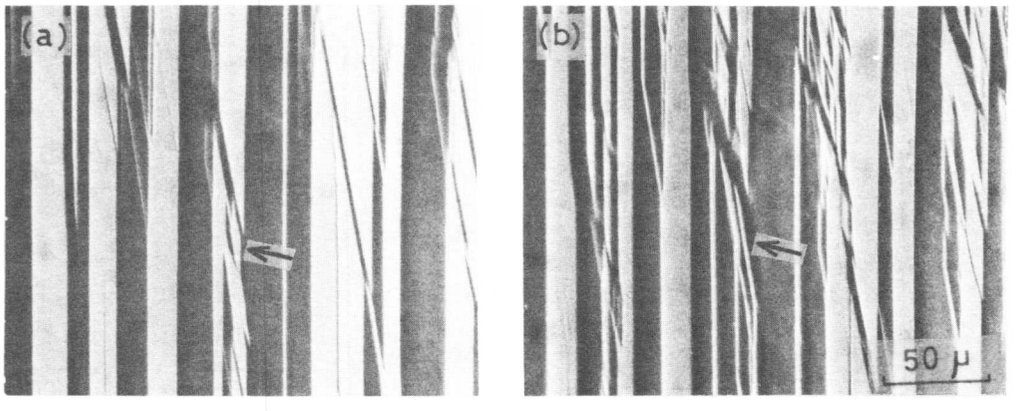

Photo. 2 Metallographs showing a difference in appearance of β_1' martensites at the low temperauture. (a) without load (b) under load
The arrow indicates the place where a different β_1' is formed by the applied stress.

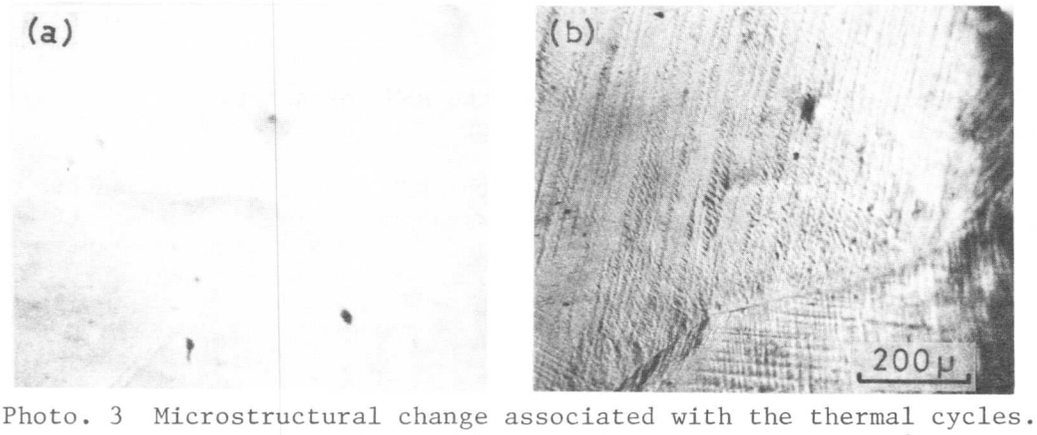

Photo. 3 Microstructural change associated with the thermal cycles.
(a) Electropolished surface (b) After 40 cycles between 60°C and -10°C

Shape Memory Effect and Pseudoelasticity in Fe-Al Alloys.

J.Y. Guédou and J. Rieu

Tensile, compressive and shear tests have been carried out at room temperature on Fe_3Al oriented single crystals and have revealed a pseudoelastic behaviour. Moreover, after deformation at 77K, a shape memory effect is observed on the same alloys when reheated to room temperature. Such phenomena are usually related to a reversible martensitic transformation. However, no transformation of this kind has been observed in Fe_3Al. The investigation of the influence of various parameters, especially the crystallographic orientation, suggests a twinning-untwinning mechanism, as for Fe-Be alloys. Nevertheless, the phenomenon is more complex for Fe_3Al since the deformation does not only occur by twinning, but mainly by glide. The formation of micro-twins whose stability depends upon the degree of order of the alloy, enables us to account for the observations which have been made on Fe_3Al.

This system appears to be a rather unusual case of pseudoelasticity in which no stress-induced martensitic transformation is involved, but where a twinning mechanism in the ordered state seems to operate.

I. Introduction

Martensitic transformations are characterized by a diffusionless phase change. Thermoelastic martensites are induced both by lowering the temperature and by applying an external stress ; they disappear when the temperature is increased or when the stress is removed and may give rise to macroscopic mechanical effects, such as the shape memory effect or the pseudoelasticity [1]. This type of mechanical behaviour can be related to the following processes [2] :

- Superelasticity due to a reversible thermoelastic martensitic transformation ;
- Rubberlike behaviour in internally twinned martensites ;
- Bending pseudoelasticity where a reorientation of the twins takes place according to the direction of the applied stress ;
- Pseudoelastic behaviour which results from an unstable twinning mechanism in an ordered alloy.

The difference between martensite and fine twins is not always obvious. The simplest type of martensite, i.e. coherent martensite, involves a lattice change which is very close to that of a twinning deformation [3]. Certain thermoelastic martensitic transformations (e.g. TiNi) could be described by the formation of microtwins resulting from an inhomogeneous shear [4]. Likewise, mechanical twinning might be considered as the result of a double stress-induced martensitic transformation [5].

Ecole Nationale Supérieure des Mines, 158 Cours Fauriel
42023 Saint-Etienne Cédex, FRANCE

We have observed deformation twinning, a shape memory effect and pseudoelasticity on single crystals Fe-Al alloys [6, 7, 8]. However, no martensitic transformation could be detected between 77K and 300K. The mechanical behaviour has therefore been explained by an unstable twinning mechanism [8], similar to the process that accounts for pseudoelasticity in Fe-Be alloys [9]. Tension-compression cycling tests have confirmed the above conclusion. The mechanical behaviour of Fe-Al alloys is indeed analogous to that of several metals and alloys which exhibit twinning-untwinning on reversing the stress direction.

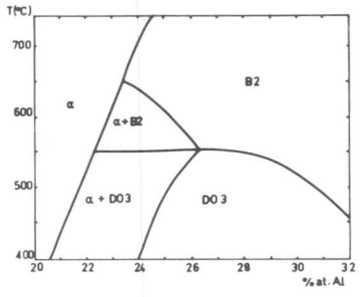

Fig. 1 : Fe-Al phase diagram [10].

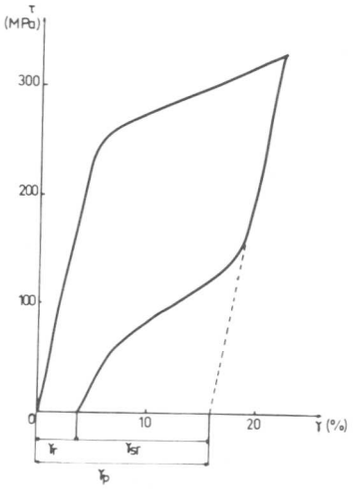

Fig. 2 : Stress-Strain curve of 23 at. % Al sheared specimen

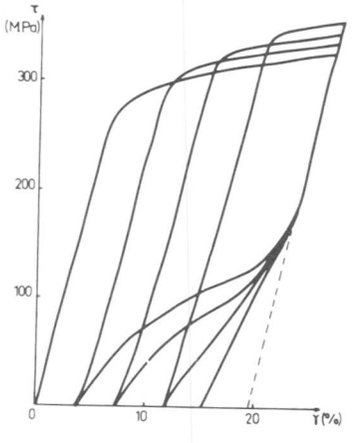

Fig. 3 : Effect of repeated deformation on pseudoelasticity

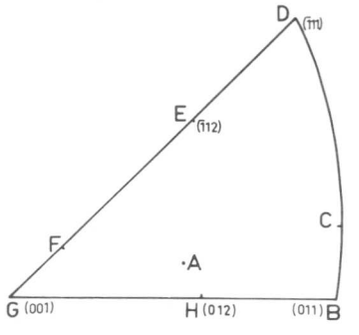

Fig. 4 : Stress axis orientation

II. Experimental Procedure

The shear and compression tests which demonstrate the pseudoelasticity and the shape memory effect on single crystals Fe-Al alloys, have been previously described [6, 7, 8]. Tension-compression cycling tests have been carried out at room temperature on an Instron machine at a nominal strain rate of 10^{-3} s^{-1}. The specimens are oriented parallelepipedic single crystals of 4 x 4 mm^2 section and 40 mm length. They are heat treated [8] to obtain the equilibrium state α, α + DO_3 or DO_3 [10] according to the aluminium content (Fig. 1), i.e. a vacuum anneal for 6 h at 900°C followed by slow cooling at 50°C/h. Two threaded heads were then brazed onto the ends of the sample. The tests were performed in a device [11] using liquid metal grips to obtain a correct alignment.

III. Results of Shear and Compression Tests

A. Pseudoelastic behaviour.

Shear tests on DO_3 or α + DO_3 single crystals containing 21 to 26 at. % Al [6, 7], have shown a pseudoelastic behaviour (Fig. 2) at room temperature. Pseudoelasticity is not observed when the specimen is quenched from 600°C to the B_2 ordered state, but appears after tempering at a temperature below 500°C which restores the DO_3 order. In addition, on repeated loading between constant deformations, the plastic recovery decreases at every cycle (Fig. 3).

Compression tests [8] confirm those results and also show that the pseudoelastic behaviour is only observed when the compression axis favours twinning, i.e. A, B, C and H in Fig. 4. However, the amount of the plastic recovery may be reduced by the possibility of multiple slip (for instance orientation B). Pseudoelasticity does not occur when twins are formed after large deformations [8].

B. Shape memory effect.

At 77K, no pseudoelasticity is observed, whatever the orientation and the composition of the Fe-Al alloy. On reheating to room temperature the α + DO_3 or DO_3 specimens (21 to 26 at. % Al) which have been compressed and unloaded at 77K, the plastic deformation is partially recovered in a continuous manner (Fig. 5). This phenomenon is similar to the shape memory effect observed on many alloys exhibiting a thermoelastic martensitic transformation [12]. However, an isothermal anneal at 200 K on sheared and unloaded specimens at 77K seems to indicate that the plastic recovery amount does not depend on temperature. Resistivity measurements between 77K and 300K have shown no particular inflexion on the ρ (T) curve, although in alloys in which a thermoelastic martensitic transformation occurs, changes in slope on the ρ (T) curve may be used to indicate such transformation [13, 14].

Another property of quenched B_2 alloys (24 at. % Al) compressed at 77K, is that they only deform by twinning. Moreover, on unloading, the deformation is partially recovered by untwinning [15] (Fig. 6). The twins developped during low temperature deformation are unstable on account of the ordered state, as in Fe-Be alloys [9].

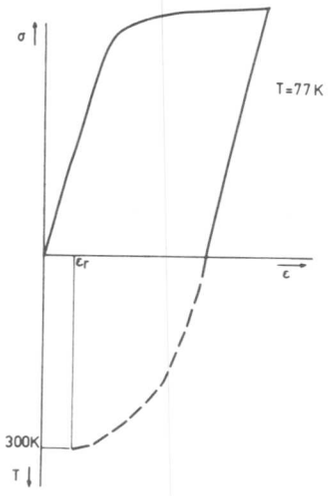

Fig. 5 : Shape memory effect on 23 at. % Al compressed specimen

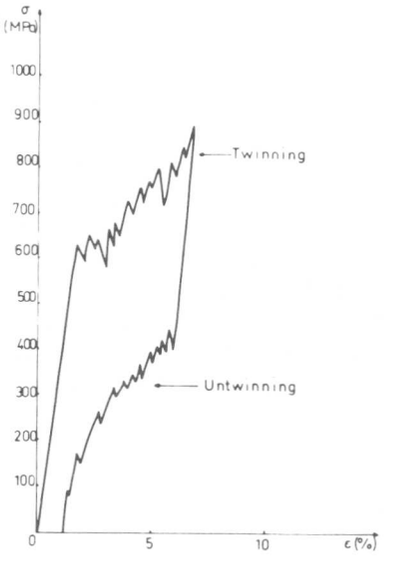

Fig. 6 : Stress-strain curve of 24 at. % Al-B_2 compressed specimen (77K)

IV. Results of Tension-Compression Cycling Tests

These tests have been carried out at room temperature on single crystals strained along the A, F or H axis (Fig. 4) which are favourably oriented for twinning in tension. Figure 7 shows the stress-strain curves σ (ε) as a function of the aluminium content of the alloy. The disordered α samples (17 to 21 at. % Al) do not exhibit pseudoelasticity in tension, but part of the deformation is recovered when the direction of the stress is reversed (Fig. 7 a and b). At higher aluminium content (23 at. % Al) the pseudoelastic behaviour is observed both in tension and in compression for A orientation which favours twinning in the two directions (Fig. 7c). The DO_3 perfectly ordered alloys (27 at. % Al) do not exhibit pseudoelasticity[3](Fig. 7 d).

The results are similar to those which have been obtained on polycristalline Fe-Al alloys containing 18 at. % Al [16]. A reversible glide and twinning process is suggested to account for these observations. Nevertheless, we pointed out that a mechanism involving glide is unlikely to explain the pseudoelastic behaviour in Fe-Al alloys [17].

V. Discussion

The tension-compression cycling tests confirm the mechanism that we have proposed to account for pseudoelasticity in partially ordered Fe-Al alloys [8] : microtwins are formed under stress but are unstable for a sufficiently ordered state and so they untwin when the stress is removed [8, 15]. The DO_3 ordered alloys (> 25 at. % Al) do not twin since perfect order impedes this deformation mode (Fig. 7 d), so the pseudoelastic behaviour is not observed in these alloys. At lower aluminium contents

(23 at. % Al) twinning is possible but the twins are unstable and destabilize on unloading (Fig. 7 c). Finally, the disordered alloys (17 to 21 at. % Al) deform easily by twinning and the twins are stable in the disordered state. To induce untwinning, it is necessary to reverse the stress direction (Fig. 7 a and b). An analogous phenomenon is observed on many metals and alloys such as Zn [18], Mg [19], Ti [20]. Nimonic 80 [21] and 80 Ni - 20 Nb [22].

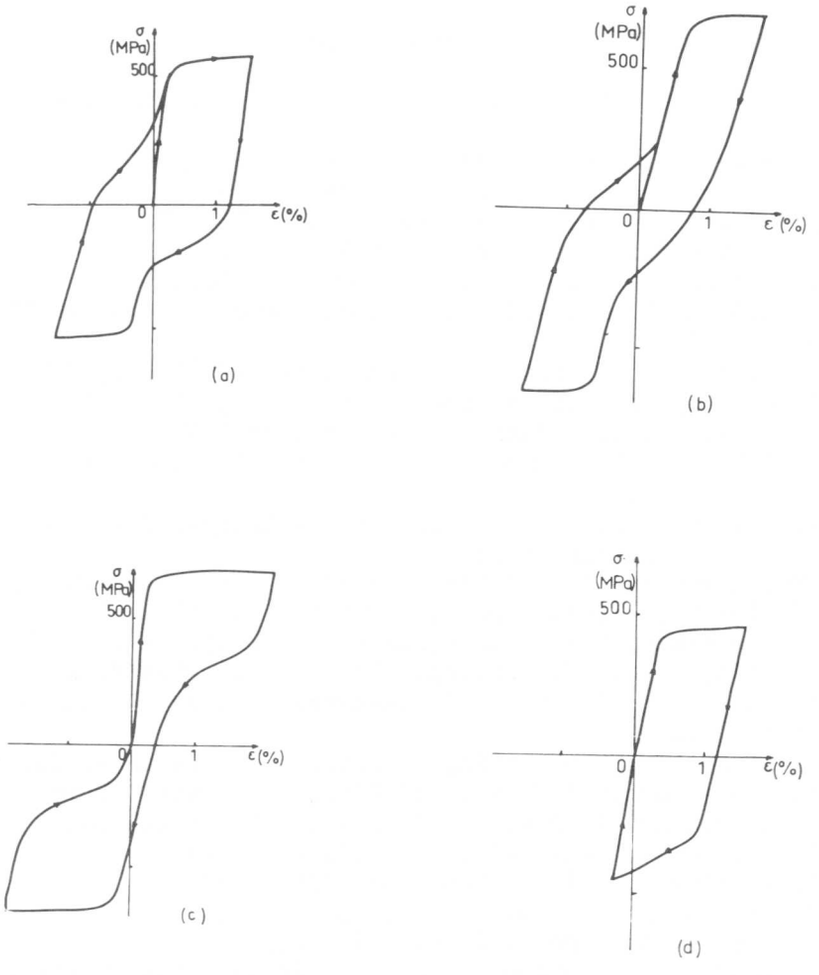

Fig. 7 : Tension-compression curves
a) 17 at. % Al (α) - H axis. b) 21 at. % Al ($\alpha + DO_3$) - F axis
c) 24 at. % Al ($\alpha + DO_3$) - A axis d) 27 at. % Al (DO_3) - A axis

In the cases where the pseudoelastic behaviour is observed (favourable crystallographic orientation, aluminium content, temperature...) pseudoelasticity seems to be related to the formation of reversible microtwins rather than to a martensitic transformation. Likewise, the shape memory effect which is measured after straining at low temperature, appears to be related to a destabilization of the twins nucleated at 77K (where they are stable), as the temperature is increased. The formation of twins in ordered alloys is thermodynamically possible [23], but the twins are then unstable. Neverthess, their very small dimension is presumed to impede their detailed characterization, which is currently under study by means of in-situ deformation tests in a high voltage microscope.

References

[1] L. Delaey, R.V. Krishnan, H. Tas and H. Warlimont : J. Mat. Sci., 9 (1974), 1521.
[2] K. Otsuka, H. Sakamoto and K. Shimizu : Scripta Met., 11 (1977), 41.
[3] J.W. Christian : J. Phys., 35 (1974), C 7-65.
[4] F.E. Wang : J. Appl. Phys., 40 (1972), 92 ; 97.
[5] R.J. Wasilewski : Met. Trans., 8 A (1977), 391.
[6] J.Y. Guédou, M. Paliard and J. Rieu : Scripta Met., 10 (1976), 631.
[7] J.Y. Guédou, M. Paliard and J. Rieu : Proceedings of ICSMA 4, Nancy, (1976), 1209.
[8] J.Y. Guédou and J. Rieu : Scripta Met., 12 (1978), 927.
[9] G.F. Bolling and R.H. Richman : Acta Met., 13 (1965), 709.
[10] S.M. Allen and J.W. Cahn : Acta Met., 23 (1975), 1017.
[11] T. Woillez, B. Gingembre, J. Driver and J. Rieu : Mém. Sci. Rev. Mét., 74 (1977), 583.
[12] C.M. Wayman : Shape Memory Effects in Alloys, Ed. by J. Perkins, Plemum Press, New York, (1975), 1.
[13] S. Vatanayon and R.F. Hehemann : Shape Memory Effects in Alloys, Ed. by J. Perkins, Plenum Press, New York, (1975), 115.
[14] D.S. Lieberman, M.A. Schmerling and R.W. Karz : Shape Memory Effects in Alloys, Ed. by J. Perkins, Plenum Press, New York, (1975), 203.
[15] J.Y. Guédou and J. Rieu : Proceedings of ICSMA 5, Aachen, (1979) to be published.
[16] R.J. Asaro : Work hardening in Tension and Fatigue, Ed. by A.W. Thompson, Metallurgical Society of AIME, Cincinnati, Ohio, (1975), 206.
[17] J.Y. Guédou and J. Rieu : C.R. Acad. Sci. Paris, 286 (1978), 327.
[18] D.C. Jillson : Trans. AIME, 188 (1950), 1009.
[19] R.L. Woolley : J. inst. Met., 83 (1954), 57.
[20] A.T. Churchman : J. Inst. Met., 83 (1954), 39.
[21] R.J. Asaro : Acta Met., 23 (1975), 1255.
[22] P.R. Bhowal, K.M. Prewo and A.J. Mc Evily : Met. Trans., 9 A (1978), 747.
[23] J.W. Cahn : Acta Met., 25 (1977), 1021.

Martensitic transformations in γ - Mn alloys and shape memory effect.

Vintaikin E.Z., Litvin D.F., Udovenko V.A., Shcherbedinskij G.V.+

In γ - Mn alloys martensitic transformations take place which are caused by antiferromagnetic ordering of Mn atoms. Results of investigations of Mn - Cu, Mn - Fe, Mn - Ni, Mn - Ge, Mn - Ga made it possible to divide them in three groups. The first is characterised by the coinsidence of Neel temperature (T_N) and the temperature of martensitic transformation (M_S) at which fcc structure transforms into fct structure with $c/a < 1$.

For the alloys belonging to the second group $M_S < T_N$ and the fct structure is characterised by $c/a > 1$.

In the intermediate narrow concentration fields alloys exist where rhombic structure (R) is formed and the chain of martensitic transformations can take place: fcc→ fct-($c/a < 1$) → R.

Specific features of the martensitic transformations in γ - Mn alloys are very small hysteresis and formation of twin structure with boundaries along {110} . Due to these features shape memory effect has its peculiarities. In γ - Mn alloys shape recovery is not complete at all degrees of deformation, and two - way memory effect can be clearly observed, i.e. shape change takes place both during the direct and reverse transformations. Two - way memory effect appears due to the oriented stresses caused by the ingomogenions local contributions of twinning and slip mechanism to the plastic deformation of the alloy.

From among the four crystallograghy modifications of pure manganese, the fcc structure (γ - Mn) is stable in the temperature range from 1079 to 1143 °C. When melting manganese with certain elements - stabilizers of the fcc structure (Cu, Ni, Fe, Ge, Ga, Pd, Au ets.) γ - phase can be fixed by quenching in water. Typical for the primary solid solution of γ - Mn is the existence of low - temperature phase transformation leading to the lattice symmetry descends from cubic to tetragonal (fcc → fct). By its external manifestations this transformation is a diffusionless martensitic one. There occurs a relief on the surface., there are temperature points of the start and

+ Centr. Res. Inst. of Ferr. Met. USSR.

finish of the transformation, and as result there arises an internal twinning structure with boundaries along {110}. By its nature this transformation is magnetic, and connected with an antiferromagnetic ordering of magnetic moment of manganese atoms.

On the basis of the data available in literature [1 - 6] and the results our investigations [7 - 13] , all the γ - Mn alloys can be broken down into three classes. The first class involves alloys with Neel's temperature (T_N) coinciding with that of the martensitic transformation (M_S). The transformation temperatures for Mn - Cu, Mn -Ga, Mn - Ge alloys are represented in Fig.1 belonging to this class. A tetragonal structure with an axial ratio $c/a < 1$ arises as a result of that transformation. The magnetic structure presented in Fig.2a, let us see that magnetic moments are directed along the tetragonal axis.

The second class alloys have martensitic temperature lower than Neel's point and martensitic structure with $c/a > 1$. As is seen in Fig.3, the Mn - Fe alloys containing small amouts of alloying additives are ascribed to the first class. When raising the alloying additive content a transition of the Mn - Fe alloys into the second class observed. The atomic magnetic moments of manganese are perpendicular to the tetragonal axis and oriented along one of the two axes a (Fig.2c). The first and second class alloys are separated in the phase diagram by the alloy region of the transition compositions (the third class) possessing a orthorhombic symmetry at room temperature. The atomic magnetic moments of manganese alloys lying in this region are oriented along the axis which corresponds to the least orthorhombic cell parameter (Fig.2b). With an increase in temperature the concentration boundaries of region III narrows so that the transition chain takes place: orthorhombic → fct (with $c/a < 1$) → fcc. The alloys of the second class between T_N and M_S show a cubic structure. However, the diffractional pictures are characterised by the broadening of lines 200, 220, 311, ets. (i.e. the lines which are split during the tetragonal structure formation), which points to a tetragonal distortion. The ordering of the magnetic moments parallel to axis a causes distortion of the lattice due to the difference in the a and c parameters (Fig. 2c). The direction of axes a and c is likely chaotic at small supercooling relatively T_N (a local order of displacement), but under substantial supercooling ordering of these displacement takes place and a tetragonal structure with $c/a > 1$ arises.

Our investigations show that the local atomic order has an influence on the martensitic transformation. For instance the tempering of Mn - Ga and Mn - Ge alloys induces an local range atomic ordering and correspondingly a decrease in the number of the neighbouring Mn - Mn pairs, which leads to the suppression of the martensitic transfor-

nation. The tempering of Mn - Cu alloys, leading to clustering, stimulates this transformation. These facts give evidence for determining role of the magnetic interaction of manganese atoms in γ - Mn alloys.

The above circumstance is due to a variety of specific peculiarities of martensitic transformation in γ - Mn alloys distinguishing them from the classical martensitic alloys. First of all one should note the extraordinarily small hysteresis of transformation. The points M_s and A_f (as well as M_f and A_s) coincide practically in all the transforming γ - Mn alloys. The transformation embraces at once the whole volume of the crystal in the vicinity of M_s temperature. With further cooling one can observe a smooth increas in the degree of tetragonal distortion (1 - c/a) which takes place according to the law close to that of variation of the magneticity of tetragonal antiferromagnetic sublattice. It should be noted that in Mn-Ge and Mn - Ga alloys with small a content of alloying additives this dependence has a jump in the vicinity of M_s (Fig.4) characteristic of phase transition of first order. With increasing of the alloy additive content the jump decreases to the very small value, i.e. the phase transformation becomes close to the transformation of the second kind. The behavioure of the third class alloys is quite peculiar. Fig.5 shows the gradual change of the lattice parameters in the course of the martensitic transformations in the third class alloys.

The behaviour of the martensitic transformations in γ - Mn alloys determines the feature of the shape memory effect in them. The temperature change in the form of the Mn - 15,8% Cu (1 class)quenched alloy plate with a deformed bend at room temperature is shown in Fig.6. When the temperature is falling (interval 1) the plate spontaneously deforms in the direction coinciding with the sign of preliminary plastic deformation. With in temperature rising (interval 2) the plate bends in the opposite direction; last deformation is known as the form recovering. At $T = M_s$ the restoration of form practically ceases, the restitution of the deformation comprising $\sim 60\%$ of the initial deformation. With decreasing in temperature the plate deforms spontaneously tending to reach the form which was made at room temperature. With further cyclic variation of temperature no matter how many times it has been made the bending of the plate is reversible along curve 3 with a very small hysteresis ($\sim 1^{\circ}$).

The available structural data allow one to understand the mechanism of the phenomenon. A deformation at the room temperature proceeds by means two mechanism: twinning and ordinary slipping, which have a different local contribution. Upon heating a local deformation by twinning anneals while deformation by slipping does not anneal. As a result the partial form recovering proceeds and the orienting microstresses arise in the sample. When the cooling occurs

these form a texturic martensite and a sample shape is changed in opposite direction.

The character of the shape memory effect described is assigned to all the γ- Mn first class alloys. However in alloys with a jump in the tetragonality degree, the restoration and reversible deformation in the vicinity of M_s occur sharply.

The character of the shape memory effect in γ- Mn second class alloys is some differentiated. According to Fig.7 we observe here a recovering and a subsequent reversible non - hysteresis deformation. The peculiarity of these alloys lies in the fact that upon heating the change in the form goes on up to T_N which is higher than M_s.

In the third class alloys one observes a quality new phenomenon: "a sign - variable reversible deformation" (Fig.8). During the first heating a usual incomplete restoration of the shape is seen to take place, whereas in the subsequent cooling and heating cycles a non - hysteresis deformation occurs, a chang in the effect sign taking place. The temperature of the sign variation corresponds to transition temperature of the fct ($c/a < 1$) to a orthorhombic phase.

References

[1] R.S. Dean, E.V. Potter, I.R. Long, R.W. Huber: Trans. ASM., 34 (1945), 465.

[2] H. Uchishiba: J. Phys. Soc. Japan, 31 (1971), 436.

[3] H. Uchishiba, T. Hori, J. Nakagawa: J. Phys. Soc. Japan, 30, (1970), 792.

[4] N. Cowlam, G. Al-Shahery: Physica, 86-88B,(1977),267.

[5] N. Honda, Y. Tanji, Y. Nakagawa: J. Phys. Soc. Japan, 41, (1976), 1931.

[6] T. Yamaoka: J. Phys. Soc. Japan, 36, (1974), 445.

[7] А.И.Бичинашвили,Е.З.Винтайкин,Д.Ф.Литвин,В.А.Удовенко: Физика металлов и металловед.,41,(1976),130.

[8] Е.З.Винтайкин,В.А.Удовенко,В.Б.Дмитриев,А.И.Бичинашвили Сб."Проблемы металловед.и физ.металлов",в.3,(1976),48.

[9] Е.З.Винтайкин,В.А.Удовенко,Л.Д.Гогуа;Известия вузов "Физика",№7,(1978),146.

[10] Е.З.Винтайкин,В.А.Удовенко,С.Ю.Макушев,Д.Ф.Литвин: Физика металлов и металловед.,45,(1978),8407

[11] Е.З.Винтайкин,В.А.Удовенко,А.И.Бичинашвили,Д.Ф.Литвин: Доклады АН СССР,222,(1975),322.

[12] Е.З.Винтайкин,В.М.Сахно,В.А.Удовенко:Физика металлов и металловед.,46,(1978),641.

[13] Е.З.Винтайкин,В.А.Удовенко,Л.Д.Гогуа:Доклады АН СССР 234,(1977),1309.

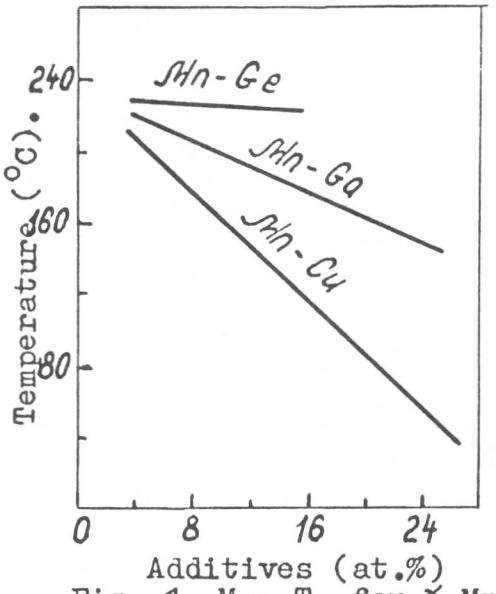

Fig. 1. $M_s = T_N$ for γ-Mn alloys (I^s class).

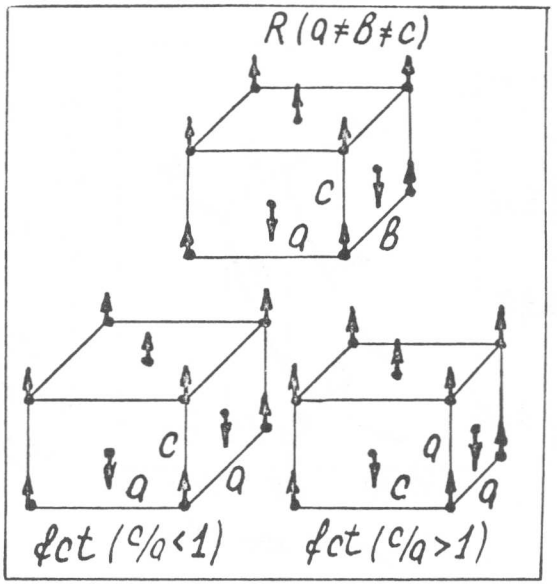

Fig. 2. The magnetic structure in γ-Mn alloys.

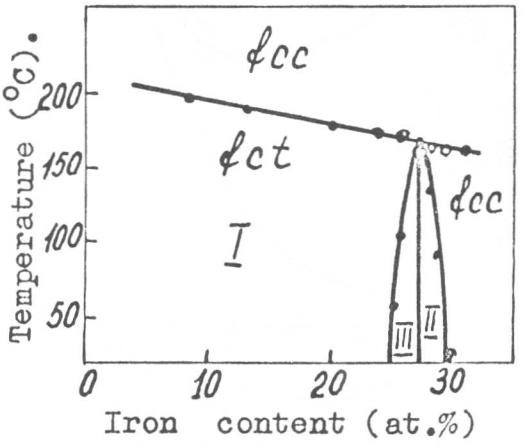

Fig. 3. The phase diagram for Mn - Fe.

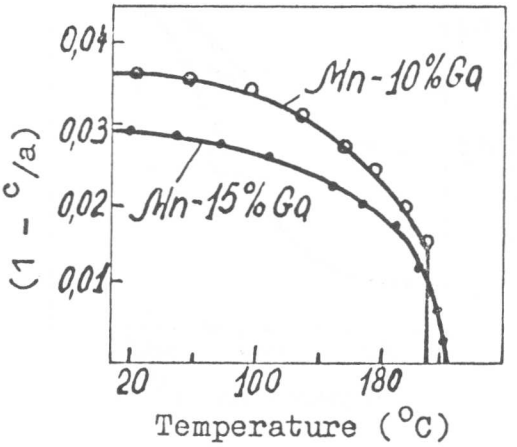

Fig. 4. The temperature dependency of $(1-c/a)$ for Mn - Ga.

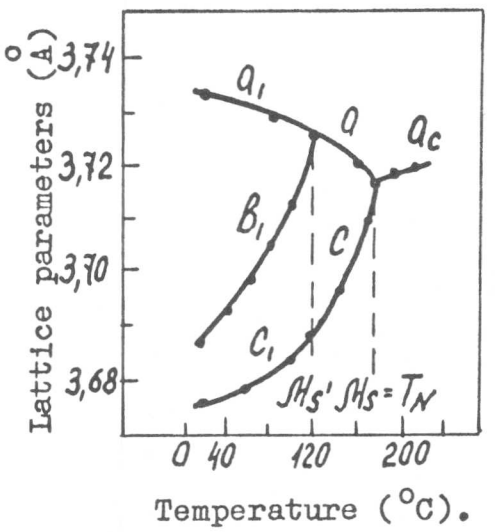

Fig. 5. The temperature dependency of lattice parameters for Mn - 15%Ni.

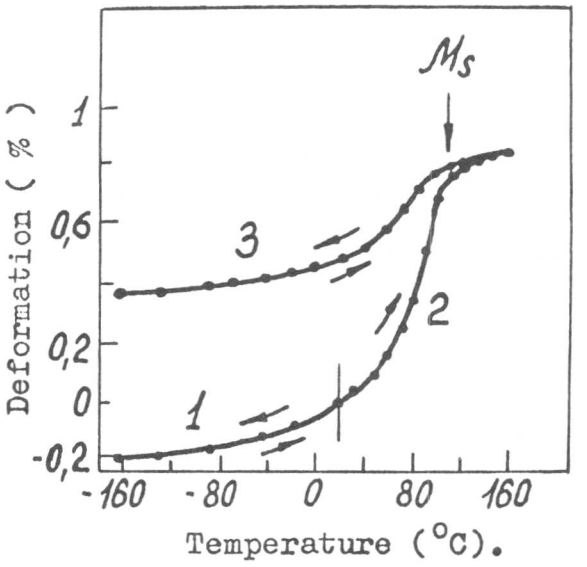

Fig. 6. The shape memory effect in Mn - 15,8% Cu (I class).

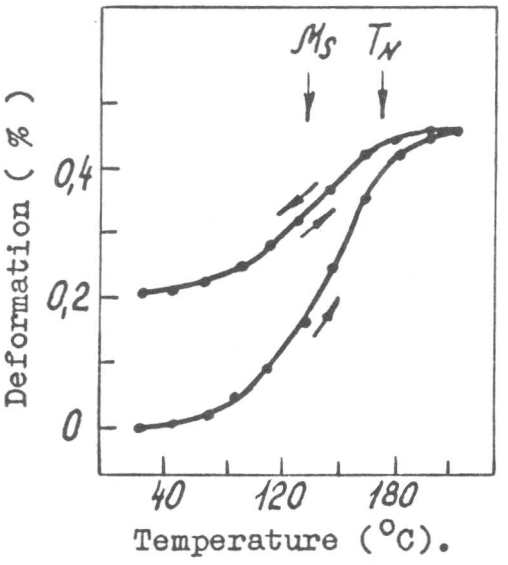

Fig. 7. The shape memory effect in Mn - 17% Ni (II class).

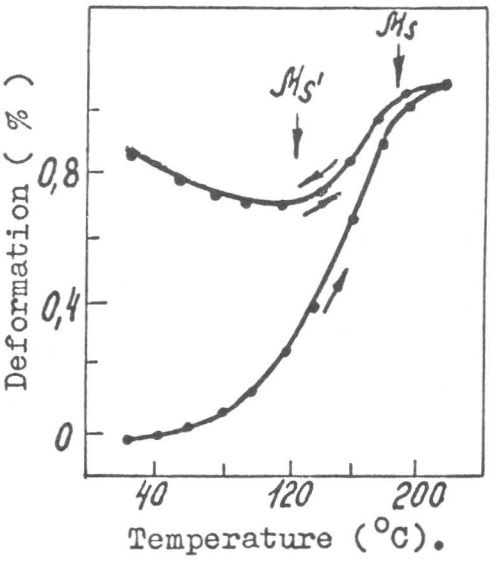

Fig. 8. The shape memory effect in Mn - 15%Ni (III class).

Martensitic Phase Transformation in Shape-memory Alloys

A. A. Golestaneh

This paper describes isothermal studies of the shape-recovery phenomenon, stress-strain behavior, electrical resistivity and thermoelectric power associated with the martensite-parent phase reaction in the Ni-Ti shape-memory alloys. The energy-balance equation that links the reaction kinetics with the strain energy change during the "cooling-deforming and heating" cycle is analyzed. The strain range in which the Clausius-Clapeyron equation satisfactorily describes this reaction is determined. A large change in the Young's modulus of the specimen is found to be associated with the M↔P reaction. A hysteresis loop in the resistivity-temperature plot is found and related to the anomaly in the athermal resistivity changes during cyclic M↔P↔M transformation. An explanation for the resistivity anomaly is offered. The M structure is found to be electrically negative relative to the P structure. A thermal emf of $\gtrsim$0.12 mV is found at the M-P interface.

I. Introduction

The purpose of the present paper is to report on several features of martensitic transformation in Nitinol alloys [1], a subgroup of the shape-memory (SM) alloys. The overall objective is to correlate the kinetics of this reaction with the parameters that characterize the material structure and with the thermodynamic parameters temperature, stress, and strain (T, σ and ε). The martensitic transformation is known to exhibit a marked sensitivity to internal stresses and, at least for Nitinol alloys, to material composition [2]. Also, the heat-transfer coefficient between the specimen and the cold reservoir (CR) or hot reservoir (HR) affects the kinetics of the shape-recovery phenomenon (SRP). To analyze these effects we have performed isothermal and isobaric experiments involving (T, σ, ε) and time t. The cooling and heating medium is water, or water plus some antifreeze substance for T either below 0°C or above 100°C. The phenomena under study are the SRP, variation of Young's modulus and electrical resistivity, and generation of thermoelectric power. Because of the technological interest in Nitinol and because of some anomalies observed in the martensite (M)-parent (P) phase reaction in these alloys, our initial studies have utilized a Ti-Ni binary alloy of 50-50 composition. The generalization of our results requires study of other binary and ternary Nitinol alloys as well as other SM materials. Because single-crystal Nitinol specimens are difficult to prepare and too expensive for practical applications, we have used polycrystalline specimens. The best isothermal test results are obtained with a wire specimen of 0.5 to

---

Materials Science Division, Argonne National Laboratory, Argonne, IL 60439, USA.

1 mm dia. The specimens are trained to have a particular form (either straight or curved with a desired radius). Inasmuch as the accurate chemical analysis of Nitinol is difficult and expensive, we characterize our specimens in terms of the M→P transition temperature T_o, the SR critical temperature T_C, and the temperature spreads $\pm\Delta T_o$ and $\pm\Delta T_C$, which will be defined below.

For discussion of the experimental data we use the following notations. The quench-induced martensite under zero external stress will be called γ_1', while the stress-induced martensite will be called β_1'. The P phase will be designated β_1. Since our specimens are in ordered states and we are considering only reactions in which the ordering is conserved, we will henceforth omit the subscript 1. We will refer to the martensitic transformation as the M→P or P→M reaction.

II. The Thermomechanical Energy Equation Associated with Martensitic Transformation

We recall that shape recovery (SR) in the SM alloys is energetic and is accompanied by forces which depend on the specimen geometry and the resistance encountered. Since the magnitude and direction of the SR force are difficult to evaluate directly, we will consider the energy-balance equation that governs the SRP. The SRP is associated with the β' martensite structure, and the energy source for this phenomenon is the latent heat of the $\beta' \rightarrow \beta$ transformation $\Delta H_{\beta'\beta}$ (henceforth ΔH). For a closed martensitic transformation M→P→M (which does not change the geometrical or structural configuration of the specimen), the Gibbs free-energy evaluation yields the energy-balance equation [3, 4]

$$\alpha\delta\Delta H = W_o(T_H) - W_i(T_L) \quad . \tag{1}$$

Here δ is the material density, W_i is the energy required for specimen deformation at temperature $T_L < T_C$, W_o is the mechanical energy recovered in the $\beta' \rightarrow \beta$ transformation at temperature $T_H > T_C$, and α is a coefficient which relates the energy of the SR to the fraction of the M→P transformation completed. In an energetic SR, α represents the portion of the γ' martensite which transforms via the channel

$$\gamma' \rightarrow \beta' \rightarrow \beta \tag{2}$$

and not the direct $\gamma' \rightarrow \beta$ channel [3, 4]. Reaction (2) can occur, by the so-called "reshuffling" process, because of the instability (soft mode) of the γ' martensite under the combined influence of temperature and applied stress. The coefficient α, which is always less than unity and on the order of 0.15 for binary Nitinol alloys [4], is a function of material structural parameters in addition to temperature and initial material strain, ε, and applied stress.

To evaluate α we have conducted a series of isothermal experiments. Figure 1 shows a series of isothermal stress-strain (σ-ε) tests conducted at temperatures from 20 to 105°C, a range which encompasses

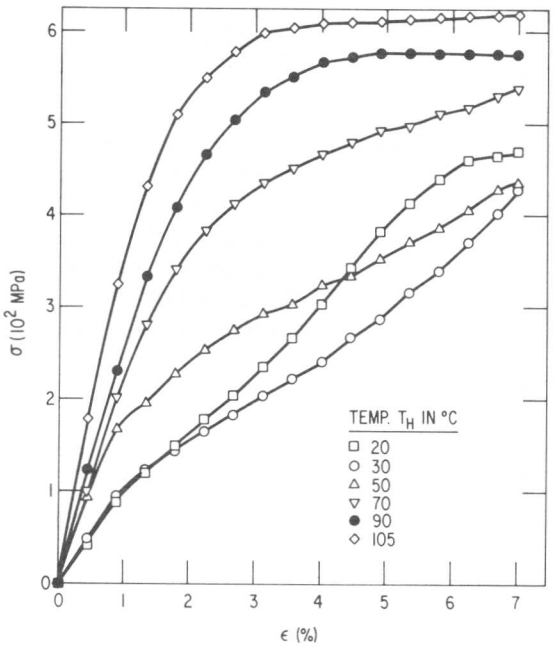

Fig. 1. Isothermally obtained stress-strain (σ-ε) curves for a Nitinol wire specimen (1 mm dia x 56 mm) with $T_C \approx 33 \pm 7$°C.

the T_C ($\approx$ 40°C) of our specimen. Figure 2 shows the results of transient tests in which the specimen is strained to a certain level and its temperature is then rapidly increased from T_L to T_H. A quantity of interest is

$$\Sigma = \sigma_r(T_H) - \sigma_i(T_L) \ , \tag{3}$$

where σ_r and σ_i are, respectively, the recovery and initial stresses in the specimen. This Σ, which can be obtained from the transient curves in Fig. 2, is close to the stress difference measured in isothermal σ-ε tests (shown in Fig. 1). From the variation of the Σ value versus ε shown in Fig. 3, it is seen that for ε within the range 1.5-3.5% in our specimen, one may write

$$W_o - W_i = \frac{1}{2}\,\varepsilon_o^2\,\Delta E(T_H, T_L) + \Sigma\varepsilon \approx \Sigma\varepsilon \ . \tag{4}$$

Here ΔE is the change in the Young's modulus of the specimen due to the M$\leftrightarrow$P transition, and ε_o is the elastic strain limit in the specimen. By combining Eqs. (1) and (3), we obtain

$$\Sigma\varepsilon \simeq \alpha\delta\Delta H \ . \tag{5}$$

The form of this equation is identical to the integrated Clausius-Clapeyron (CC) equation [5]

$$\Sigma\varepsilon = \delta\Delta H \ln\left(\frac{T_H}{T_C}\right) \qquad \text{for } T_H \lesssim A_f \ , \tag{6}$$

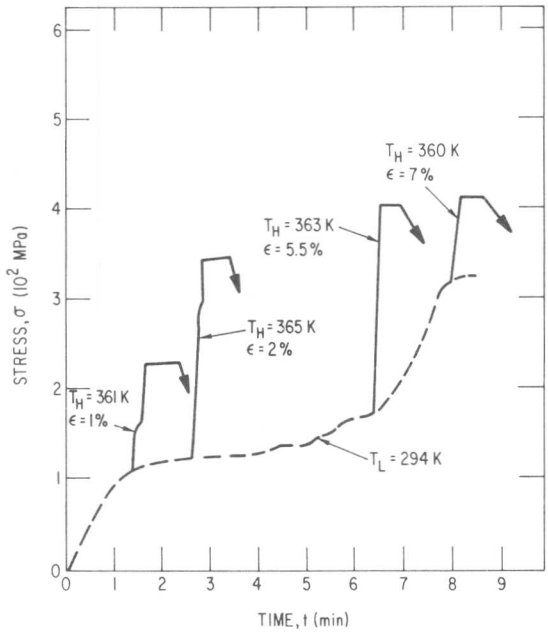

Fig. 2. Transient (σ-ε) response of a Nitinol wire specimen subjected to rapid temperature changes.

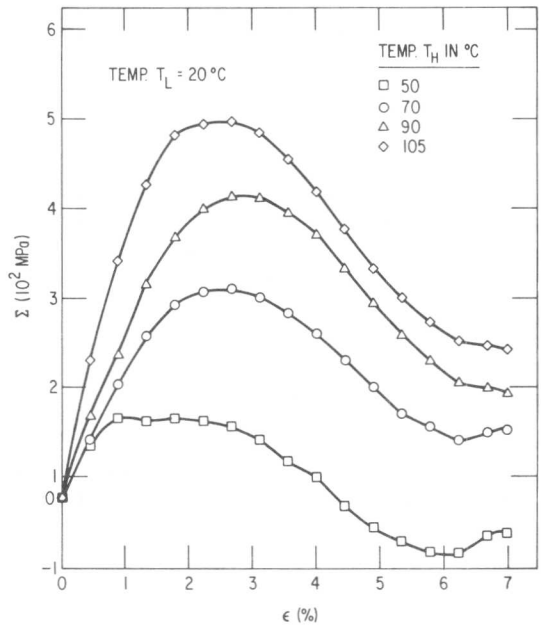

Fig. 3. Variation of $\Sigma = \sigma_r(T_H) - \sigma_i(T_L)$ with strain ε at various temperatures.

Using the data of Fig. 3, we have verified that in the range $1.5\% < \varepsilon < 3.5\%$, and for $T_L \gtrsim 0$ to 20°C, the Σ data vary fairly linearly with $\ln T_H/T_C$. The slope of this line gives, according to Eq. (6), $\Delta H = 1.2\text{-}2.8$ cal/g ($\delta = 6.3$ g/cm^3 for Nitinol alloys), which is close to $\Delta H = 1.57\text{-}2.4$ cal/g obtained previously by calorimetry [6]. This result indicates the ε range in which the CC [7] equation can be used satisfactorily. In this range Eqs. (1) and (6) give the maximum value of α, as

$$\alpha_o = \ln\left(\frac{T_H}{T_C}\right) \qquad \text{for } 1.5\% < \varepsilon < 3.5\%,\ T_H \lesssim A_f \ . \tag{7}$$

For our Nitinol alloy specimen, which has $T_C \gtrsim 313$ K and $T_H = 360$ K, Eq. (7) gives $\alpha_o = 0.140$.

To summarize the above results, (a) the CC equation is applicable in the strain range that corresponds to the bulk of the M→P transition, and (b) the coefficient α in the energy-balance equation for the above ε range depends logarithmically on T_H and T_C. It should be noted that the energetic SR depends on α and t. However, the experimental data on the SR strain ε_r in a uniaxial system fit the expression

$$\varepsilon_r = \varepsilon_i \left\{1 - \left[\exp -\left(\frac{t}{\tau}\right)^{1/2}\right]\right\} \tag{8}$$

where ε_i is the maximum shape recovery and τ is a time constant, dependent on T_H, T_C, and ΔT_C, which arises as the result of structural inhomogeneity, the external stresses exerted on the specimen, and the heat transfer rate between the specimen and its heating medium. The factor τ is a measure of the internal friction in the specimen; thus it depends on the material structural parameters. For our annealed specimen undergoing a free SR in water, τ is about 10^{-1} sec for T_H between A_s and A_f, and it becomes much larger in the presence of a constraint stress that exceeds the σ value for a given T_H (shown in Fig. 1).

To see the effect of the grain size on α_o, we reevaluate the energy-balance equation (1) for a given grain within the specimen. For this we recall one of the conditions for the occurrence of a complete SR in an SM element, which is the conservation of the mass of the individual grains during the cooling-deformation and heating of the specimen. Thus at the onset of the SR of a grain with, say, γ' structure, volume v, and surface area s, we have

$$v\Delta W_v - s\Delta W_s = 0 \ . \tag{9}$$

Here ΔW_v and ΔW_s are, respectively, the averaged volume and surface energy densities of the grain, which appear as a result of the grain, which appear as a result of the heating of the specimen to temperature T_H. In a specimen for which a uniaxial stress is dominant

(e.g., a long, thin wire), we have $\Delta W_V = \Sigma\varepsilon$, and $\Delta W_S \propto \Sigma\varepsilon$. Thus, assuming all grains in the specimen have more or less the same size and are uniformly distributed, Eqs. (6) and (9) give

$$T_\sigma = T_C \left[1 + \frac{6N^{1/2}}{\delta d} \frac{\Delta W_s}{\Delta H} \right]. \tag{10}$$

Here $T_\sigma = T_H$ is the SR critical temperature corresponding to a given set of Σ and ε values, d is the average diameter of the specimen cross section, and N is the average number of grains in the cross section. Equation (10) shows that T_σ increases with d^{-1} (as reported in Ref. 8 and seen in Fig. 5 below) and with $N^{1/2}$.

III. The SRP and Other Features of the Martensitic Transformation

It is understood that the direct $\gamma' \rightarrow \beta$ transition does not directly contribute to the SRP, and that the $\beta' \rightarrow \beta$ transformation does not coincide with the SR behavior with respect to time or temperature. It is reasonable to assume that the M↦P reaction begins earlier than the SR, since the reaction must overcome the internal friction and stresses before the SR can start. Isothermal tests show that in the existing SM alloys under zero stress, there is a temperature T_C^- below which no SR occurs, and a temperature T_C^+ above which a complete SR occurs; the spread, $\pm\Delta T_C$, of T_C is defined by the expression $2\Delta T_C = T_C^+ - T_C^-$. One would expect $T_C^- \geq M_s$ and $T_C^+ \geq A_s$, but T_C cannot be evaluated in terms of the usual M and A temperatures, which are not themselves well defined and measurable. Rather, T_C may be determined for a thin wire by carefully deforming the specimen to a certain degree (at a temperature at which no SR can occur), quenching it in an HR at a constant temperature, and measuring the fraction of the SR. The test results in Fig. 4 show that T_C and ΔT_C depend on the specimen size and structure, with ΔT_C ranging from $\sim$7 to 15°C.

To relate the temperature T_C to the M↦P transition temperature T_o, we have studied other isothermal phenomena. The investigation of those features that are associated with the $\gamma' \rightleftarrows \beta$ reactions under zero stress is reported in the present work. The effect of the applied stress, which elicits the $\beta' \rightleftarrows \beta$ reactions, will be presented in a separate article.

(a) Study of the Young's modulus of the material. One of the striking observations in the pattern of the σ-ε curves describing the M↦P reaction is the substantial variation of Young's modulus and other elastic constants with T [9]. Study of Young's modulus in a polycrystalline wire specimen by the sonic technique is difficult and expensive. A major problem is that to maintain a constant and uniform temperature, the specimen has to be thin, a feature which makes it unsuitable for the sonic tests. We have therefore carried out arranged conventional stress-strain measurements, using a 1-mm-dia x 56 mm wire for which a uniaxial stress can be assumed. The specimen is surrounded by water, the temperature of which can be changed at a controlled rate. A fixed strain below 0.4%, which is well within the

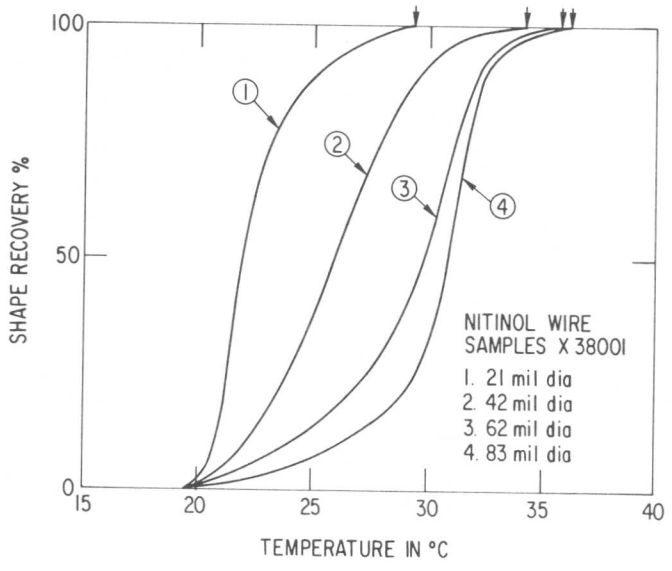

Fig. 4. Fractional shape recovery versus temperature.

elastic state of the Nitinol material, is applied to the specimen, and the variation of σ with T is recorded. At fixed $\varepsilon \leq 0.4\%$, $\Delta\sigma$ is related to ΔE by

$$\Delta E = \frac{1}{\varepsilon} \Delta\sigma \ . \tag{11a}$$

Figure 5 shows the test results for $\varepsilon \approx 0$, 0.18, and 0.36%. Curve (3), corresponding to $\varepsilon \approx 0$, indicates the change $\Delta\sigma$ which is due to the constraint force of the machine jaws (this force prevents the specimen's expansion as T increases). Taking this constraint force into account, the test results give

$$\left\langle \frac{\Delta E}{E} \right\rangle = 4 \ , \tag{11b}$$

where E, defined for 0.05% deviation from linearity, is Young's modulus for the specimen with a martensitic structure. Figure 5 shows that ΔE begins to appear at $T_C \approx 25\text{-}41°C$.

(b) Resistivity change. The athermal resistivity change $\Delta\rho$ that accompanies the change in T during the M↦P transformation have been investigated for many SM materials [10]. A plot of typical data for a Nitinol specimen, shown in Fig. 6, exhibits an anomalous shape which has not been adequately explained to date. This anomaly has been shown to be nearly independent of the heating and cooling rates [10]. Nevertheless, our studies indicate that these rates, as well as the specimen structural conditions (internal stress, impurities, etc.) do influence, to some degree, the ρ-T curves. Therefore, to analyze the relationship between the M↦P reaction and the ρ-T curves, we have conducted a series of isothermal tests; the results for one well-annealed thin-

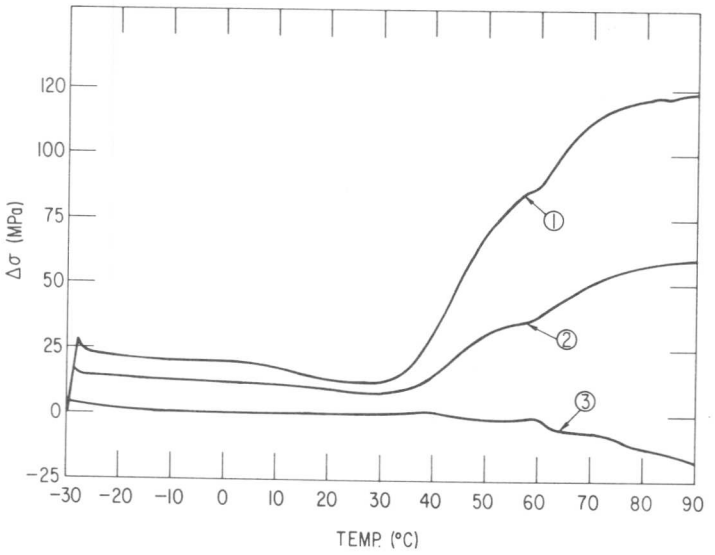

Fig. 5. Transient plots of $\Delta\sigma$ vs T for a Nitinol wir wire specimen under sub-elastic strains $\varepsilon \sim 0$ (curve 1), 0.18 (curve 2), and 0.36% (curve 3).

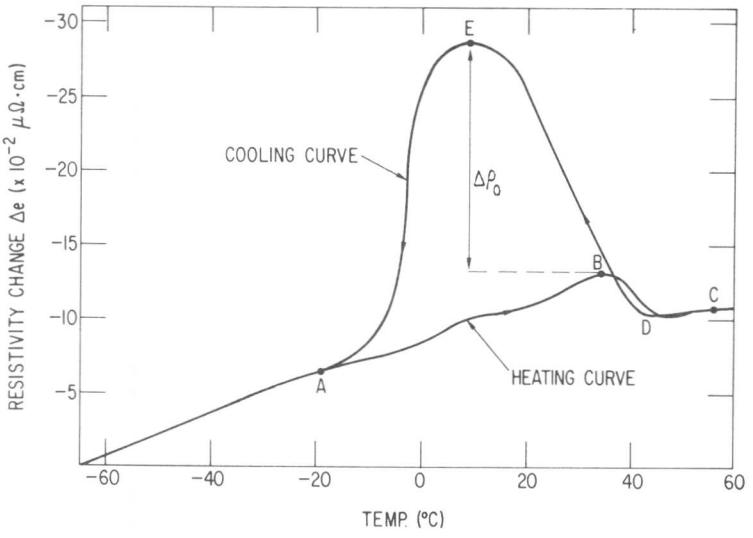

Fig. 6. Athermal resistivity change in a Nitinol wire specimen under zero stress, heated and cooled in a water reservoir at an average rate of 1°C/min.

wire Nitinol specimen, under zero stress, are shown in Fig. 7. Similar tests will be conducted in the future on other Nitinol alloys and on specimens under various combinations of temperature and stress. We note that for either below or above the transition temperature range defined by $T_o^{\pm} = T_o \pm \Delta T_o$, the variation in the resistivity ρ is dominantly ohmic in nature, and its value, denoted by ρ_T, is found as

$$\Delta\rho_T = a\Delta T \tag{12a}$$

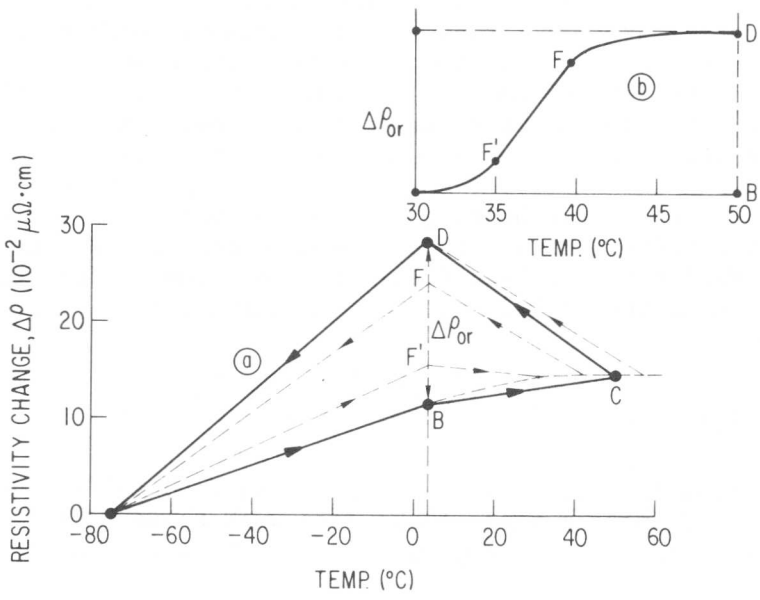

Fig. 7. (a) Hysteresis loop generated by successive isothermal resistivity measurements at temperatures of -75, 4, T_H = 50, 4, and -75°C; (b) the variation of the height of the loop, $\Delta\rho_{or}$, with temperature.

where

$$a = 0.156\ \mu\Omega\cdot\text{cm} \quad \text{for} \quad T < T_o^- \qquad (\gamma'\text{-structure}),$$

$$\simeq 0.1\ \mu\Omega\cdot\text{cm} \quad \text{for} \quad T > T_o^+ \qquad (\beta\text{-structure}). \qquad (12b)$$

However, between T_o^- and T_o^+ the ρ value depends on the structural condition, i.e., the relative proportions of β and γ', internal stresses, impurities, etc. In any case, the isothermal ρ data form a hysteresis loop if a sequence of measurements is made at temperatures T_L', T_L, and T_H, where $T_L' \lesssim M_s$ (say -75°C for our specimen) and $T_L < T_o^-$ (say 4°C). This loop, which is shown schematically by the line ABCDA in Fig. 7a, is reproducible, although it can be changed to the loop ACDA by measuring ρ over the temperature cycle T_L'-T_H-T_L-T_L'. We observe that if we vary T_H between T_o^- and T_o^+, the points A and B do not change. However, as T_H goes toward T_o^-, D approaches B; when T_H reaches T_o^-, the loop reduces to the line AB. The variation in the height of the loop, BD, with respect to T_H is seen in Fig. 7b. This height goes toward zero as the temperature T_L approaches T_H, or T_L'. So by constructing a series of loops for various T_H and T_L values, we can build up the same loop that was obtained by the athermal ρ-T experiment in Fig. 6. In doing this for our specimen, we find T_o = 35°C and $\Delta T_o = \pm 15$°C. Also from the test data we find that ρ_H and ρ_C, which denote the resistivity in heating and cooling, respectively, are functions $(T_H - T_o^+)$ and $(T_L - T_o^-)$. In fact we find phenomenologically, the resistivity changes during the M↦P and P↦M reactions, respectively, as

$$\Delta\rho_H = \Delta\rho_{or}\left[1 - e^{-K(T-T_o^-)} + e^{K'(T_o^+-T)}\,\theta(T - T_o^+)\right]\theta(T - T_o^-)\,\theta(T_o^+ - T) \qquad (13a)$$

$$\Delta\rho_C = \Delta\rho_{or}\left[e^{-K(T_o^+ - T)} + e^{-K''(T_o^- - T)}\theta(T_o^- - T)\right]\theta(T - T_o^-)\theta(T_o^+ - T) \ . \tag{13b}$$

Here $\Delta\rho_{or}$ is the maximum change in specimen resistivity during the reaction; the coefficients K, K', and K" are constants which depend on the material structural conditions and the heat-transfer coefficient between the specimen and the cooling or heating medium; T_H is the temperature at which the heating is reversed to cooling; and the θ functions guarantee the contribution of each term to a specific temperature range. Thus, $\theta(T - T_o) = 1$ for $T > T_o$, 0 for $T < T_o$, and so on. In Fig. 6 the AB portion of the heating curve OABD, and the EA portion of the cooling curve CDEAO, are due to the terms containing K' and K", respectively. Making use of Eqs. (12a) to (13b), the difference $\Delta\rho_o$ between the peaks of the cooling and heating curves, in Fig. 6, can be approximated as

$$\Delta\rho_o \simeq a(T_E - T_B) + \Delta\rho_{or}[1 + e^{-K''(T_B - T_o^-)} - e^{-K'(T_o^+ - T_E)}] \ , \tag{14}$$

From Fig. 6 we find $T_E = 10°C$ and $T_B = 35°C$, and from the isothermal data $\Delta\rho_{or} \simeq 17.5$ μΩ·cm; combining these data with those in Eqs. (12) to (14), we obtain $\Delta\rho_o \simeq 14$ μΩ·cm, which agrees with the value obtained from Fig. 6.

(c) Thermoelectric power in the M-P reaction. The measurement of the thermal emf generated at interfaces between the M and P phases is rather difficult because of the interference from the thermoelectric power generation at the specimen junctions. To eliminate this effect, we first measured the thermoelectric power of Nitinol relative to metals such as Cu, Ni, Ag, and Au. We found that the conventional polarity of Nitinol relative to these materials depends on whether the Nitinol is in the M or the P phase. For example, relative to the absolute thermoelectric power values for Cu and Ni in μV/°C, we found [11]

P-phase	Cu	Ni	M-phase
+11.7	+1.5	-16.8	-4.53

Use of a long (50-cm) specimen with copper leads minimized the junction effects satisfactorily. The specimen was curved to that any portion of it could be immersed in the water reservoir. The specimen junctions were kept at about 0°C by covering them with several layers of frozen insulating materials. The specimen was cooled in a CR to produce the M structure; a portion or the entire specimen was then rapidly immersed in an HR to produce P phase. We found that during the M↦P transition an emf of 0.1 to 0.12 mV was generated. This emf will remain constant as long as the M and P zones in the specimen are maintained. The M-phase is negatively charged relative to the P-phase, so that in conventional terms the P-phase is the positive pole. In a wire specimen in which a P zone is sandwiched between two M zones, as in Fig. 8, the sign of the emf depends on the lengths of the M zones.

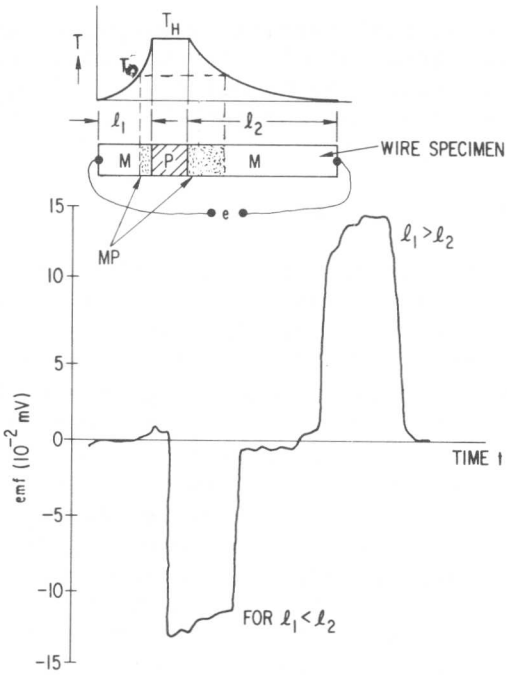

Fig. 8 The net thermal emf e generated in a long Nitinol wire specimen with a P-phase region sandwiched between two M-phase regions. PM indicates the two M-P interfacial zones.

This may be explained as follows: Assume the specimen terminal junctions are kept at $0^{\circ}C$, and the P zone is at temperature T_H, so that thermal gradients are present in the M zones (with lengths ℓ_1 and ℓ_2). Then the thermoelectric fields on the two sides of the P zones can, in general, be written as

$$E_{MP,\ell} = Q_{MP}\left(\frac{dT}{d\ell}\right)_{\ell} + T\left(\frac{dQ_{MP}}{d\ell}\right)_{\ell} \tag{15a}$$

generated by the P-M transformation. The Q_{MP} value varies from zero, in a region with $T \leq T_0$, to a maximum at a region with $T > T_0^+$. Hence we may write

$$Q_{MP} = Q\, e^{k(T-T_0^+)}\, \theta(T_0^+ - T)\, \theta(T - T_0^-), \tag{15b}$$

where k is a constant and Q depends on the variation of the P and M admixture in the interfacial zone. Now, if $\ell_1 \neq \ell_2$, the interfacial zones in fig. 8, progress in time and stop with different lengths, as they are under different thermal gradients. Hence, according to eqs. (15a) and (15b), the net emf across the specimen can be written, as

$$\mathcal{E} \simeq \frac{1}{2}\, k(T_H + T_0)\, (Q_1 - Q_2)\, \theta(T_0^+ - T)\, \theta(T - T_0^-) \tag{15c}$$

where Q_1 and Q_2 are associated with the two M-P interfacial zones shown in fig. 8. The sign and magnitude of $\mathcal{E}$ depend on the thermal gradients along the ℓ_1 and ℓ_2 portions; for $\ell_1 = \ell_2$, $Q_1 = Q_2$ and so $\mathcal{E} = 0$ in agreement with the test result in fig. 8. Also $\mathcal{E}$ varies if the specimen junctions

have different temperatures. Experimental results, a sample of which is shown Fig. 8, lead to $Q_{MP} \simeq -0.12$ mV, in agreement with the thermoelectric data given above for the P and M phases. The negative sign of Q_{MP} agrees with the general expectation that the current flows from the hot section (P-phase) to the cold one (M-phase).

IV. Concluding Remarks

It is clear that the martensitic transformation in SM alloys generates many changes in the metal properties which are nearly reversible as soon as the reverse reaction occurs. Two distinct martensitic transformations are involved in the process. The first, $\gamma' \rightarrow \beta$, is a first-order transformation in many respects. The volume change due to this transformation is apparently very small ($\sim$0.1%) in Nitinol materials. The anomalous shape of the specific-heat or resistivity change, associated with the first-order λ-type transformation, is very similar to that in ferromagnetic materials. However, unlike the ferromagnetic transformation, the present transition preserves the ordering state. The shallow minima in the ΔE variations in Fig. 5, and the broad peaks in the ρ curves in Fig. 6, is partly due to the second-order phase change caused by straining and partly due to the fact that the specimen is polycrystalline and the transition temperature exhibits a spread of $2\Delta T_o$.

The unusual change in Young's elastic modulus with temperature is readily understandable. As a well-annealed alloy with the γ' structure, Nitinol is extremely pliable, whereas the same material in the β phase is highly elastic. The mechanical properties of the M and P structures are consistent with the γ' and β' electronic states.

Note that while the increase in $\Delta E/E$ is due to the $\gamma' \rightarrow \beta$ transition, the nonzero value of $W_o - W_i = \Delta W$ in the energy-balance equation (1) is due solely to the indirect $\gamma' \rightarrow \beta' \rightarrow \beta$ reaction which takes place by "reshuffling" of the highly unstable γ' variants at a temperature $T_H > T_C$ and under an applied stress. It would be interesting to find out whether the coefficient α in Eq. (1), which leads to $\Delta W \neq 0$, can be increased from its present value of 0.14 by changing the alloy composition, impurity content, etc. The variation of T_C with the grain size and density, Eq. 10, needs future investigation.

The isothermal resistivity measurement provides a fairly accurate method of study of the M-P transition in terms of T, σ, and material parameters. It reveals the source of the anomaly in the ρ-T curves. From the test data leading to Eqs. (12a) to (13b), we find that the existence of the transition range ΔT_o, even with residual P phase below $\bar{T_o}$, cannot be responsible for the ρ-T anomaly. One then must explain how at a given $T_L < T_o$ the martensite can have two different ρ values, as shown by points D and B in Fig. 8a. To do this we note that ρ depends on the phonon-electron scattering amplitude (call it A) projected along a given crystal axis that is oriented along the current direction. In a (cubic) P-structure, A is the same for any of the crystal axes. On the other hand, in an M-structure formed by inhomogeneous rapid cooling, internal stresses cause various degrees of lattice distortion (producing a metastable M-structure); this leads to the variations of

A and "Charge Density Wave", and in turn an increase in ρ as shown by point D [12]. However, during a relaxation period which depends on $T_L - T_o$, the lattice distortion is minimized and some phonon modes are dissipated; thereby a more stable M-structure with lower ρ (shown by point D) is produced. This stabilization process is accelerated exponentially if T_L is lowered. Finally we note that the thermoelectric pulse shown in Fig. 8, arises between the P and stable M phases with a metastable M-P interfacial zone. More detailed information on the resistivity and thermopower will be presented in a separate article.

An important observation is that all these changes (in the M↔P interfacial emf, electrical resistivity, and elastic constants) share a common parameter, namely, the Debye temperature θ, which is a measure of the interaction between the thermal phonons and electronic states of the materials. The variation of θ during the M↔P reaction has already been reported for the (Cu, Au, Zn) shape-memory alloys [13]. Another important parameter seems to be the strong anisotropy factor, C_{44}/C', which appears at the SR critical temperature T_C. This phenomenon suggests that in addition to the phonon-electron interaction, the phonon-lattice interaction should be taken into account. All these points are currently under study as a continuation of the present work. Finally, the effects of stress on the resistivity thermoelectric power, etc. will be reported in a separate paper.

Work supported by the U.S. Department of Energy.

Acknowledgments

The author would like to thank Drs. W. J. Shack and F. A. Nichols for many useful comments and discussions.

References

[1] Numerous articles have been published on the shape recovery and other features of the martensitic transformation in some shape-memory alloys. However, relatively little has been presented on the Ni-Ti shape-memory alloys since the report of C. M. Jackson, R. J. Wagner, and R. J. Wasilewski: NASA-SR 5110, 1972 (unpublished).

[2] See Ref. 1 and K. H. Eckelmeyer: "Effect of Alloying on the Shape Memory Phenomenon in Nitinol," Tech. Report SAN 74-0418, Sandia Laboratories (March 1975).

[3] A. A. Golestaneh has proposed a systematic investigation of the SRP in "The Shape-Recovery Phenomenon in Shape Memory Alloys, with Particular Reference to the Nitinol Systems," Tech. Report, Argonne National Laboratory (Sept. 1978).

[4] A. A. Golestaneh: to be published.

[5] A. A. Golestaneh: J. Appl. Phys., 49, (1241), 1978.

[6] See, for instance, Jackson et al. (Ref. 1).

[7] Note that the CC equation has only been derived for first-order reactions in the liquid-gas systems. The application of this equation to a system involving stress and strain tensors needs experimental verification, as provided in the present work.

[8] For example, G. Edwards and J. Perkins: *Shape Memory Effects in Alloys*, Ed. by J. Perkins, Plenum, New York (1975), 445.

[9] Variations of the bulk of modulus, elastic constants, and Poisson's ratio in Nitinol systems have been studied by several authors, e.g., N. G. Pace and C. A. Saunders: Phil. Mag., 22 (1970), 73.

[10] F. E. Wang, B. F. DeSavage, W. Buehler, and W. R. Hosler: J. Appl. Phys., 39 (1968) 2166.

[11] A gold junction with special soldering material was used to minimize the junction thermocouple effect.

[12] The anisotropy in the A amplitude plays the same role in forming the resistivity hysteresis loop as the magnetization in the ferromagnetic case. Hence it may be possible to develop a theory for the ρ loop following the approach used for the magnetic hysteresis loop.

[13] See, for instance, N. Nakanishi, Ref. 8, p. 151. The linkage between the Debye temperature and several features of the M→P transformation in the SM is under study by A. A. Golestaneh.

Design Concepts For Actuators Using Shape Memory Effect Brasses

L. McDonald Schetky* and Roy B. Sims**

SME brasses offer significant advantages for a wide variety of actuators due to the ease with which they may be fabricated, as well as the ability to maintain composition limits, which defines M_S, to within the limits required for actuators. Actuator operating temperature, force/deflection characteristics and hysteresis control are discussed in terms of design curves. Examples of successful applications are presented as an indication of the range of devices possible.

Research was initiated in 1972 by the Delta Company in England, one of the largest copper and brass producers in Europe, to produce shape memory effect ternary brass-type alloys to operate at room temperatures, and thereabouts, for the economic reasons that Nitinol is, for many applications, too expensive to melt and fabricate. This work has produced a range of alloys, all of them comprising approximately 70% copper brass with additions of aluminum in which the shape memory effect can be produced reliably and stably at temperatures up to 120°C (approximately 250°F).

Perhaps the most useful characteristic of these SME brasses is the fact that they can be relatively easily fabricated. The lower temperature transforming alloys can be readily cold-worked, those which transform at a higher temperature cold-work with difficulty; but all of the SME brasses can be hot formed.

---

* Technical Director; International Copper Research Association, Inc., New York, New York.

** Group Vice President; Delta Metal Co., Ltd., London, England.

Shapes most useful for the range of actuators designed to date include helical coils, helical torsion springs, bi-stable wire configurations, and tubular actuators acting in torsion. These are likely to be the most useful forms for components for the measurement and control of temperature.

The first characteristic of the material to be evaluated was the variation of elastic stress/strain with temperature, and here the transition temperature T_{min} used in their work should be defined.

T_{min} is the temperature below which the material is wholly in the martensitic form. At and below this temperature the material exhibits a single elastic stress/strain curve with temperature and although Young's modulus of the material will vary because the stress/strain curve is non linear, nonetheless it has its lowest values as a function of temperature. This is shown in Fig. 1 where the curves of stress against strain in the elastic regime are shown.

All the useful SME brasses exhibit similar stress/strain characteristics with temperature, when the temperature parameter is reduced to the basis of T_{min}, that is to say, the measured values of stress and strain in a material which transforms at 0°C can be made very close to those of an alloy which transforms at 40°C if the basis of measurement is taken as increments of temperature from their respective values of T_{min}. Thus, one family of curves can be used to characterize the SME brasses, and their performance with actual temperature can be derived by inserting the appropriate value of T_{min} for the material, and thus greatly simplifying calculation. SME brasses have a long working range, although in practical design it is preferable to keep the working range to within T_{min}+ 60°C. This is sufficient to cope with most measurement and control problems met in practice.

The memory devices designed to date have been limited to a maximum shear strain of 2%. Higher values, up to 4% strain, are possible but inadvisable at the present state of the art for actuators intended to undergo a large number of strain cycles, although feasible for those intended for relatively few strain cycles or which operate in compression only Actuators operating with this 2% limit exhibit no creep and have shown no sign of fatigue failure.

Of concern to design engineers is the question of whether the memory effect decreases either with time, or with frequent strain cycling. In Fig. 2, it can be seen that the material settles down to repeatable values

after 3-5 reversals of temperature. In pieces which have been cycled for well over ½ million times, there is no measurable change in deflection characteristics with temperature after the first few cycles, unless the actuator is either over stressed or subjected to temperatures outside its working range for prolonged periods of time. This phenomenon of change in strain-temperature characteristics over the first few temperature cycles is called the 'shakedown effect' or training period and Delta eliminates it during heat treatment so that actuators are supplied fully heat treated to develop the required memory.

Probably the most troublesome phenomenon with all shape memory effect materials when used as precision actuators is the phenomenon of hysteresis. Figure 3 shows the hysteresis with temperature measured in terms of displacement of an unloaded helical actuator. It will be seen that the hysteresis is large, and is usually of the order of 15-17°C. Much of this hysteresis can be suppressed by forcing the actuator to work against a bias spring. Figure 4 shows the displacement of this combination against temperature, and two important effects can be observed.

It will be seen that the variation of displacement with temperature is decreased, and the hysteresis is reduced with increased bias spring stiffness so that with a stiff bias spring the hysteresis of the SME actuator is not more than approximately ±0.9°C. The other interesting effect is that when the material is cycled over a temperature range considerably narrower than the maximum - say over 5°C in a working range of perhaps 40°C then the hysteresis is negligible in any one cycle and there is only a very small cumulative effect if cycling is repeated over this narrow band. A typical example is a room thermostat which may have a hysteresis of ±0.9°C over its working range of 10°C to 35°C; but only ±0.2°C over its control band of 18 to 20°C.

Figure 5 shows the spectrum of stress/strain with temperature for a particular SME actuator, and the straight line represents the effect of a bias spring working in conjunction with the SME actuator. At temperatures at and below T_{min} the bias spring will compress the SME actuator to its full extent, and as temperature is increased the increase in stiffness of the actuator will overcome the bias spring progressively and as a result displacement with temperature can be read off the diagram where the straight line and the curved lines of deflection with temperature intersect. This is the basic design diagram from which the performance of actuators can be predicted. A mathematical model is being developed for a mini-computer program to ease

the labor of engineering calculations, and also to predict with some confidence the effects of hysteresis. Figure 6 shows the basic design chart for calculating SME actuators in the form of helices and you will recognise the normal engineering parameters defining helically wound compression springs, and from this diagram is predicted a force-displacement diagram with temperature shown in the previous figure and on it can be superimposed a suitable bias spring. This same type of chart has been developed for torsion springs and tubular torsion actuators.

The constraints with which a designer is faced when attempting to design with SME brass are summarized as follows: 1) Force and/or displacement required; 2) total hysteresis to be permitted within the device; 3) external frictional forces which the actuator must overcome (and which will contribute to overall hysteresis); 4) temperature range over which the material must operate; 5) dimensions into which the material must fit; 6) cost.

All these parameters interact. Furthermore, the design task is not made easier by designing in a material in which the modulus of rigidity follows a series of non-linear curves which makes the optimisation process an order of magnitude more difficult.

At the present time SME brass suffers from the disadvantage that it cannot operate continuously and indefinitely at temperatures greater than approximately 250°F (120°C). This is because the martensitic state at temperatures below T_{min} gradually transforms irreversibly to the austenitic state and the metal will lose its memory. A great deal of work is being done on the development of alloys with a wider operating band of temperature above T_{min} and also on alloys which can operate continuously at higher temperatures. Efforts are also being made to improve the cold working characteristics of the higher temperature alloys, and the performance of the alloys at high strain levels, particularly for applications where the material undergoes relatively few strain cycles. Research is also in progress to further reduce the hysteresis effect.

This material is now being produced in tonnage quantities with a tolerance on the transformation temperature T_{min} to ±7°C. It can be hot worked into all shapes normally available in brass, and this is the preferred form of fabrication. It can also be cold worked in alloys with a low transformation temperature.

The metal can be conditioned to give a stable memory and with careful design can meet almost all operating and design specifications. The absolute value of hysteresis is about 0.6°C, and this low value can only be reached with a sacrifice of other characteristics. Normally the hysteresis range is of the order of 1.2°C to 0.9°C. The design characteristics of the metal are now well understood and a number of design studies have been completed on which many variations can be based to give commercially viable components.

Three broad classes of shape memory devices are currently being explored in the U.S. and Europe: Coupling devices, devices for thermostatic actuators and various toys and amusement devices. The use of SME brass for couplings is quite feasible, however, it requires an alloy with maximum hysteresis and the use of high values of strain to cope with pipe tolerances. The paper presented by Bushell and Harrison outlines this application.

Devices which have been designed, manufactured and placed in field test by Delta Metal Company include an automotive fan with variable speed proportional demand, various thermostat devices for domestic hot water control, a greenhouse window opener, an automotive automatic choke and an automotive carburator with temperature compensated needle valve, and a broad range of electric relays.

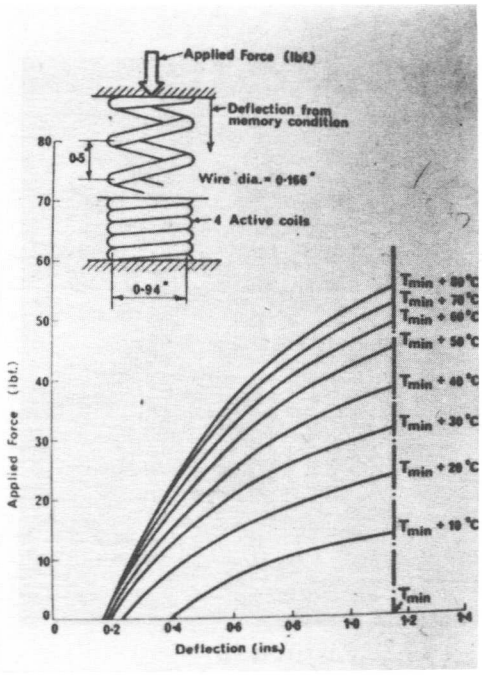

Figure 1

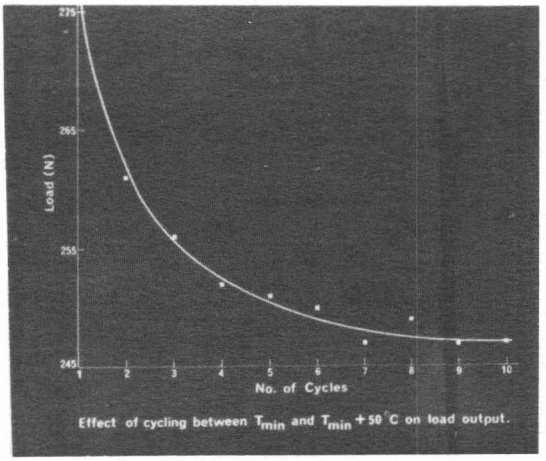

Figure 2

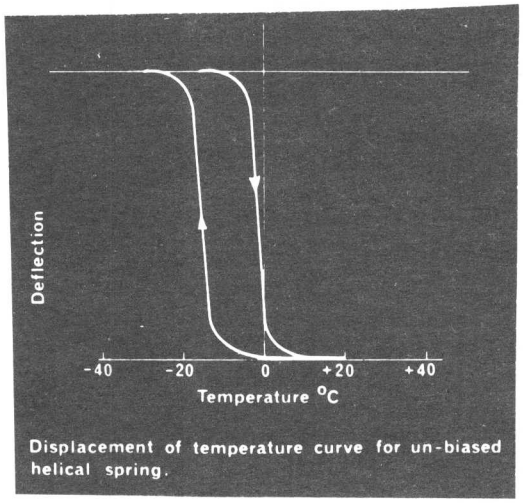

Displacement of temperature curve for un-biased helical spring.

Figure 3

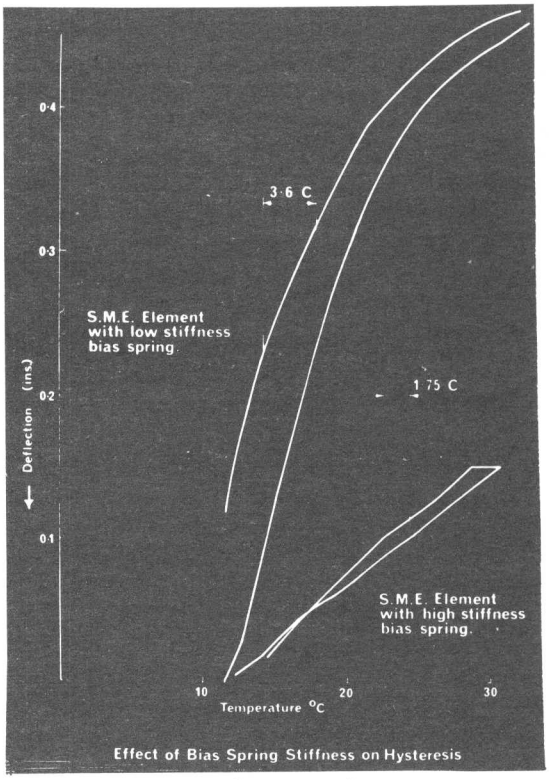

Effect of Bias Spring Stiffness on Hysteresis

Figure 4

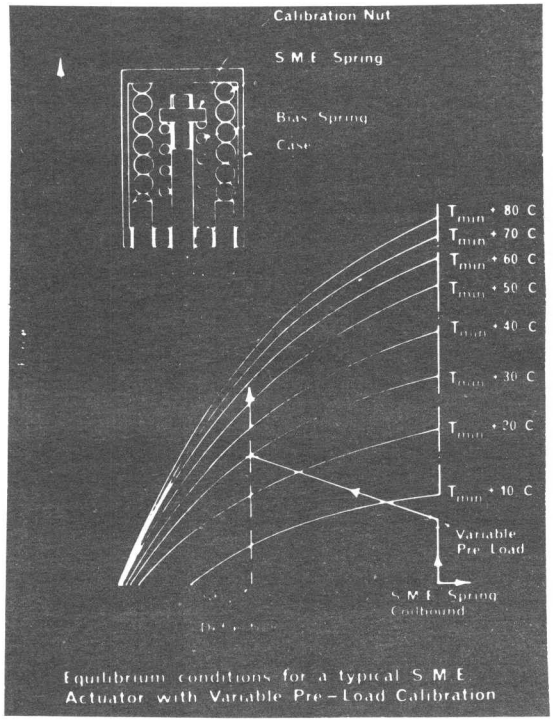

Equilibrium conditions for a typical S.M.E. Actuator with Variable Pre-Load Calibration

Figure 5

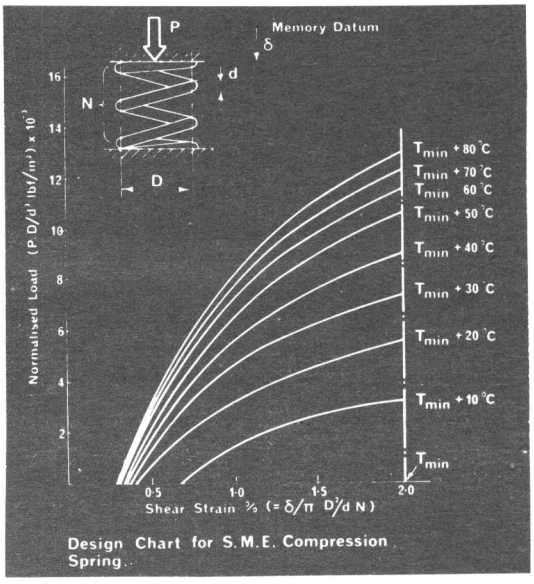

Design Chart for S.M.E. Compression Spring.

Figure 6

Use of Shape Memory in Joining Sub Sea Piping

Alan Bushell and Jack Harrison; and Les Hill*

Building on the work of Wm. J. Buehler and others at the U.S. Naval Ordnance Laboratory (now Naval Surface Weapons Center) in the late 50's, Raychem Corporation has developed a family of nickel titanium alloys which exhibit shape memory characteristics, and are sold under the registered name Tinel™. The initial application for these alloys was in a high performance coupling developed for the Grumman Aircraft Corporation to solve the problems of joining titanium tubing for the hydraulic system of the F-14 "Tomcat" fighter. This continues to be a highly successful application with in excess of 150,000 of these 3000 psi rated couplings currently in service.

This Cryofit® coupling principle involves the machining of a cylinder of Tinel™ material at room temperature, followed by cooling in liquid nitrogen, at which temperature it is expanded, shipped and stored. Installation is effected by removing the coupling from the LN_2, inserting the pipe or tubing, and allowing the coupling to recover to its original shape as it warms to the ambient temperature.

Today, a complete family of couplings serves the requirements of both the U.S. and British Navies in variously replacing welding as the method of joining 6000 psi rated power piping in destroyers, nuclear submarines and other vessels. The couplings, which are designed for both pipe and tube sizes up to 1.9 inches in diameter, have been qualified for applications on carbon-steel, 300 series stainless steels and 70/30 copper nickel.

In December 1977 a request was received for the supply of two 2" IPS size pipe (2.375" O.D.) couplings which were required to attempt the repair of a damaged Schedule 80 carbon steel pipe 100 feet beneath the surface of the southern section of the North Sea. Winter weather conditions in the North Sea are so severe (regular Force 8 gales) that maintaining a diving ship in position for the duration of a traditional repair is virtually impossible. Failure to effect the repair at this time would have meant interruption in production during the winter months when the demand for gas is high. The resulting economic impact would have been substantial.

Raychem was able to develop and build the desired couplings by extrapolating and modifying the design of the existing monolithic couplings, and the finished product was made available by mid-January. Star Sub Sea Maintenance, who specialize in North Sea offshore diving maintenance, were at the same time engaged in developing a suitable alignment/

Raychem Corporation, 300 Constitution Drive, Menlo Park, CA 94025.
*Mr. Hill is at Raychem U.K., Swindon, England.

positioning frame with integral dry environment habitat (known as a J.I.F and finalizing the procedural steps necessary for underwater handling of the couplings in liquid nitrogen.

During the location, rigging and preparation of the pipe, the diving team was blown offsite and forced to take shelter eight times. Having located and positioned the pipe within the JIF, the damaged section of th pipe was cut out and a piece of similar pipe prepared to replace the damaged section. Dummy couplings were used to check the alignment of the pipes, go/no-go gauges were employed to check pipe tolerances, and pipe ends were prepared by removing all coating material. At this point all was set to proceed with the repair.

The repair team, comprising two divers, entered the habitat and it was filled with air so that the pipe ends were entirely in a dry environment. The two couplings, held in specially-designed tooling, were then lowered into the habitat in a specially-designed pressure vessel containi liquid nitrogen. The divers removed the couplings from the container and slid one coupling onto each end of the replacement piece which was suspen from the roof of the habitat. The replacement piece was then lowered int place, the couplings slid out over the pipe ends to meet prepositioned st the tooling removed and the couplings allowed to warm to the ambient temp erature, thereby passing through their transition range from martensite t austenite (-125 to -50°C) and recovering to create a high integrity metal to-metal seal. This installation phase had required two hours from the t that the divers entered the water to the completion of the repair which, fact, utilized the entire possible operating window as a Force 8 gale necessitated immediate evacuation of the site.

Since this initial installation, signigicant advances in product, tooling and procedures have been made through the joint efforts of both Raychem and Star. Couplings are now available in 2", 4" and 6" IPS configuration and the transition range of the alloy used is now -100 to -20°C which allows more time for positioning prior to recovery. An improved integrated tool has now been created which is both the transfer vessel from surface to habitat and the installation tool. It has both the ability to accommodate the change in boiling point of the liquid nitrogen with increase of pressure at depth, and maintain the part at LN temperature until installed in place. A second generation JIF has also been built with superior alignment and handling capability.

A 4" coupling has been installed in 300 feet of water using saturati diving techniques. A further eight 2" couplings have been installed at 100 feet in the North Sea, where the use of this technique represented a savings in time of between two and three weeks to the pipeline owners. This translates into many hundreds of thousands of dollars when one recognizes the costs associated with all the support equipment for this type of offshore operation.

The coupling itself is a hollow right cylinder machined from the nickel-titanium alloy (Tinel™) in its austenitic phase condition. This cylinder, which contains annular sealing lands on the inside diameter, has a bore somewhat smaller than the outside diameter of the pipe to be joined. The coupling is then cryogenically cooled using LN_2 (Temp. -196° causing a transition of the alloy to its martensitic phase, at which point

its bore is mechanically expanded to a size larger than the upper limit of the particular pipe O.D. Expanded couplings retain this deformation by being stored in liquid nitrogen which ensures that the alloy remains martensitic. Upon removal from the liquid nitrogen, the alloy warms to the ambient temperature, passing through the transition point at which it reverts to austenite with the accompanying activation of the shape memory characteristic. The coupling attempts to revert to its original dimension but is designed to interface with the pipe wall such that the two metal surfaces go into yield with one another thereby achieving a high integrity metal to metal seal.

The couplings, which are rated for operating pressures up to 6000 psi for temperatures from -20°C to 300°C, have been subjected to extremely severe tensile, torque, bend and burst testing and in all cases are superior in performance to the top grade pipe used in the industry. Preliminary tests show the couplings to be cathodic relative to steel pipes and are thus galvanically protected should the protective coating be removed. The effect of sour crude is still under investigation. Elaborate quality assurance procedures are also enforced throughout manufacture to ensure that each supplied coupling will satisfy the demanding performance requirements of the sub sea environment. These procedures, in turn, minimize the amount of post-installation inspection to a simple insertion inspection, as opposed to radiography of welds, which represents a significant improvement in providing the industry with a simple and cost-effective solution.

Internal Friction Peaks Associated with the Martensitic Phase Transformation of NiTi and NiTiCu Alloys

O. Mercier*, E. Török**, B. Tirbonod***.

Anelastic measurements in the low and medium frequency range have been made on a martensitic equiatomic NiTi alloy and on a series of $(Ni_{1-x}Cu_x)Ti$ alloys. An internal friction peak and a change in modulus are observed during cooling and heating through the phase transformation. In some specimens, a second internal friction peak is found, with no frequency minimum. In comparing the anelastic curves with resistivity measurements, these peaks are associated on the one hand with premartensitic phase transformation and on the other hand with the martensitic transformation itself. These peaks as a function of heating and cooling rate and as a function of the amplitude of measurement have been studied in the low frequency range with an inverted pendulum and in the medium frequency range with a resonnant bar apparatus. The experimental results are in good agreement with the predictions of different theories explaining the internal friction observed during the phase transformations. However no explanation was found to explain why the binary NiTi, after some heat treatments, has a premartensitic transformation, which results in a supplementary peak and in a sharp minimum of modulus, whereas in substituting Ni by Cu this premartensitic transformation is no longer observed, and in substituting Ni by Fe the temperature separation of the premartensitic transformation and of the martensitic one is enhanced.

I. Introduction

The near equiatomic NiTi and $(Ni_{1-x}Cu_x)Ti$ alloys undergo a martensitic transformation around room temperature [1,2]; and internal friction peak and a large modulus change are observed on heating and cooling samples of these alloys through the phase transformation [3,4,5]. The general behaviour of these peaks is similar to those observed in other martensitic alloys, such as CuAlNi [6] or CuZnAl [7], except that sometimes 2 peaks are observed and the modulus has a sharp minimum near the temperature of the phase transformation [5]. The results of further investigations on this subject,especially in relation with the effect of substituting Ni by Cu in NiTi are presented in this paper.

II. Experimental

The NiTi and $(Ni_{1-x}Cu_x)Ti$ alloys were prepared using standard technique [8]. The composition and the transformation temperature M_s of the dif-

---

*Brown Boveri Research Centre, 5401 Baden,
**Institut Straumann, 4437 Waldenburg,
*** Laboratoire de Génie Atomique, EPF-L, 1007 Lausanne, Switzerland

ferent alloys are given in table I. The transformation temperatures were determined by an AC electrical resistivity technique (Fig.1). The internal friction measurements were made during thermal cycling between -200°C and +200°C. The measurements made at low frequency (∿1Hz) were done on an inverted pendulum [9] on wires of 1 mm in diameter and of 100 mm in length; the measurements at medium frequency (0.5-20KHz) were done on a resonnant bar apparatus [10] on plate of 50 mm x 5 mm x 1 mm in dimensions.

III. Results and Discussion.

(1) Anelastic effects associated with the martensitic phase transition.

The value of the internal friction and of the measurement frequency of the alloy 3(Table I), measured on the pendullum during heating and cooling at a constant rate of 3,5 K/min is shown in Fig.2. A peak of internal friction and a change of frequency, located between 300 K and 330K during the heating and between 300 K and 270 K during the cooling, are observed. For the same alloy, during the same temperature intervals a change of resistivity is ovserved (Fig.1), which is due to the martensiti phase transition [2]. This peak and this change of frequency are therefor due to this latter. When the alloy is martensitic, a very high damping (∿ 0.01) is also observed. At medium frequency (∿ 1kHz), similar results are observed for the change in modulus (or in measurement frequency) (Fig.3) and for the internal friction of the martensitic phase, but the peaks associated with the phase transition are hardly detectable (Fig.4). This result is in agreement with previous results [5], which have shown that the internal friction measured at low frequency can be divided in 2 parts, one including essentially the transformation peaks and the other the high damping of th martensitic phase (see for example Fig.7). The part A, dashed on Fig.7, which depends on the cooling and hea ting rate $\dot{T}$ and on the measurement frequency was interpreted as the result of a plastic strain due to the preferential growth of the martensitic plates in the direction of the applied stress (Delorme's model) [5] This part should only appear at low frequency, which agrees with our mea surements. We have also observed tha the internal friction of Fig.4 was heating and cooling rate independan as expected. The part B, independen of $\dot{T}$ was attributed to the viscous motion of dislocations, probably

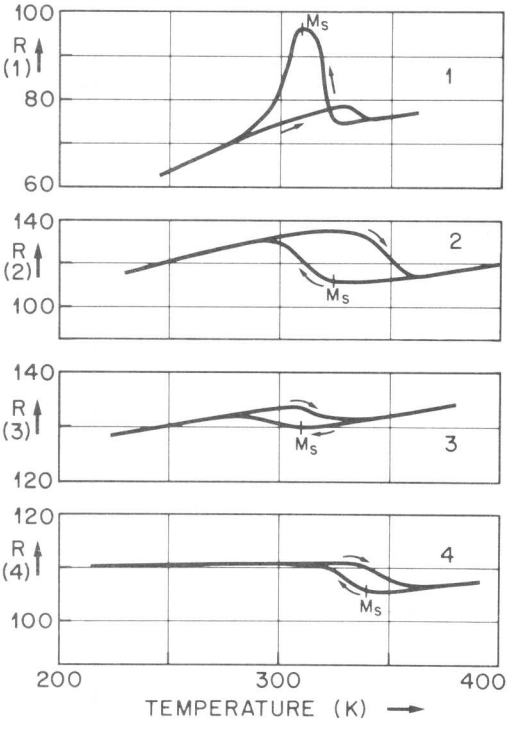

Fig. 1: Resistance, in arbitrary units, as a function of temperature, of the 4 alloys defined in Table I.

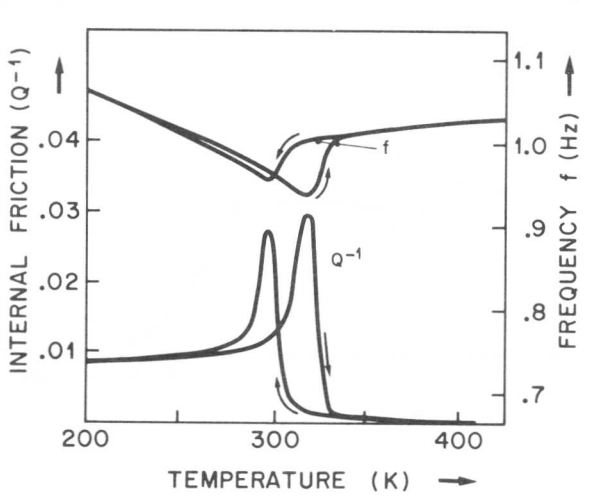

Fig. 2: Internal friction and frequency of measurement as a function of temperature, measured on the alloy 3 at low frequency ($\varepsilon=1.5\times10^{-5}$, $\dot{T}=3.5$ K/min)

twin dislocations [5]. This part of the internal friction should be also approximately frequency independent which agrees also with our measurements; it is also independent of the measurement amplitude ε below a critical value (2×10^{-5}) and increases then strongly with it [11]. During the phase transition, the shear and the Young's modulus go through a minimum, as shown for the alloy 3 on the Fig.3. The decrease in Young's modulus is particular large (about 50%). From the values of these 2 modulus, the Poisson ratio and the compressibility factor can be calculated; it is found that the compressibility factor goes almost to zero at the beginning of the phase transition. This is verified for all the NiTi base alloys, whereas this effect is not found on the CuZnAl and CuAlNi alloys [12].

The internal friction of alloys 2 and 4, measured on the pendulum are shown in the Fig. 5 and 6 respectively. Each time, the internal friction peak and the change in frequency correspond to the change of resistivity, reported in Fig. 1. The internal friction peaks are narrower and higher for the alloys 2 and 4 than for the alloy 3; however, in computing the area of each, it is found that this latter decreases slightly as a function of increasing Cu content. The change of modulus is also larger and the internal friction of the martensite higher for the alloy 4 than for the alloys 2 and 3. These results are also relatively similar to those obtained for the binary NiTi (Fig.7), in regard to the peaks corresponding to the martensitic transformation (peaks at 310 K on cooling and at 360 K on heating [5]) and to the internal friction of the martensite. These results show that in substituting Ni by Cu in the ternary system $(Ni_{1-x}Cu_x)Ti$, only small changes are observed in the high internal friction spectrum, associated with the martensite and the martensitic phase transformation; this is in agreement with the other results on this system, which have

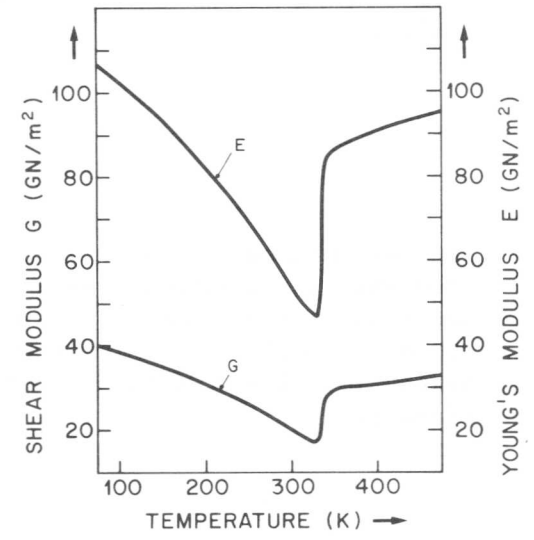

Fig. 3: Shear and Young's modulus as a function of temperature, measured on the alloy 3 during heating at 11.5 kHz and 1 kHz respectively.

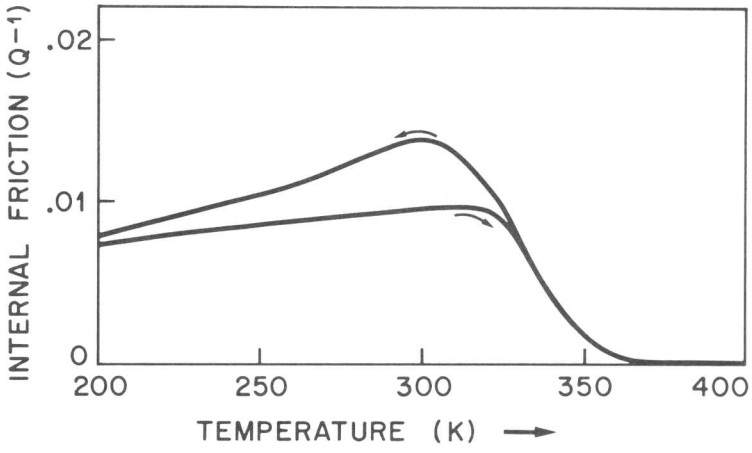

Fig. 4: Internal friction as a function of temperature, measured on the alloy 3 at medium frequency (1000Hz) ($\varepsilon = 5 \times 10^{-5}$, $\dot{T} = 5$ K/min.).

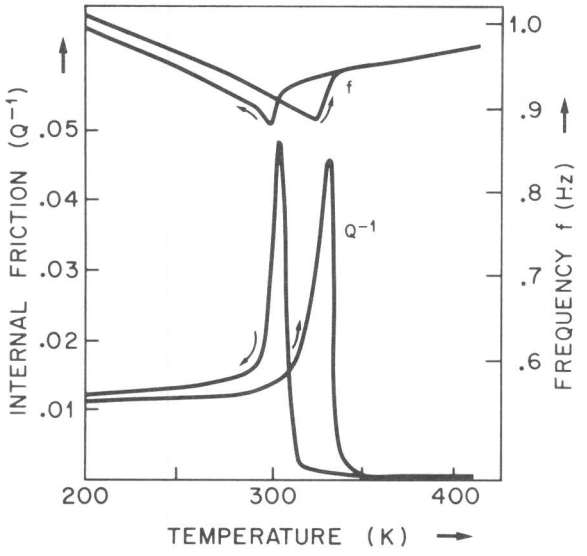

Fig. 5: Internal friction and frequency of measurement as a function of temperature, measured on the alloy 2 at low frequency ($\varepsilon = 1.5 \times 10^{-5}$, $\dot{T} = 3.5$ K/min.).

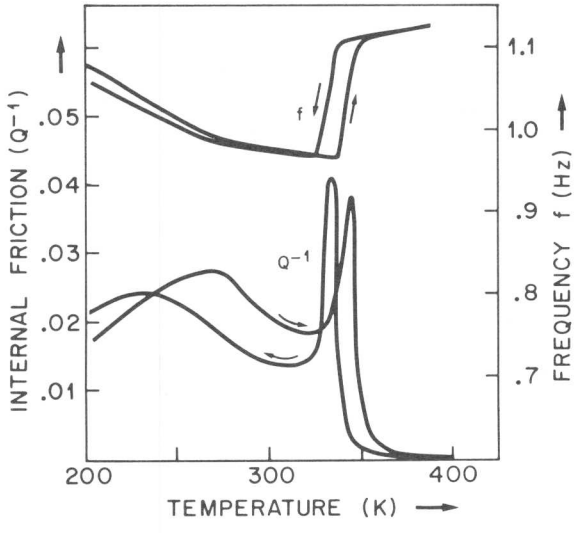

Fig. 6: Internal friction and frequency of measurement as a function of temperature, measured on the alloy 4 at low frequency ($\varepsilon = 1.4 \times 10^{-5}$, $\dot{T} = 3.5$ K/min.).

shown that the martensite type and the martensite transformation temperature is almost unaffected by the replacement of Ni by Cu [2,13].

(2) Anelastic effects associated with a premartensitic transformation.

On some binary alloys (Fig.7), as well as on ternary or quaternary (NiCuFe)Ti alloys, [12], 2 internal friction peaks appear on cooling. One, located at the lower temperature is attributed to the martensitic transformation, whereas the one at higher temperature is attributed to a premartensitic phase transition [5]. This latter is associated with a sharp minimum in modulus. For the binary NiTi, these premartensitic effects appear only when the specimen is quenched or cycled through the phase transformation, as soon as an increase of resistivity is observed (Fig. 1). However, for this alloy the 2 phase transformations are almost at the same temperature, which makes it difficult to study it. On the contrary, on some NiTiFe, of composition given by [14], the 2 phase transformations are well separated in temperature. First measurements of the internal friction and of the modulus have been made on such an alloy at medium frequency [12]. They show that a narrow internal friction peak and a sharp minimum in modulus are also associated with the premartensitic phase transition, like it was observed on the binary NiTi of Fig. 7. It can also be noticed that the internal friction below the premartensitic peak is also relatively high, only about 3 times lower than the one of the martensite. From this study, it is however not clearly understood why the premartensitic transformation is observed only on some NiTi base alloys. At least 3 hypothesis are possible: (1) The premartensitic transformation is only necessary for the binary NiTi, because it has the largest distortion between the martensite and β cells [12] and not for the ternary NiTiCu, where the distortion decreases with Cu increase, (2) the premartensitic phase is unstable in the ternary alloys with Cu and therefore the martensitic transformation follows immediately the premartensitic one, which makes invisible this latter, (3) the premartensitic transformation is independant of the martensitic one and its appearance is related to a still yet unknown parameter. On the basis of these measurements, no answer can be given, even if the sharp decrease in modulus, observed on all the specimens at the beginning of the phase transformation, and which is similar to the one observed at the temperature of the premartensitic transformation in the NiTiFe gives a support to the second hypothesis.

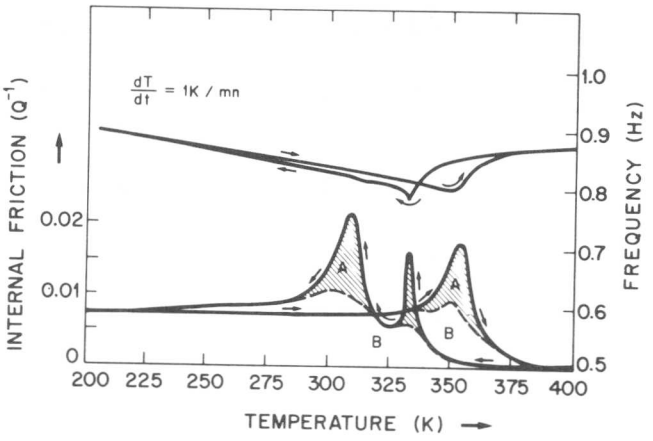

Fig. 7: Internal friction and frequency of measurement as a function of temperature, measured on the alloy 1 at low frequency ($\varepsilon = 1.5 \times 10^{-5}$, $\dot{T}$ = 1 K/min.)

Measurements were also done on alloys, based on the CuZnAl and CuAlNi system. At medium frequency, only one peak of internal friction, associated with a relatively small change of modulus was observed around the temperature of the phase transformation [12], no such effect like in the binary NiTi was observed, which indicates also that the premartensitic phase transition of the NiTi is not of the same nature as that observed in CuZnAl and CuAlNi alloys.

References

[1] F.E. Wang, W.T. Buehler and S.J. Pickart: J. Appl. Phys., 36 (1965), 3232

[2] O. Mercier and K.N. Melton: Met. Trans. in press

[3] G.J. Wasilewski: Trans. Met. Soc. AIME, 233 (1965), 1961

[4] R.R. Hasiguti and K. Iwasaki: J. Appl. Phys. 39 (1968), 2182

[5] O. Mercier, K.N. Melton, Y. De Préville: Acta Met. in press

[6] K. Sugimoto, T. Mori, K. Otsuka and K. Shimizu: Scripta Met. 8 (1974), 1341

[7] W. Dejonghe, R. Debatist, L. Delay and M. Debonte: *Shape Memory Effects in Alloys*, Ed. J. Perkins, Plenum Press, (1975), 451

[8] C.M. Jackson, J.J. Wagner and R.J. Wasilewski: NASA report, NASA SP 5110, (1972)

[9] G. Gremaud: J. of Appl. Math. and Phys. 28 (1977), 368

[10] G. Hausch and E. Török: Phys. Stat. Sol. (a) 40 (1977), 55

[11] B. Tirbonod: unpublished research

[12] O. Mercier, E. Török: unpublished research

[13] R.H. Bricknell, K.N. Melton and O. Mercier: Met. Trans in press

[14] M. Matsumoto and T. Honma: *New Aspects of Martensitic Transformation*, J.I. M., Kobe (1976), 199

Table I: Composition and transformation temperature M_s of the different alloys

Alloy No	Nominal Composition (wt%) Ni	Ti	Cu	M_s
1	55	45	-	310 K
2	49	46	5	325 K
3	44.5	45.5	10	310 K
4	39	46	15	340 K

ANELASTIC BEHAVIOUR OF Cu Zn Al ALLOYS

S. Koshimizu*, M. Mondino and W. Benoit**

The internal friction (IF) spectra of samples with a nominal content of 17 wt% Zn, 7 wt% Al and the balance Cu have been determined in the temperature range 220-380 K under different strain amplitudes and heating and cooling rates.

The main features of the IF peak related to the transformation, which appears below Ms are the following: (i) the peak height shows a significant amplitude dependence in the range 10^{-8} to 10^{-5} and does not depend on the thermal rate for T between 0.8 K/min and 3.0 K/min; (ii) the peak height is systematically lower by 15-20% on cooling than on heating; (iii) it is not affected by thermal cycling between 220 and 380 K.

Moreover, the IF on both sides of the peak has the same amplitude dependence as the peak itself.

Measurements have been performed to observe the effect of isochronal thermal treatments on the annealing out of the peak.

I. Introduction

Due to its sensitivity to atomic rearrangements, IF has been widely utilized in the study of martensitic transformation in alloys such as Ti Ni [1, 2, 3], Mn Cu [4], Cu Al Ni [5, 6] and Co Ni [7, 8]. In particular, the martensitic transformation in Cu Zn Al-β alloys has been extensively studied by internal friction methods in the low frequency range by De Jonghe et al. [9, 10]. Their results show that the internal friction depends on the temperature variation rate and on the measuring strain amplitude. It has been also observed that the IF peak due to the martensitic transformation differs in the cooling and heating. Furthermore, difficulties to obtain good reproductibility of the measurements have been noted [6].

In general, the IF spectrum of phase transitions is divided into three regions [4]. The first one, the β range, shows a very low IF; the second one presents a very large peak between Ms and Mf on cooling or between As and Af on heating; and the third one is the IF of martensite itself.

The results in the kHz range reported in the present paper differ from those obtained in the low frequency range. The observed differences may be useful to the understanding of the martensitic transformations and to the interpretation of the IF mechanism itself in Cu Zn Al alloys.

II. Experimental Procedure

Cu Zn Al alloys with a nominal composition of 17 wt% Zn, 7 wt% Al balance Cu were prepared by induction melting under an argon atmosphere. The casting was then treated at 800 C followed by water quenched.

* On leave from CNEN-Rio de Janeiro and IEA-Sao Paulo

** Laboratoire de génie atomique, EPF-Lausanne, Switzerland

The IF and frequency measurements were carried out in parallelepiped samples (2 mm x 4mm x 40 mm) under flexural vibrations. The accuracy of the frequency measurements is higher than 99.9%, the dispersion of the IF value is 2% for 5×10^{-3} and the accuracy of the temperature measurement is ± 1 K [11]. All the measurements are recorded digitally, tape-punched, and afterwards read and interpreted by computer.

III. Results

The IF and frequency as a function of temperature at a constant heating and cooling rate are presented in figure 1. The IF curves follow the general description discussed in Section I. There is a rapid increase in IF and corresponding rapid decrease in frequency on approaching Ms during cooling. The maximum of IF is accompanied by a minimum in the frequency. The shift in the peak temperature between cooling and heating characteristic of martensitic transformation is here observed.

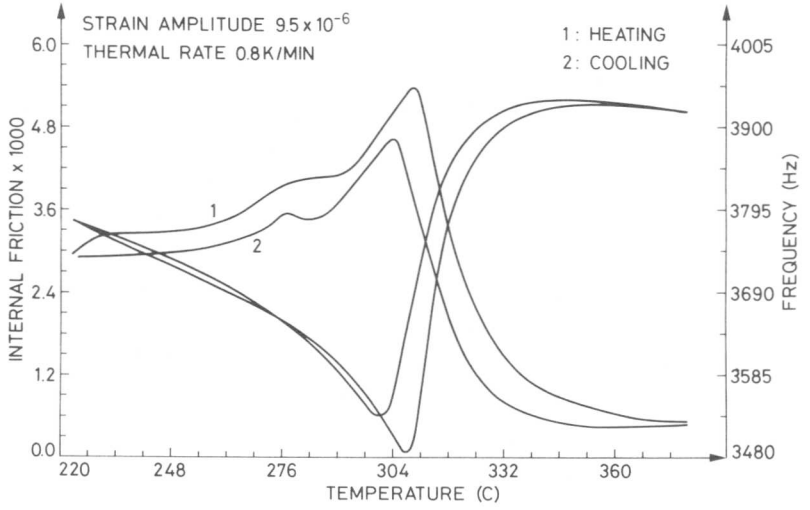

Figure 1 Internal friction and frequency variations between 220 and 380 K

The peak height is about 15 to 20% higher on heating than on cooling, and the same behaviour is observed for the background of the martensitic phase.

In order to have a comparison with low frequencies results, we have studied the influence on the IF spectrum and frequency of two main variables: the heating and cooling rate and the measuring strain amplitude. Figure 2 shows the observations as a function of thermal rate at two strain amplitudes for the peak height (A) and for the martensitic phase background (B). It is found that the thermal rates between 0.8 K/min and 3 K/min have no influence on the IF. On the

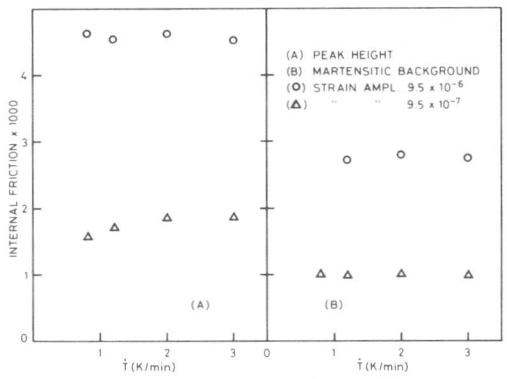

other hand, as shown in figure 3, the strain amplitude has a considerable influence. In fact the peak height varies from 6.3×10^{-3} for $\epsilon = 2.7 \times 10^{-5}$ to 2.0×10^{-3} for $\epsilon = 9.5 \times 10^{-7}$. This result is very important, for it implies that at very small strain amplitude the IF peak disappears; and this in turn implies that the IF peak is due probably to the dislocation mobility.

Figure 2 Influence of the thermal rate on peak height and martensitic background

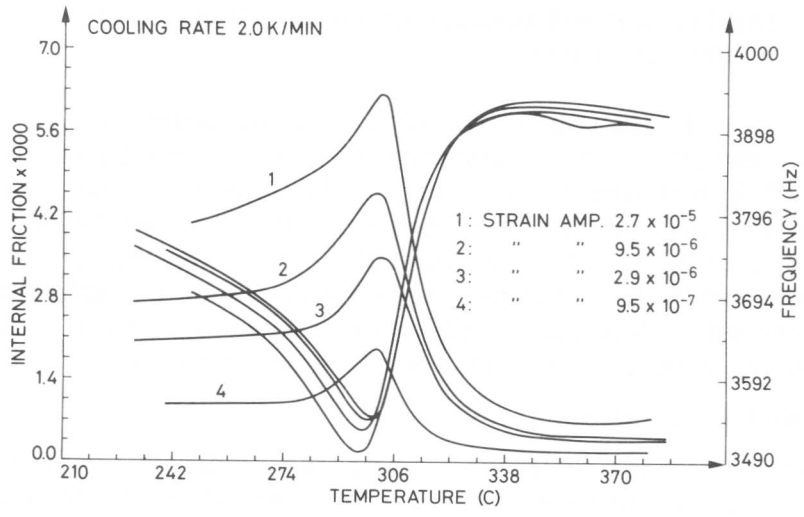

Figure 3 Internal friction and frequency as function of temperature for different strain amplitudes

Observations have also been carried out on the annealing out of the peak. Figure 4 presents the evolution of the IF spectrum during isochronal treatment up to 573 K. A treatment of 15 minutes at 423 K has no effect, but annealing at higher temperature lowers the entire IF spectrum. After 15 minutes at 573 K the peak is no longer observable, and the spectrum becomes a step-like function.

IV. Discussion

(a) Dependence on temperature variation rate

The results at low frequency (for instance, in Cu Zn Al [9]) described by the phenomenological model of De Jonghe et al. [10], have shown that the IF can be divided into two components: the first one depending on thermal rate and frequency ($\dot{T}/f$) and the second one depending on stress

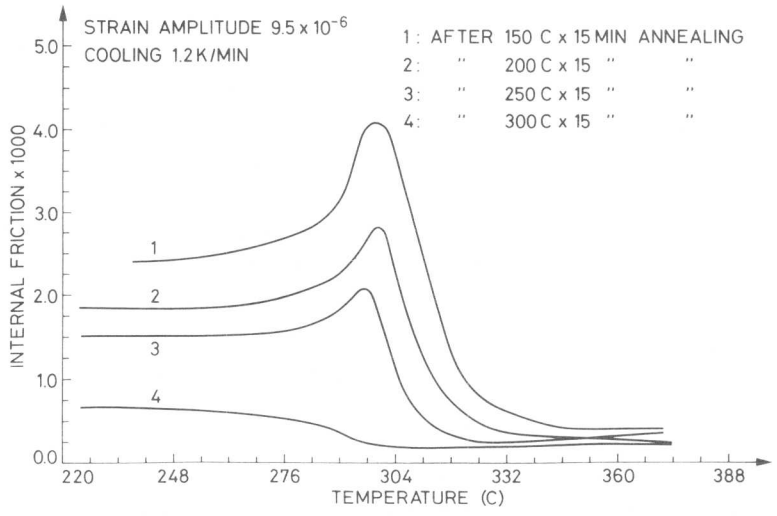

Figure 4 Diminution and disappearance of IF peak with isochronal annealing

amplitude. In the kHz range, the IF spectrum including the peak height does not show any dependence with the temperature change rate, between 0.8 K/min and 3.0 K/min (fig. 2). The dependence on the temperature variation rate becomes negligible at high frequency (kHz range) owing to the $\dot{T}/f$ factor, whereby the IF coming from T is masked at high frequency. This non-dependence on $\dot{T}$ is similar to the result reported by Mercier et al [2] in Ti Ni measured in a static process, that is, with the temperature variation rate null.

(b) Amplitude dependence

As pointed out in Section III the dependence of the entire IF spectrum (fig. 3) on strain amplitude implies a relationship with dislocation motion. Therefore, the results of the strain amplitude dependence were plotted according to the Granato-Lücke dislocation damping theory [13], which explains the amplitude dependent IF as being caused by breakaway of dislocations from pinning impurities. This theory predicts that $\ln Q^{-1} \times \varepsilon$ versus ε^{-1} is a straight line whose slope is given by [14] as:

$$C_2 = \frac{\Gamma}{G} \qquad (1)$$

where Γ is the stress required for freeing the dislocation from its pinning point and G is the shear modulus.

The Granato-Lücke plot shown in figure 5 was corrected taking into account the fact that the strain amplitude is not maximum along the sample [15]. It is worthwhile to observe that the three slopes in fig. 5 are nearly the same. The slopes in the β phase background, peak

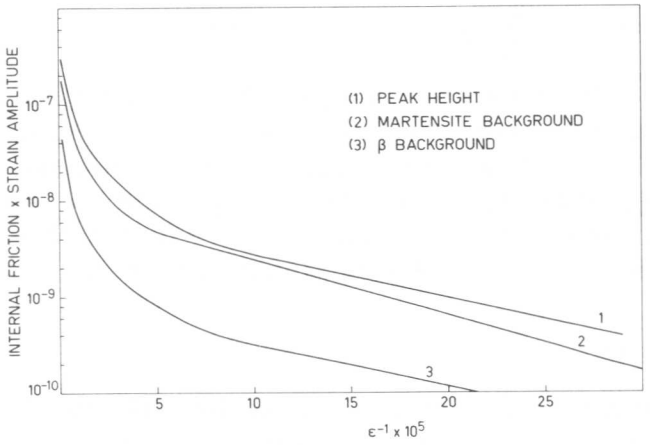

Figure 5 Granato-Lücke plot for peak height, martensitic phase background and β phase background

height and martensitic phase background are 1.01×10^{-6}, 1.03×10^{-6} and 1.34×10^{-6} respectively. Although a quantitative analysis of these results is difficult because Γ in equation (1) involves unmeasured parameters, they indicate that the amplitude dependent IF is of the same origin in the three regions, due to dislocation movements.

(c) Model

According to the observed amplitude dependence in figures 3 and 5, our results can be interpreted by the Granato-Lücke model of amplitude dependent IF [13], but with the addition of the anisotropy factor A (as used by Mercier et al [16] for the amplitude independent case).

The amplitude dependent IF is given by the expression [14]:

$$Q^{-1} = \frac{C_1}{\varepsilon_0} \exp\left(-\frac{C_2}{\varepsilon_0}\right) \qquad (2)$$

with $$C_1 = \Omega\, \Delta_0\, L^3/\pi^2\, \ell\, G \qquad (3)$$

and $$C_2 = \Gamma/G \qquad (1)$$

In equation (3), Ω is an orientation factor; $\Delta_0 = 4(1-\nu)/\pi^2$; ν is Poisson's ratio; L is the dislocation length; ℓ is the average distance between impurity pinning points and G is the shear modulus. The stress required for freeing the dislocation from its pinning point can be written [14]:

$$\Gamma = \pi\, F/4\, a\, L \qquad (4)$$

with $$F = 4\, G\, \varepsilon^0\, a^4/d^2 \qquad (5)$$

where ε^0 is the Cottrell misfit parameter, d is the distance between the impurity atom and dislocation and a is the interatomic distance.

From equations (1), (3), (4) and (5), C_1 depends on the elastic constants through G while C_2 is independent of the elastic constants. One can rewrite equation (2):

$$Q^{-1} = \frac{C_1(A)}{\epsilon_0} \exp\left(-\frac{C_2}{\epsilon_0}\right) \qquad (6)$$

wherein C_1 now is a function of the anisotropy factor. Now, if we take into account that the shear elastic constant $C' = C_{11} - C_{12}/2$ diminishes and hence the anisotropy factor $A = C_{44}/C'$ increases at the martensitic transformations [17, 18, 19], then Q^{-1} also increases at the transformation; and the frequency, which is proportional to $G^{1/2}$ diminishes. Thereby, equation (6) explains the IF during a martensitic transformation.

(d) Effect of isochronal annealing

The progressive diminution of internal friction with isochronal annealing (fig. 4) seems to confirm the assumption that dislocation motion is responsible for the amplitude dependent IF during the martensitic transformation. The diminution of the entire IF spectrum following the decomposition of the β phase, indicates that there are fewer and fewer dislocations which contribute to IF. After 15 minutes at 573 K there is no peak, but rather a step-like function, indicating that the transformation is still present but that there is no longer a sufficient dislocation density for the peak. On the other hand, if one assumes that the volume of martensite is proportional to the peak area, one can represent the change in volume fraction of martensite as a function of annealing temperature, as shown in the figure 6.

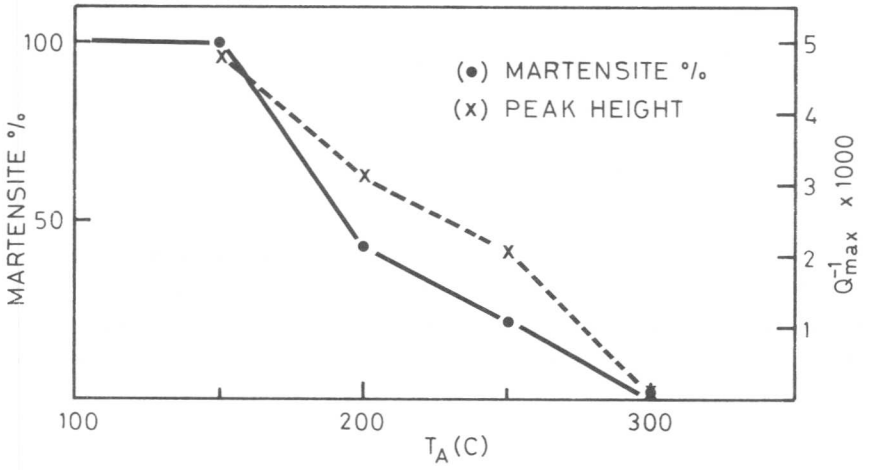

Figure 6 Evolution of internal friction peak with annealing temperature The assumed volume fraction is also shown.

References

[1] C. M. Jackson, H. J. Wagner and R. J. Wasilewski, Nasa - SP 5110 (1972)

[2] O. Mercier, K. N. Melton and Y. De Préville - to be published
[3] R. R. Hasiguti and K. Iwasaki - J. Appl. Phys. 39, 2182 (1968)
[4] K. Sugimoto - Mem. Inst. Sci. Ind. Res., Osaka Univ., 35, 31 (1978)
[5] V. S. Postnikov, I. M. Sharshakov and V. G. Komarov - Phys. of Metals and Metallurgy (Fiz. Metal. Metalloved.) 33, 218 (1972)
[6] K. Sugimoto, T. Mori, K. Otsuka and K. Shimizu - Scripta Met. 8, 1341 (1974)
[7] V. S. Postnikov, V. N. Belko and I. M. Sharshakov - Physics of Metals and Metallurgy (Fiz. Metal. Metalloved.) 26, 92 (1968)
[8] V. N. Belko, B. M. Darinskiy, V. S. Postnikov and I. M. Sharshakov - Physics of Metals and Metallurgy (Fiz. Metal. Metalloved.) 27, 140 (1969)
[9] W. De Jonghe, R. De Batist, L. Delaey and M. De Bonte - Shape Memory Effects in Alloys - Edited by J. Perkins - Plenum Press, 451 (1975)
[10] W. De Jonghe, R. De Batist and L. Delaey - Scripta Met. 10, 1125 (1976)
[11] P. Stadelmann - Thesis EPF Lausanne, 11 (1978)
[12] G. Guenin, M. Morin and P. F. Gobin - "Anelastic properties of Ti Ni alloy before and during martensitic transformation"
[13] A. Granato and K. Lücke - J. of Appl. Phys. 27, 583 (1956)
[14] R. De Batist - "Internal Friction of structural defects in crystalline solids" - North-Holland Publishing Co., 341 (1972)
[15] T. Jalanti - Thesis EPF Lausanne, 1975
[16] O. Mercier and K. N. Melton - Scripta Met. 10, 1075 (1976)
[17] Y. Murakami - J. of the Phys. Soc. of Jap. 33, 1350 (1972)
[18] N. Nakanishi - Shape Memory Effects in Alloys - Edited by J. Perkins - Plenum Press, 147 (1975)
[19] S. Koshida and H. Kaga - J. of the Phys. Soc. of Jap. 42, 499 (1977)

The Crystallography of Microcracking in Ferrous Martensites

B.C. Muddle* and J.S. Bowles**

The crystallography of transverse microcracks formed in high carbon ferrous martensite plates with both $(225)_F$ and $(259)_F$ habit planes has been examined by trace analysis. In $(259)_F$ plates, cracking occurs predominantly on a plane approximately parallel to the $(001)_B$ plane of the martensite, the usual cleavage plane of b.c.c.(t) metals. In contrast, cracks in $(225)_F$ plates occur on the plane normal to the close-packed direction, $[1\bar{1}0]_F$, in the $(225)_F$ habit plane. This cracking occurs without external influence and, since it implies that the plates have been in tension parallel to $[1\bar{1}0]_F$, seems likely to be associated with the need to accommodate the contraction in interatomic spacing that accompanies the transformation of $[1\bar{1}0]_F$ into $[11\bar{1}]_B$. Although shape strain measurements on $(225)_F$ plates seem to indicate that this contraction is accommodated by plastic deformation in the austenite, microcracking of the martensite on a plane normal to $[11\bar{1}]_B$ provides another means of accommodation. The extent of cracking is, however, inadequate to account for the necessary contraction and it seems likely that cracking complements plastic deformation of the austenite as a means of accommodation, occurring if there is any breakdown in the mechanism of plastic accommodation in the austenite.

I. Introduction

The transverse microcracks commonly observed in high carbon ($\geq$0.8%C) ferrous martensites are generally considered [1-3] to be associated with impingement between martensite plates. It has not been made clear, however, whether impingement is considered a direct cause of cracking or whether the cracking has its origin in internal stresses within a plate and the impingement is of secondary importance. It has, for example, been suggested [4] that the microcracks observed in $(225)_F$ martensite plates imply the existence of volume and/or interfacial constraints to plate growth, but the possibility that the occurrence of cracking may be related directly to the mechanism and hence crystallography of the transformation has received little attention.

A recent reassessment [5] of shape strain measurements on $(225)_F$ plates has revealed that the change in volume produced by the invariant plane strain exceeds the total volume change accompanying the transformation as calculated from the lattice parameters. This result, which is in conflict with the phenomenological theories of martensitic transformations [6,7], was originally thought [8] to imply that the invariant plane strain was accompanied by a uniform contraction but, in later work [9,10] has been considered to reflect the level of experimental error. However, recent shape strain determinations [5], incorporating for the

* Dept. of Metallurgy and Mining Engineering and Materials Research Laboratory, University of Illinois, Urbana, Illinois 61801, U.S.A.
** School of Metallurgy, The University of N.S.W., Kensington, N.S.W. 2033, Australia.

first time measurements of length changes produced by the shape strain, have established unequivocally that the habit plane is invariant and that the volume discrepancy must thus be attributed wholly to an increase in plate thickness. A systematic discrepancy in plate thickness approaching 2% is not so readily attributed to experimental error. The mean values of g_s/g, where g_s is the ratio of final to initial volume in the measured shape strain and g is the ratio calculated from the lattice parameters, are shown in Table I. Values obtained for $(225)_F$ plates by different observers using different techniques and measuring instruments are all significantly greater than unity. In contrast, the mean ratios obtained in studies of $(3,10,15)_F$ martensite plates and $(301)_B$ mechanical twins in tin do not differ significantly from unity.

It has been suggested [5] that this volume discrepancy might be caused by atoms being displaced into the transforming region by the generation of dislocations at the interface and their movement into the austenite. The plastic accommodation model [11] of the transformation involved a similar proposal, an accommodation strain in the austenite being invoked to accommodate the contraction in interatomic spacing that accompanies the transformation of the close packed line $[1\bar{1}0]_F$ lying in the $(225)_F$ habit plane, into $[11\bar{1}]_B$. In that model, however, the accommodation strain was assumed to cause no change in volume. If the contraction of the plate parallel to $[1\bar{1}0]_F$ is accommodated entirely by the displacement of atoms into the transforming volume then the measured volume ratio would be expected to exceed g by a factor equal to the ratio of the initial to the final interatomic spacing. As shown in Table I, this ratio is in good agreement with the mean experimental values.

It remains difficult to obtain direct evidence that a plastic accommodation strain in the austenite forms an integral part of the $(225)_F$ transformation mechanism. If, however, it may be established that crackin of the martensite occurs as a result of the constraints on a growing plate then it would indicate indirectly the importance of an accommodation of the austenite to plate growth. This possibility prompted the present examination of the role of microcracking in the $(225)_F$ transformation and a comparison with behaviour in $(259)_F$ martensite plates.

II. Experimental Procedure

Coarse-grained specimens of an homogenised Fe-8.03%Cr-1.11%C alloy were polished metallographically and cooled to -40°C to produce 5-10% martensite. The orientations of grains containing cracked martensite plates were determined from back reflection Laue photographs and the $(225)_F$ habit plane variant and the direction of transverse cracks within plates derived from single surface trace measurements. For $(259)_F$ martensite specimens of an Fe-1.84%C alloy were austenitised at 1150°C for 24hrs and water-quenched, producing austenite grains 2-3mm in diameter containin approximately 20% martensite. Austenite orientations were determined usin the traces of $(111)_F$ annealing twins in two surfaces, the habit planes of the plates from two-surface trace analysis of the mid-rib planes and the directions of transverse cracks within the plates from single surface trac measurements. For some plates in both alloys cracking was observed in two surfaces and a two surface analysis of the cracking plane carried out.

III. Experimental Results

Transverse microcracking of martensite plates in both alloys was observed. In $(225)_F$ plates cracking was evident in the pre-polished relief surfaces of all specimens (Fig.1) but was restricted to those plates for which the close-packed direction in the habit plane was within approximately 30° of the specimen surface (Fig.2). When the habit plane was indexed as $(225)_F$ the trace normals to the microcracks all passed within approximately 5° of $(1\bar{1}0)_F$; an average trace normal for each plate examined is shown in Fig.2. For two plates for which cracks were measured in two surfaces the cracks defined planes within approximately 3° of $(1\bar{1}0)_F$.

In contrast to the consistency of these measurements, a relatively wide scatter in results for $(259)_F$ plates was observed (Fig.3). The extent of this scatter probably reflects the less regular nature of the cracking and the necessity, in most cases, of determining the direction of each crack from segments only about 10μm in length. In spite of the scatter the majority of trace normals to the microcracks appear to converge about a pole near to $(0\bar{1}0)_F$ when the habit plane is indexed as $(259)_F$. Two surface analyses of the plane of cracking are consistent with this conclusion.

Metallographic examination of cracked plates in both alloys confirmed the crystallographic nature of the cracking. Sections through plates polished approximately parallel to the habit plane reveal predominantly long, straight cracks. In $(225)_F$ plates, in particular, these cracks are stepped in a regular manner across other defects within the plate (Fig.4); some branching of the cracks occurs but the predominant direction of cracking is parallel to the trace of $(1\bar{1}0)_F$. Serial sectioning of cracked $(225)_F$ plates revealed that the average direction of cracking remains constant and parallel to the trace of $(1\bar{1}0)_F$ through a series of surfaces polished parallel to the original relief surface.

IV. Discussion

The present results indicate that microcracking of $(259)_F$ martensite plates occurs predominantly on a plane approximately parallel to $(0\bar{1}0)_F$. For the selected habit plane variant, the $[010]_F$ axis becomes on transformation the c axis of the body-centred tetragonal martensite and the plane of cracking is thus in turn approximately parallel to the $(001)_B$ plane of the martensite, the usual cleavage plane of b.c.c.(t) materials. As shown in Fig.3, a systematic displacement of up to 15° from $(001)_B$ is observed for these results and, at present, the source of this discrepancy is not understood. It is noted, however, that because of the strong texture of the parent austenite, the present results are drawn from plates in a limited range of orientations and may not be truly representative of transformation behaviour. It is difficult from these limited measurements to reach a conclusion regarding the origin of the cracks, although the metallographic evidence often lends support to earlier results [1,3] associating cracking with impingement between martensite plates.

Since microcracks are observed in isolated $(225)_F$ plates, their presence here can not readily be attributed to external influence such as the impingement of other plates. The occurrence of the cracks, predominantly

on the plane normal to the close-packed direction in the habit plane, implies that the martensite has been in tension along an axis parallel to $[1\bar{1}0]_F$ and it seems likely that cracking is associated with the need to accommodate the contraction in interatomic spacing that accompanies the transformation of $[1\bar{1}0]_F$ into $[11\bar{1}]_B$. The observation that cracking on a plane normal to $[1\bar{1}0]_F$ is confined to the $(225)_F$ transformation would support this view. In $(259)_F$ martensite the $[1\bar{1}0]_F$ direction does not lie in the habit plane and is distorted to its final length by the shape strain. There will be, therefore, no tension developed parallel to the habit plane and transverse microcracking would not be expected in isolated $(259)_F$ plates. Although it has not been possible to confirm this experimentally in the present work, it would seem to be consistent with previous observations [2] that there is a greater incidence of microcracking in $(225)_F$ martensite than in $(259)_F$ martensite.

It has been suggested [5] that the discrepancy between the volume ratio defined by the lattice parameters and that detected in recent shape strain measurements on $(225)_F$ plates, indicates that the contraction in interatomic spacing parallel to $[1\bar{1}0]_F$ is accommodated by plastic deformation of the austenite. Cracking of the martensite on a plane normal to the $[11\bar{1}]_B$ direction would provide an alternative mechanism for accommodation and a plausible origin of the volume discrepancy. However, not all $(225)_F$ plates exhibit cracking and in those that are cracked the volume of cracks is generally inadequate to account for the necessary contraction Furthermore, the observed volume discrepancy can not be attributed to cracking because the shape strain measurements defining the volume ratio were made on un-cracked plates or un-cracked regions of plates.

Although incapable of accommodating the necessary adjustment in interatomic spacing, by revealing that $(225)_F$ plates are in tension along $[11\bar{1}]_B$ the microcracks emphasise the need for such accommodation and thus provide indirect evidence for a plastic accommodation strain in the austenite. Microcracking seems to complement plastic deformation in the austenite as a means of accommodating the required contraction and apparently occurs if for any reason there is a breakdown in the mechanism of plastic accommodation in the austenite.

References

1. A.R. Marder and A.O. Benscoter: Trans. A.S.M., 61(1968), 293.
2. R.G. Davies and C.L. Magee: Met. Trans., 3(1972), 307.
3. A.R. Marder, A.O. Benscoter and G. Krauss: Met. Trans., 1(1970), 1545.
4. C.M. Wayman, J.E. Hanafee and T.A. Read: Acta Met., 9(1961), 392.
5. B.C. Muddle, P. Krauklis and J.S. Bowles: Acta Met., 24(1976), 371.
6. J.S. Bowles and J.K. Mackenzie: Acta Met., 2(1954), 129.
7. M.S. Wechsler, D.S. Lieberman and T.A. Read: Trans. A.I.M.E., 197(1953), 1503.
8. A. Morton and C.M. Wayman: Acta Met., 14(1966), 1567.
9. D.P. Dunne and J.S. Bowles: Acta Met., 17(1969), 201.
10. S. Jana and C.M. Wayman: Met. Trans., 1(1970), 2815.
11. J.S. Bowles and D.P. Dunne: Acta Met., 17(1969), 677.
12. M. Watanabe and C.M. Wayman: Met. Trans., 2(1971), 2229.
13. E.J. Efsic and C.M. Wayman: Trans. A.I.M.E., 239(1967), 873.
14. D.P. Dunne and C.M. Wayman: Acta Met., 18(1970), 981.

Table I: Mean Values of the Ratios of Measured to Calculated Volume Change

Transformation	g_S/g	No. of Individual Measurements	$d_{[1\bar{1}0]_F}/d_{[11\bar{1}]_B}$
$(225)_F$			
Fe-Cr-C (5)	1.0192 ± 0.0048*	149	1.0185
Fe-Cr-C (8)	1.0372 ± 0.0320	26	1.0184
Fe-Mn-C (9)	1.0142 ± 0.0065	35	1.0179
Fe-Mn-Cr-C (10)	1.0143 ± 0.0056	110	1.0189
Mean :	1.0184 ± 0.0036	320	
$(3,10,15)_F$			
Fe-Ni-C (9)	1.0043 ± 0.0052	45	
Fe-Al-C (12)	1.0056 ± 0.0078	-	
Fe-Pt (13)	0.9896 ± 0.0079	18	
Twinning of Tin			
Muddle et al (5)	1.0045 ± 0.0043	18	
Dunne & Wayman (14)	0.9987 ± 0.0041	-	

* The error limits given are 99% confidence limits.

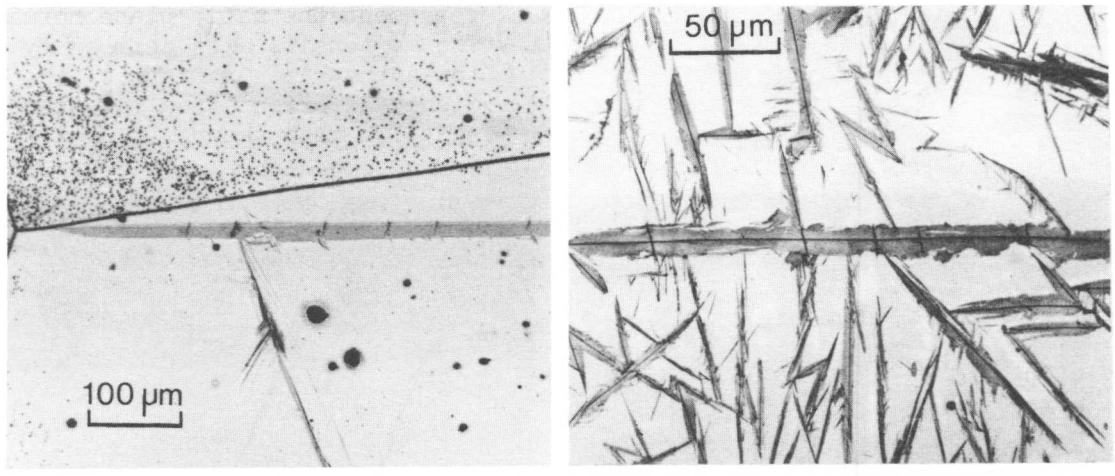

(a) (b)

Fig. 1: Photomicrographs showing transverse microcracks in
(a) a $(225)_F$ martensite plate in the relief surface, and
(b) a polished and etched section of a $(259)_F$ plate.

Fig. 2:
Stereographic projection showing results of trace analysis for $(225)_F$ plates. (●) indicate surface traces of cracked plates. Trace normals (----) to the transverse cracks pass near to $(1\bar{1}0)_F$. (▲) identify normals to crack planes defined by two surface analysis and (•) represent corresponding habit plane normals. ▶

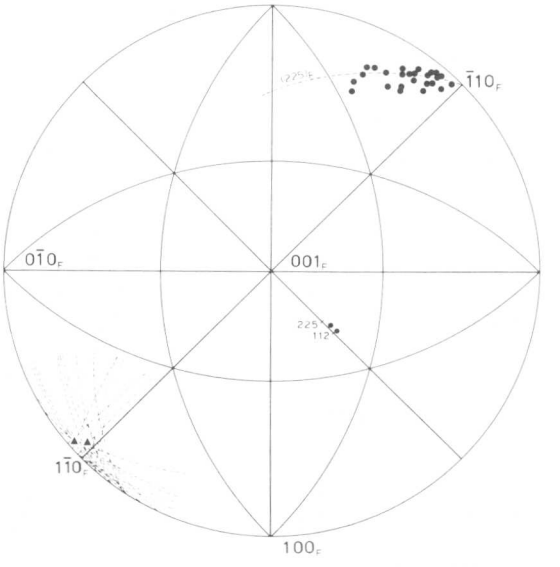

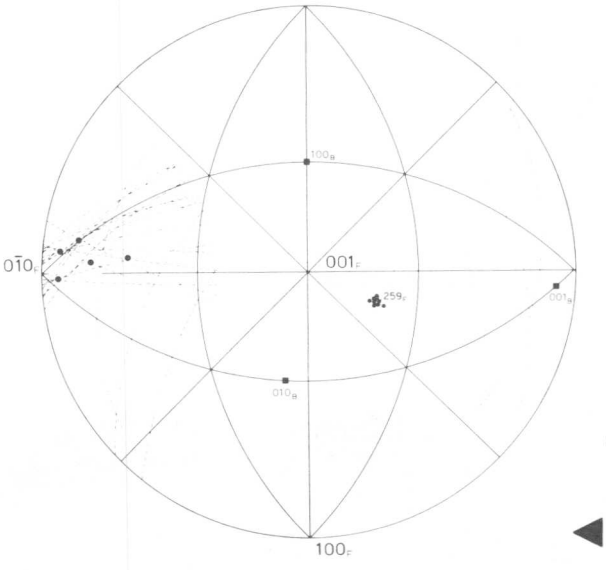

Fig. 3:
Stereographic projection summarising results of trace analysis for $(259)_F$ plates. Trace normals (----) to cracking planes converge near to $(0\bar{1}0)_F$. (●) indicate normals to crack planes defined by two surface analysis and (•) represent the habit plane normals. The martensite axes defined by the appropriate variant of the Nishiyama orientation relationship are also shown. ◀

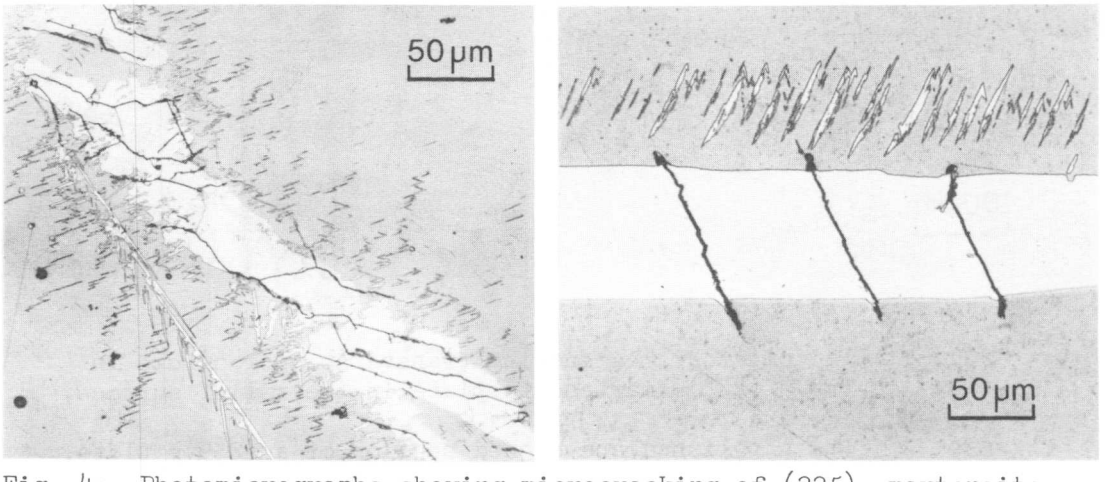

Fig. 4: Photomicrographs showing microcracking of $(225)_F$ martensite plates, sectioned and polished approximately parallel to the habit plane.